Muhammad Rahman

Numerical Solutions of Three-Dimensional Von Kármán and Bödewadt Heat and Fluid Flow Problems

Thesis for the degree of Philosophiae Doctor

Trondheim, January 3, 2018

Norwegian University of Science and Technology
Faculty of Engineering Science and Technology
Department of Energy and Process Engineering

NTNU
Innovation and Creativity

NTNU

Norwegian University of Science and Technology

Thesis for the degree of Philosophiae Doctor

Faculty of Engineering Science and Technology
Department of Energy and Process Engineering

© Muhammad Rahman.

ISBN (printed version)
ISBN (electronic version)
ISSN 1503-8181

Doctoral theses at NTNU,

Printed by NTNU

I dedicate this work to my beloved parents

"Life consists of two days , one for you and one against of you. So when it’s for you don’t be proud or reckless, and when it’s against you be patient, for both days are test for you."

Imam Ali (AS)

Preface

This doctoral thesis in fluids engineering is based mainly on theoretical and numerical work to investigate an area of fluid mechanics. Thesis discusses the laminar boundary layer of swirling, rotating-disk and generalized vortex flow. The thesis is divided into two parts; the first part consists of an introduction, background theory, as well as a summary and the conclusion of the research papers. The second part contains six papers. The format of the papers may vary from the published format to align with the formatting of this thesis. The thesis is also available as a PDF file at the NTNU library.

This doctoral thesis is apparently submitted to describe the investigations authentically performed during a period from February 2014 to January 2018 at Norwegian University of Science and Technology (NTNU), Faculty of Engineering Science and Technology, Department of Energy and Process Engineering. The department of Human Resource Development (HRD) of Pakistan has provided the main financial support.

Acknowledgments

This study has been supported by the HRD of Pakistan. I think it's impossible to describe everything here to thank people who helped me during my doctoral work. Without the support from them, I could not have succeeded with my doctoral work and life in Norway. Therefore, even if you do not find your name in my acknowledgments, you should not be disappointed. I really appreciate the support of everyone I have met during this period. First of all, I would like to thank my main supervisor Prof. Helge I. Andersson, who gave me a chance to work under his kind supervision. I was able to do my research in a very nice environment and atmosphere during this doctoral work. You taught me how a researcher should be in many different aspects. In particular, I am really grateful for your contribution in making me learn the art of writing a scientific paper. Therefore, this four years of life at NTNU was extremely worthwhile and makes a huge impact on my future. Many thanks also to my co-supervisor Dr. Nils Erland Haugen. I appreciate Faisal and Salman Ejaz for providing me assistance in writing Matlab code.

I am very grateful to people in the Department of EPT, NTNU. They provided me a very nice atmosphere and I was able to study with a lot of fun. Thanks to Åsmund, Kun, Niranjan, Jørgen, Wenjun, Elin, and Rohit for sharing an office with me during my stay in the fluid building.

During my stay in Norway, I have met many friends who have supported me outside of the research world and who have shared fun time, BBQ, traveling and many experiences with me. Especially, I would like to acknowledge my friends, Adil, Qasim, Khuram, Shafique, Asif, Salman, Shebaz, Usman. You have made my life more meaningful, thanks a lot! Finally, I appreciate my sister, brothers, cousins, my uncle, and In particular, my mother for supporting me and permitting me to choose my own path and those people who prayed for me. Thanks to you, I was able to experience the diverse world and have great experiences.

Muhammad Rahman

Contents

Part I **1**

1 Introduction **3**

1.1 Swirling flow 3

1.2 Rotating disk flow 5

1.3 Vortex flow 6

1.4 Objectives 7

2 Background Theory **9**

2.1 Flow equations for fluid phase 9

2.1.1 Flow equations in cylindrical coordinate system (for fluid phase) 10

2.2 Flow equations for continuous particle phase 12

2.2.1 Flow equations in cylindrical coordinate system (for particle phase) 12

2.3 Similarity transformation 14

2.3.1 Steady flow 14

2.3.2 Generalized steady flow 15

2.3.3 Unsteady flow 16

2.4 Boundary conditions 17

2.5 Numerical approach 18

3 Summary of research papers 21
3.1 List of papers 21

4 Conclusions and Future Work 25
4.1 Future work 27

Bibliography 28

Part II 33

Paper1. On heat transfer flow in Bödewadt flow 35

Paper2. Revolving flow of a fluid-particle suspension with suction 43

Paper3. Bödewadt flow of a fluid-particle suspension with strong suction 51

Paper4. On heat transfer in unsteady von Kármán flow 59

Paper5. A note on buoyancy effects in von Kármán flow over a rotating disk 67

Paper6. Heat transfer in generalized vortex flow over a permeable surface 77

List of Figures

2.1 Sketch of the three-dimensional flow field set up by a steadily revolving flow high above the shaded surface. The variations of the radial (u) and circumferential (v) velocity components are indicated. The axial velocity component (w) is shown upward. 18

2.2 Sketch of the three-dimensional flow field set up by a steadily revolving flow high above the shaded surface. The variations of the radial (u) and circumferential (v) velocity components are indicated. The axial velocity component (w) is shown upward, as in the classical Bödewadt problem [1]. In presence of strong suction, as considered herein, the axial velocity is downward. 19

2.3 Sketch of the three-dimensional flow field set up by a revolving infinite rotating disk. The variations of the radial velocity (u), circumferential velocity (v), and axial velocity (w) components are indicated. This is adopted from Imayama & Lingwood [2]. 20

Part I

Chapter 1

Introduction

There is air around us, and there are rivers and seas near us. "The flow of a river never ceases to go past, nevertheless it is not the same water as before. Bubbles floating along on the stagnant water now vanish and then develop but have never remained". So stated Chohmei Kamo, the famous thirteenth century essayist of Japan, in the prologue of Hohjohki, his collection of essays. In this way, the air and the water of rivers and seas are always moving. Such a movement of gas or liquid (collectively called fluid) is called the 'flow', and the study of this is fluid mechanics. While the flow of the air and the water of rivers and seas are flows of our concern, so also are the flows of water, sewage and gas in pipes, in irrigation canals, and around rockets, aircraft, express trains, automobiles and boats. And so too is the resistance which acts on such flows. Throwing baseballs and hitting golf balls are all acts of flow. Furthermore, the movement of people on the platform of a railway station or at the intersection of streets can be regarded as forms of flow. In a wider sense, the movement of social phenomena, information or history could be regarded as a flow, too. In this way, we are in so close a relationship to flow that the fluid mechanics which studies flow is really a very familiar thing to us, is quoted from Nakayama [3]. In the same way in our daily life there are many applications of swirling flow in diverse fields, such as rotating machines, filtering systems, computer storage devices, heat and mass transfer, planetary formations and geophysics etc. To elaborate the theoretical basis of flow problems, the introduction section is divided into three parts:

- Swirling flow
- Rotating disk flow
- Vortex flow

1.1 Swirling flow

The steadily revolving flow of a viscous fluid above a solid surface was first studied by Bödewadt [1] who transformed the governing partial differential equations into a set of ordinary differential equations by means of the same similarity transformation as originally used by Von Kármán[4] in his classical study of the swirling flow driven by a constantly rotating disk. The Bödewadt flow can be considered as a reversed Von Kármán flow with the axial velocity component directed away from the planar surface rather than towards the rotating disk. However, the three velocity components in the Bödewadt flow exhibit a more complex variation than in the Von Kármán flow and the Bödewadt boundary layer is substantially thicker than the corresponding Von Kármán boundary layer.

The fluid motion well above the surface is characterised by a uniform angular velocity, which is reduced through a viscous boundary layer in order for the fluid to adhere to the no-slip condition at the solid surface. The reduction of the circumferential velocity component in the vicinity of the surface reduces the radially directed centripetal acceleration (or centrifugal force) such that the prevailing radial pressure gradient induces an inward fluid motion. In order to assure mass conservation, this inward fluid motion gives in turn rise to an axial upward flow. Such a spiralling flow exists near the planar surface, although more complex variations of the velocity field have been reported further away, but yet before the uniformly rotating flow conditions are reached. The oscillatory nature of the three velocity components reported by Bödewadt [1] has been subject to criticism, but this criticism was deem unjustified by Zandbergen & Dijkstra [5]. It is interesting to notice that these oscillations are damped and even suppressed in presence of a magnetic field (King & Lewellen [6]), partial slip (Sahoo, Abbasbandy & Poncet [7]), stretching surface (Turkyilmazolgu [8]) or suction (Nath & Venkatachala [9]). With a sufficiently high suction velocity through the planar surface, the axial flow is directed in the downward direction rather than upward, as is the case in the classical Bödewadt flow. In view of its fundamental importance as a prototype swirling flow the Bödewadt flow has received renewed focus in recent years. The inviscid instability of the Bödewadt boundary layer was examined by MacKerrell [10] whereas Sahoo [11, 12] and Sahoo & Poncet [13] demonstrated that also such revolving flows of a non-Newtonian Reiner-Rivlin fluid admit exact similarity solutions. Zung [14] studied a Von Kármán flow of a fluid-particle suspension and his analysis was subsequently extended by Sankara & Sarma [15] to include surface suction and further explored by Allaham & Peddieson [16].

Studies of suspensions of small particles in a continuous medium (either gas or liquid) are of fundamental interest in fluid mechanics and yet with numerous applications like, for instance, aerosol clouds and erosion protection. Additional applications were recently pointed out by Turkyilmazolgu [17]. A daily life example is the characteristic flow-induced sedimentation of tea leaves in a flat-bottomed cup of tea, as discussed by Einstein [18] . Some sample solution have computed for strong suction by Rahman & Andersson [19].

In this study we consider the heat transfer in steadily revolving Bödewadt flow. The heat transfer in this prototype flow seems to have received only negligible attention in comparison with the heat transfer in the Von Kármán flow. Heat transfer in flow above a rotating disk was first studied by Millsaps & Pohlhausen [20] and Sparrow & Gregg [21], followed by many others. See, e.g., the book by Shevchuk [22]. Shevchuk & Buschmann [23], for instance, found self-similar solutions for the flow and heat transfer in a fluid co-rotating with a rotating disk with a radially varying disk temperature. One may speculate whether the lack of studies of heat transfer in B*ö*dewadt flow is due the relatively higher complexity of the three-dimensional flow field.

The only earlier studies that we are aware of are the recent papers by Sahoo [11], Sahoo et al. [24], and Turkyilmazoglu [8]. Sahoo [11] included heat transfer analysis in his study of B*ö*dewadt flow of an electrically conducting fluid with partial slip. Some temperature profiles were presented, but not for pure B*ö*dewadt flow of a Newtonian fluid with no-slip at the solid surface. Sahoo et al. [24] also focussed on non-Newtonian fluid properties and the majority of their results were concerned with the flow field, but two figures showing heat transfer results for Newtonian fluids were also included. As we will see later, these results might be questionable. Even more recently, Turkyilmazoglu [8] studied the heat transfer in B*ö*dewadt flow over a stretching but non-rotating disk. In the absence of stretching, however, his results suggested a constant temperature all across the viscous boundary layer and therefore failed to satisfy the outer boundary condition for the thermal field. The auxiliary condition is commonly overlooked in analysis of thermal boundary layers, similarly as the auxiliary conditions for the momentum boundary layer are discussed in the paper Andersson [25] and Pantokratoras [26]. In-depth discussions on high-Prandtl-number effects on the thermal boundary layer thickness and the surface heat transfer can be found in Shevchuk [23, 27].

1.2 Rotating disk flow

The steadily revolving motion of a viscous fluid driven solely by a rotating disk in an otherwise quiescent and unbounded ambient has evolved into a canonical flow problem in fluid mechanics. The problem was first formulated by Von K*á*rm*á*n [4] by means of the axisymmetric Navier-Stokes equations. He moreover devised an ingenious similarity transformation which elegantly transformed the governing partial differential equations (PDEs) to a set of ordinary differential equations (ODEs). The review article by Zandbergen & Dijkstra [5] provided a comprehensive survey of the vast attention devoted to the Von K*á*rm*á*n swirling flow. Throughout the century that has elapsed since Von K*á*rm*á*n's work appeared, the vast majority of investigations have been concerned solely with various aspects of the mathematical problem formulation and the resulting three-componential velocity field. However, Von K*á*rm*á*n [4] pointed out that also the associated pressure field can be obtained from an ODE that results from the axial momentum equation as soon as the velocity field has been determined, but the pressure variation over the rotating disk was neither addressed by Von K*á*rm*á*n [4] nor by Zandbergen & Dijkstra [5]. This is likely due to the fact that the Von K*á*rm*á*n flow is often considered as a three-dimensional boundary layer flow, in which the pressure gradient across the boundary layer is negligible.

The accompanying heat transfer problem was apparently first studied by Millsaps & Pohlhausen [20] and Sparrow & Gregg [21]. Only recently, however, buoyancy was included in analyses of Von K*á*rm*á*n swirling flows by Sibanda & Makinde [28] and Guha & Sengupta [29] by solving ODEs and PDEs, respectively.

While Von K$\acute{a}$rm$\acute{a}$n [4] obtained approximate solutions for the three velocity components by means of the momentum integral method approach, more accurate solutions were obtained by Cochran [30] and Rogers & Lance [31]; see also the review article by Zandbergen & Dijkstra [5]. The accompanying heat transfer problem was first studied by Millsaps & Pohlhausen [20] and Sparrow & Gregg [21], followed by several others and Turkyilmazoglu [32] shown that the axial velocity component of the Von K$\acute{a}$rm$\acute{a}$n flow becomes constant in presence of strong suction. Lingwood & Alfredsson [33] shown that Von K$\acute{a}$rm$\acute{a}$n flow will be unstable and eventually turbulent at higher Reynolds numbers.

A prerequisite for steady-state solutions to exist is that the disk is rotating steadily with a constant angular velocity Ω_0. Unsteady flows induced by a time-varying angular velocity $\Omega(t)$ of the disk has also received considerable attention in the past, for instance by consideration of a step-change in Ω, the impulsively start-up from rest, and a torsionally oscillating disk. A particularly attractive case is a decelerating disk for which the angular velocity Ω decreases inversely proportional to time, i.e. $\Omega(t) = \Omega_0(1 - \alpha t)^{-1}$ where α is a constant measured in sec^{-1} which discriminates between an accelerating $(\alpha > 0)$ and a decelerating $(\alpha < 0)$ disk. Similarity solutions of the unsteady Navier-Stokes equations are rare (see the review by Wang [34]), but Watson & Wang [35] nevertheless obtained a transformation which exactly transformed the time-dependent Navier-Stokes equations to ODEs in the similarity variable. A particularly peculiar observation made by Watson & Wang [35] was that the fluid in the vicinity of the disk rotates faster rather than slower than the disk for a sufficiently fast deceleration of the disk. One may wonder if and how these circumstances may affect the temperature distribution in the fluid and, in particular, the heat transfer between the decelerating disk and the fluid. unstable and eventually turbulent at higher Reynolds numbers.

1.3 Vortex flow

B$\ddot{o}$dewadt [1] considered the steadily revolving flow of a viscous fluid above an impermeable solid surface. The fluid far above the planar surface was assumed to be in a state of rigid-body rotation so that the tangential velocity component v increased linearly with the distance r from the axis of rotation. The presence of viscous shear stresses inevitably slowed down the revolving fluid motion in the viscous boundary layer adjacent to the surface. A resulting imbalance between the radial pressure gradient and the centrifugal force gave rise to a velocity component directed towards the axis of rotation. Finally, to secure mass conservation, an axial flow away from the surface arose and a three-dimensional boundary layer flow was established. The effects of alternative boundary conditions at the planar surface have been examined by Nath & Venkatachala [36], Sahoo et al. [37] and Turkyilmazoglu [8]. They considered suction, partial slip, and stretching, respectively.

The classical B$\ddot{o}$dewadt problem was later generalized by King & Lewellen [6] who assumed the tangential velocity to vary as $v \sim r^m$ where m is dimensionless constant. They were partly concerned with the effect of the parameter m and partly with the effect of a magnetic body-force term on the fluid motion. Their study was extended by Venkatachala & Nath [38] to include also the effects of suction through the surface. The generalized B$\ddot{o}$dewadt flow was also considered as a part of an extensive paper by Kuo [39] focused on tornado-like vertices. In addition to the conventional no-slip conditions at the solid surface, Kuo [39] also allowed for partial surface slip. This was referred to as a geophysical boundary condition.

It was suggested by Moore [40] that the generalized Bödewadt flow does not admit similarity solutions for $m = -1$, i.e. when the revolving flow behaves as a potential vortex. The non-existence of similarity solutions was later proved by King & Lewellen [6]. However, as demonstrated by Nanbu [41] and Venkatachala & Nath [38], similarity solutions do exist in the presence of suction through the surface.

1.4 Objectives

The overall objective of this thesis is to provide a theoretical and numerical underpinning on the nonexistence of thermal energy of swirling, rotating disk and vortex flow with and without suction, to investigate the characteristics of particle phase near the vicinity of the surface of disk, and to explore the effect of buoyancy on the pressure field of a rotating disk. In the following, the objective is divided into three major strands.

- To provide the numerical solution, using $similarity\ solution$, to show how the particle phase is revolving along with the fluid and how the presence of particles affects the swirling motion of the fluid phase.
- To explore how the pressure field of a rotating disk is affected by buoyancy (parameterized by the Grashof number), and to investigate the unsteady heat transfer on an isothermal disk and the Prandtl number.
- To investigate the heat transfer between a generalized Bödewadt flow and the planar surface above which the fluid revolves, and the similarity solutions of the thermal energy equation for different revolving flows, including solid-body rotation $(m = +1)$ and potential vortex flow $(m = -1)$, and for different Prandtl numbers.

Chapter 2

Background Theory

The study on two-fluids modelling is fairly extensive in fluid mechanics considering different forms, such as the cases of external heating transition of liquid into vapor, dispersed and separated flows in the form of droplets, and particles phase with fluid flow (i.e. gas or liquid). The following sections elucidate relevant mathematical model of the two-fluid theory.

2.1 Flow equations for fluid phase

The governing equations for fluid phase are taken as that considered by Zung [14] for swirling von Kármán flow of a fluid phase above a steadily rotating disk. We consider a Newtonian fluid and apply the Eulerian approach on mass, momentum, and energy, thus giving the following equations:

Mass conservation equation (continuity equation):

$$\nabla.\mathbf{U} = 0, \tag{2.1}$$

which means that the velocity field of an incompressible flow is divergence free for the fluid. Here, $\mathbf{U}$ denotes the velocity of the fluid.

Momentum equation (the Navier-stokes equation) :

$$\rho\left(\frac{\partial \mathbf{U}}{\partial t} + (\mathbf{U}.\nabla)\mathbf{U}\right) = -\nabla p + \mu\nabla^2\mathbf{U} + F, \tag{2.2}$$

where p and ρ denote pressure and constant density, respectively. The terms μ and F are the viscosity and the external body force acting per unit mass (i.e. drag force) of the fluid, respectively.

Energy equation:

$$\rho c_p \left(\frac{\partial T}{\partial t} + (\mathbf{U}.\nabla)T \right) = k\nabla^2 T + \Phi, \tag{2.3}$$

where the term c_p (energy per unit mass per degree Kelvin) is the specific heat at constant pressure. The terms k and T refer to thermal conductivity and temperature, respectively. Whereas Φ is the dissipation function. Note that for liquids, $c_p \approx c_v$ for incompressible flows.

2.1.1 Flow equations in cylindrical coordinate system (for fluid phase)

In cylindrical polar coordinates (r, θ, and z directions), the mass conservation, momentum and energy equations can be written as follows:

Mass conservation equation (continuity equation):

$$\frac{\partial}{\partial r}(ru) + \frac{\partial}{\partial \theta}(rv) + \frac{\partial}{\partial z}(rw) = 0, \tag{2.4}$$

Momentum equation (The Navier-stokes equation):

$$\begin{aligned} r \quad direction: \quad & \rho \left(\frac{\partial u}{\partial t} + u\frac{\partial u}{\partial r} + \frac{v}{r}\frac{\partial u}{\partial \theta} - \frac{v^2}{r} + w\frac{\partial u}{\partial z} \right) = \\ & -\frac{\partial p}{\partial r} + \mu \left[\frac{\partial^2 u}{\partial r^2} + \frac{\partial}{\partial r}\left(\frac{u}{r}\right) + \frac{1}{r^2}\frac{\partial^2 u}{\partial \theta^2} + \frac{\partial^2 u}{\partial z^2} - \frac{2}{r^2}\frac{\partial u}{\partial \theta} \right] + F_r, \end{aligned} \tag{2.5}$$

$$\begin{aligned} \theta \quad direction: \quad & \rho \left(\frac{\partial v}{\partial t} + u\frac{\partial v}{\partial r} + \frac{v}{r}\frac{\partial v}{\partial \theta} - \frac{uv}{r} + w\frac{\partial v}{\partial z} \right) = \\ & -\frac{1}{r}\frac{\partial p}{\partial \theta} + \mu \left[\frac{\partial^2 v}{\partial r^2} + \frac{\partial}{\partial r}\left(\frac{v}{r}\right) + \frac{1}{r^2}\frac{\partial^2 v}{\partial \theta^2} + \frac{\partial^2 v}{\partial z^2} + \frac{2}{r^2}\frac{\partial u}{\partial \theta} \right] + F_\theta, \end{aligned} \tag{2.6}$$

$$\begin{aligned} z \quad direction: \quad & \rho \left(\frac{\partial w}{\partial t} + u\frac{\partial w}{\partial r} + \frac{v}{r}\frac{\partial w}{\partial \theta} + w\frac{\partial w}{\partial z} \right) = \\ & -\frac{\partial p}{\partial z} + \mu \left[\frac{\partial^2 w}{\partial r^2} + \frac{1}{r}\frac{\partial w}{\partial r} + \frac{1}{r^2}\frac{\partial^2 w}{\partial \theta^2} + \frac{\partial^2 w}{\partial z^2} \right] + F_w, \end{aligned} \tag{2.7}$$

Energy equation:

$$\rho c_p \left(\frac{\partial T}{\partial t} + u\frac{\partial T}{\partial r} + \frac{v}{r}\frac{\partial T}{\partial \theta} + w\frac{\partial T}{\partial z} \right) = k \left[\frac{\partial^2 T}{\partial r^2} + \frac{1}{r}\frac{\partial T}{\partial r} + \frac{1}{r^2}\frac{\partial^2 T}{\partial \theta^2} + \frac{\partial^2 T}{\partial z^2} \right] + \Phi, \tag{2.8}$$

where (u, v, w) and (F_r, F_θ, F_z) are the velocity components and body forces (i.e drag force) of the fluid, given in the radial, circumferential and axial directions, respectively.

The equations (2.5)-(2.8) are divided by fluid density ρ and we assume rotational symmetry about the vertical z-axis, i.e. $\partial/\partial\theta = 0$ and dissipation function $\Phi = 0$. Hence the equations (2.4)-(2.8) can be reduced to:

$$\frac{\partial}{\partial r}(ru) + \frac{\partial}{\partial z}(rw) = 0, \tag{2.9}$$

$$\frac{\partial u}{\partial t} + u\frac{\partial u}{\partial r} - \frac{v^2}{r} + w\frac{\partial u}{\partial z} = -\frac{1}{\rho}\frac{\partial p}{\partial r} + \nu\left[\frac{\partial^2 u}{\partial r^2} + \frac{\partial}{\partial r}\left(\frac{u}{r}\right) + \frac{\partial^2 u}{\partial z^2}\right] + \frac{F_r}{\rho}, \tag{2.10}$$

$$\frac{\partial v}{\partial t} + u\frac{\partial v}{\partial r} + \frac{uv}{r} + w\frac{\partial v}{\partial z} = \nu\left[\frac{\partial^2 v}{\partial r^2} + \frac{\partial}{\partial r}\left(\frac{v}{r}\right) + \frac{\partial^2 v}{\partial z^2}\right] + \frac{F_\theta}{\rho}, \tag{2.11}$$

$$\frac{\partial w}{\partial t} + u\frac{\partial w}{\partial r} + w\frac{\partial w}{\partial z} = -\frac{1}{\rho}\frac{\partial p}{\partial z} + \nu\left[\frac{\partial^2 w}{\partial r^2} + \frac{1}{r}\frac{\partial w}{\partial r} + \frac{\partial^2 w}{\partial z^2}\right] + \frac{F_z}{\rho}, \tag{2.12}$$

$$\frac{\partial T}{\partial t} + u\frac{\partial T}{\partial r} + w\frac{\partial T}{\partial z} = \frac{k}{\rho c_p}\left[\frac{\partial^2 T}{\partial r^2} + \frac{1}{r}\frac{\partial T}{\partial r} + \frac{\partial^2 T}{\partial z^2}\right], \tag{2.13}$$

where $\nu = \mu/\rho$ is the kinematic viscosity of the fluid. Note that in paper 4, we employed equations (2.9)-(2.13) without considering body force, i.e. $(F_r, F_\theta, F_z) = 0$, also assumed that flow is steady, i.e. $\partial/\partial t = 0$. Therefore, equations (2.10)-(2.13) can be written as:

$$u\frac{\partial u}{\partial r} - \frac{v^2}{r} + w\frac{\partial u}{\partial z} = -\frac{1}{\rho}\frac{\partial p}{\partial r} + \nu\left[\frac{\partial^2 u}{\partial r^2} + \frac{\partial}{\partial r}\left(\frac{u}{r}\right) + \frac{\partial^2 u}{\partial z^2}\right] + \frac{F_r}{\rho}, \tag{2.14}$$

$$u\frac{\partial v}{\partial r} + \frac{uv}{r} + w\frac{\partial v}{\partial z} = \nu\left[\frac{\partial^2 v}{\partial r^2} + \frac{\partial}{\partial r}\left(\frac{v}{r}\right) + \frac{\partial^2 v}{\partial z^2}\right] + \frac{F_\theta}{\rho}, \tag{2.15}$$

$$u\frac{\partial w}{\partial r} + w\frac{\partial w}{\partial z} = -\frac{1}{\rho}\frac{\partial p}{\partial z} + \nu\left[\frac{\partial^2 w}{\partial r^2} + \frac{1}{r}\frac{\partial w}{\partial r} + \frac{\partial^2 w}{\partial z^2}\right] + \frac{F_z}{\rho}, \tag{2.16}$$

$$u\frac{\partial T}{\partial r} + w\frac{\partial T}{\partial z} = \frac{k}{\rho c_p}\left[\frac{\partial^2 T}{\partial r^2} + \frac{1}{r}\frac{\partial T}{\partial r} + \frac{\partial^2 T}{\partial z^2}\right]. \tag{2.17}$$

We assume that the body force, i.e. $(F_r, F_\theta, F_z) = 0$. Therefore, equations (2.14)-(2.17) reduce to:

$$u\frac{\partial u}{\partial r} - \frac{v^2}{r} + w\frac{\partial u}{\partial z} = -\frac{1}{\rho}\frac{\partial p}{\partial r} + \nu\left[\frac{\partial^2 u}{\partial r^2} + \frac{\partial}{\partial r}\left(\frac{u}{r}\right) + \frac{\partial^2 u}{\partial z^2}\right], \tag{2.18}$$

$$u\frac{\partial v}{\partial r} + \frac{uv}{r} + w\frac{\partial v}{\partial z} = \nu\left[\frac{\partial^2 v}{\partial r^2} + \frac{\partial}{\partial r}\left(\frac{v}{r}\right) + \frac{\partial^2 v}{\partial z^2}\right], \tag{2.19}$$

$$u\frac{\partial w}{\partial r} + w\frac{\partial w}{\partial z} = -\frac{1}{\rho}\frac{\partial p}{\partial z} + \nu\left[\frac{\partial^2 w}{\partial r^2} + \frac{1}{r}\frac{\partial w}{\partial r} + \frac{\partial^2 w}{\partial z^2}\right], \tag{2.20}$$

$$u\frac{\partial T}{\partial r} + w\frac{\partial T}{\partial z} = \frac{k}{\rho c_p}\left[\frac{\partial^2 T}{\partial r^2} + \frac{1}{r}\frac{\partial T}{\partial r} + \frac{\partial^2 T}{\partial z^2}\right]. \tag{2.21}$$

In the papers (1 & 5), we applied equations (2.9) and (2.18)-(2.20) in the radial, circumferential, and axial directions.

2.2 Flow equations for continuous particle phase

The governing equations for continuous particle phase are taken as those considered by Zung [14] and Sankara & Sarma [15] for swirling von Kármán flow for particle phase above a steadily rotating disk except a case that a priori unknown pressure p is assigned only to the fluid phase. We apply the Eulerian approach on mass and momentum equations.

Mass conservation equation:

$$\nabla.\mathbf{U_p} = 0, \tag{2.22}$$

which means that the velocity field of a incompressible flow is divergence free for the particles. Here, $\mathbf{U}_p$ denotes the velocity of particles.

Momentum equation :

$$\rho_p\left(\frac{\partial \mathbf{U}_p}{\partial t} + (\mathbf{U}_p.\nabla)\mathbf{U}_p\right) = -\nabla p + \mu_p \nabla^2 \mathbf{U}_p - F, \tag{2.23}$$

where ρ_p and μ_p are the constant density and viscosity of the particles, respectively.

2.2.1 Flow equations in cylindrical coordinate system (for particle phase)

In cylindrical polar coordinates (r, θ, and z directions), the particle phase, mass conservation, momentum, and energy equations can be written as follows:

Mass conservation equation:

$$\frac{\partial}{\partial r}(\rho_p u_p) + \frac{\partial}{\partial \theta}(\rho_p v_p) + \frac{\partial}{\partial z}(\rho_p w_p) = 0, \tag{2.24}$$

Momentum equation :

$$r \quad direction: \quad \rho_p\left(\frac{\partial u_p}{\partial t} + u_p\frac{\partial u_p}{\partial r} + \frac{v_p}{r}\frac{\partial u_p}{\partial \theta} - \frac{{v_p}^2}{r} + w_p\frac{\partial u_p}{\partial z}\right) = -\frac{\partial p}{\partial r}$$
$$+\mu_p\left[\frac{\partial^2 u_p}{\partial r^2} + \frac{\partial}{\partial r}\left(\frac{u_p}{r}\right) + \frac{1}{r^2}\frac{\partial^2 u_p}{\partial \theta^2} + \frac{\partial^2 u_p}{\partial z^2} - \frac{2}{r^2}\frac{\partial u_p}{\partial \theta}\right] - F_r, \tag{2.25}$$

$$\theta \quad direction: \quad \rho_p\left(\frac{\partial v_p}{\partial t} + u_p\frac{\partial v_p}{\partial r} + \frac{v_p}{r}\frac{\partial v_p}{\partial \theta} - \frac{u_p v_p}{r} + w_p\frac{\partial v_p}{\partial z}\right) = -\frac{1}{r}\frac{\partial p}{\partial \theta}$$
$$+\mu_p\left[\frac{\partial^2 v_p}{\partial r^2} + \frac{\partial}{\partial r}\left(\frac{v_p}{r}\right) + \frac{1}{r^2}\frac{\partial^2 v_p}{\partial \theta^2} + \frac{\partial^2 v_p}{\partial z^2} + \frac{2}{r^2}\frac{\partial u_p}{\partial \theta}\right] - F_\theta, \tag{2.26}$$

$$z \quad direction: \quad \rho_p\left(\frac{\partial w_p}{\partial t}+u_p\frac{\partial w_p}{\partial r}+\frac{v_p}{r}\frac{\partial w_p}{\partial \theta}+w_p\frac{\partial w_p}{\partial z}\right)=-\frac{\partial p}{\partial z}$$
$$+\mu\left[\frac{\partial^2 w_p}{\partial r^2}+\frac{1}{r}\frac{\partial w_p}{\partial r}+\frac{1}{r^2}\frac{\partial^2 w_p}{\partial \theta^2}+\frac{\partial^2 w_p}{\partial z^2}\right]-F_w, \quad (2.27)$$

In the present study, however, pressure gradients are shared by the two phases in proportion to their density ratios. This alternative formulation was suggested by Allaham & Peddeison [16], but was not adopted in their subsequent calculations. However, it is essential to include pressure gradient terms also in the particle phase equations of motion. In fact, a radial pressure gradient is required to balance the centripetal acceleration in the far field as dictated in equation (2.25). Here (u_p, v_p, w_p) are the velocity components of the particle phases. Dividing the equations (2.25)-(2.27) by particle density ρ_p and assuming rotational symmetry about the vertical z-axis, i.e. $\partial/\partial\theta = 0$, we can write equations (2.24)-(2.27) as follows:

$$\frac{\partial}{\partial r}(\rho_p u_p)+\frac{\partial}{\partial z}(\rho_p w_p)=0, \quad (2.28)$$

$$\frac{\partial u_p}{\partial t}+u_p\frac{\partial u_p}{\partial r}-\frac{{v_p}^2}{r}+w_p\frac{\partial u_p}{\partial z}=-\frac{1}{\rho_p}\frac{\partial p}{\partial r}+\nu_p\left[\frac{\partial^2 u_p}{\partial r^2}+\frac{\partial}{\partial r}\left(\frac{u_p}{r}\right)+\frac{\partial^2 u_p}{\partial z^2}\right]-\frac{F_r}{\rho_p}, \quad (2.29)$$

$$\frac{\partial v_p}{\partial t}+u_p\frac{\partial v_p}{\partial r}+\frac{u_p v_p}{r}+w_p\frac{\partial v_p}{\partial z}=\nu_p\left[\frac{\partial^2 v_p}{\partial r^2}+\frac{\partial}{\partial r}\left(\frac{v_p}{r}\right)+\frac{\partial^2 v_p}{\partial z^2}\right]-\frac{F_\theta}{\rho_p}, \quad (2.30)$$

$$\frac{\partial w_p}{\partial t}+u_p\frac{\partial w_p}{\partial r}+w_p\frac{\partial w_p}{\partial z}=-\frac{1}{\rho_p}\frac{\partial p}{\partial z}+\nu_p\left[\frac{\partial^2 w_p}{\partial r^2}+\frac{1}{r}\frac{\partial w_p}{\partial r}+\frac{\partial^2 w_p}{\partial z^2}\right]-\frac{F_z}{\rho_p}, \quad (2.31)$$

where $\nu_p = \mu_p/\rho_p$ is the kinematic viscosity of the particle. Assuming that the flow is steady, i.e. $\partial/\partial t = 0$, equations (2.28)-(2.31) can be written as follows:

$$u_p\frac{\partial u_p}{\partial r}-\frac{{v_p}^2}{r}+w_p\frac{\partial u_p}{\partial z}=-\frac{1}{\rho_p}\frac{\partial p}{\partial r}+\nu_p\left[\frac{\partial^2 u_p}{\partial r^2}+\frac{\partial}{\partial r}\left(\frac{u_p}{r}\right)+\frac{\partial^2 u_p}{\partial z^2}\right]-\frac{F_r}{\rho_p}, \quad (2.32)$$

$$u_p\frac{\partial v_p}{\partial r}+\frac{u_p v_p}{r}+w_p\frac{\partial v_p}{\partial z}=\nu_p\left[\frac{\partial^2 v_p}{\partial r^2}+\frac{\partial}{\partial r}\left(\frac{v_p}{r}\right)+\frac{\partial^2 v_p}{\partial z^2}\right]-\frac{F_\theta}{\rho_p}, \quad (2.33)$$

$$u_p\frac{\partial w_p}{\partial r}+w_p\frac{\partial w_p}{\partial z}=-\frac{1}{\rho_p}\frac{\partial p}{\partial z}+\nu_p\left[\frac{\partial^2 w_p}{\partial r^2}+\frac{1}{r}\frac{\partial w_p}{\partial r}+\frac{\partial^2 w_p}{\partial z^2}\right]-\frac{F_z}{\rho_p}. \quad (2.34)$$

The linear drag law assumes that the fluid is viscous and the particles are small. Therefore, we can treat only inviscid momentum equation for particle phase with body force (F_r, F_θ, F_z), and we obtain the following equations:

$$u_p\frac{\partial u_p}{\partial r}-\frac{{v_p}^2}{r}+w_p\frac{\partial u_p}{\partial z}=-\frac{1}{\rho_p}\frac{\partial p}{\partial r}-\frac{F_r}{\rho_p}, \quad (2.35)$$

$$u_p\frac{\partial v_p}{\partial r}+\frac{u_p v_p}{r}+w_p\frac{\partial v_p}{\partial z}=-\frac{F_\theta}{\rho_p}, \quad (2.36)$$

$$u_p\frac{\partial w_p}{\partial r}+w_p\frac{\partial w_p}{\partial z}=-\frac{1}{\rho_p}\frac{\partial p}{\partial z}-\frac{F_z}{\rho_p}, \quad (2.37)$$

In the papers (2 & 3), we applied equations (2.28) and (2.35)-(2.37) in order to calculate particle phase with body force (F_r, F_θ, F_z).

Particle-fluid interactions are described using the following force components

$$F_r = \rho_p(u_p - u)/\tau, \tag{2.38}$$

$$F_\theta = \rho_p(v_p - v)/\tau, \tag{2.39}$$

$$F_z = \rho_p(w_p - w)/\tau, \tag{2.40}$$

which are included in the fluid phase equations (2.14)-(2.16) and in the particle phase equations (2.35)-(2.37). The force components represent force per volume, and are based on the assumption of a linear drag law, i.e. Stokes drag, which is mainly represented as:

$$\tau = m/6\pi\mu a, \tag{2.41}$$

is the relaxation time of a single spherical particle of mass m, and radius a, immersed in a fluid with dynamic viscosity $\mu = \rho\nu$.

2.3 Similarity transformation

2.3.1 Steady flow

The two-phase flow that arises above the planar surface can be characterized by the length scale $\sqrt{\nu/\Omega}$, the time scale Ω^{-1} and the velocity scale $\sqrt{\nu\Omega}$. Therefore, we employ the same dimensionless similarity variables, which are introduced by Von K$\acute{a}$rm$\acute{a}$n [4] and B$\ddot{o}$dewadt [1]:

$$\eta = z\sqrt{\Omega/\nu}. \tag{2.42}$$

The same similarity transformations are utilized for the derivation of fluid phase velocities and pressure:

$$\left.\begin{aligned} u(r,z) &= r\Omega F(\eta), \\ v(r,z) &= r\Omega G(\eta), \\ w(r,z) &= \sqrt{\nu\Omega}H(\eta), \\ p(r,z) &= \rho(-\nu\Omega P(\eta) + \tfrac{1}{2}r^2\Omega^2), \end{aligned}\right\} \tag{2.43}$$

$$and \quad T(r,z,t) = T_\infty + (T_w - T_\infty)\Theta(\eta). \tag{2.44}$$

The pressure transformation was not required in B$\ddot{o}$dewadt's original approach, which was based on the boundary layer approximations which imply that the pressure is constant across the boundary layer. Here, Ω and T_∞ are the angular velocity and temperature of the revolving fluid highly above the surface at infinite distances, far away from the disk, respectively, while T_w is the temperature at the solid surface, at $z = 0$.

In terms of the non-dimensional variables defined by equations (2.42)-(2.44), the equations (2.9) and (2.18)-(2.21) can be written as follows:

$$2F + H' = 0, \tag{2.45}$$

$$F'' - HF' - F^2 + G^2 = 1, \tag{2.46}$$

$$G'' - HG' - 2FG = 0, \tag{2.47}$$

$$P' + 2FH - 2F' = 0, \tag{2.48}$$

$$\Theta'' - PrH\Theta' = 0, \tag{2.49}$$

where Pr is the Prandtl number, $Pr = C_p\mu/k$. We applied equations (2.45)-(2.49) in paper 1, where, the temperature T_w of the stationary disk is considered constant.

The variables characterizing the particle phase can be recast into dimensionless forms by means of the transformation, which is used for Von K*á*rm*á*n flow by Sankara & Sarma [42]:

$$\left.\begin{aligned} u_p(r,z) &= r\Omega F_p(\eta), \\ v_p(r,z) &= r\Omega G_p(\eta), \\ w_p(r,z) &= \sqrt{\nu\Omega}H_p(\eta), \\ \rho_p(r,z) &= \rho Q(\eta), \end{aligned}\right\} \tag{2.50}$$

where Q is the ratio between the densities of the two phases.

The set of partial differential equations (2.9)-(2.16), (2.28), and (2.35)-(2.37) can be transformed into a set of ordinary differential equations:

$$2F + H' = 0, \tag{2.51}$$

$$Q'H_p + QH_p{}' + 2QF_p = 0, \tag{2.52}$$

$$F'' - HF' - F^2 + G^2 + \beta Q(F_p - F) = 1, \tag{2.53}$$

$$G'' - HG' - 2FG + \beta Q(G_p - G) = 0, \tag{2.54}$$

$$P' = -2FH + 2F' - \beta Q(H_p - H), \tag{2.55}$$

$$F_p{}'H_p + F_p^2 - G_p^2 + \beta(F_p - F) = -1/Q, \tag{2.56}$$

$$G_p{}'H_p + 2F_pG_p + \beta(G_p - G) = 0, \tag{2.57}$$

$$QH_p{}'H_p + \beta Q(H_p - H) = P', \tag{2.58}$$

where the prime denotes differentiation with respect to the similarity variable η. We employ equations (2.51), (2.58) in papers 2 & 3.

2.3.2 Generalized steady flow

For generalized steady flow, define the similarity transformations as:

$$\left.\begin{aligned} u(r,z) &= -v_0\left[\tfrac{r}{r_0}\right]^{2n-1} F(\eta), \\ v(r,z) &= v_0\left[\tfrac{r}{r_0}\right]^{2n-1} G(\eta), \\ w(r,z) &= v_0\sqrt{\tfrac{\nu}{v_0 r_0}}\left[\tfrac{r}{r_0}\right]^{n-1}\left[(n+1)H(\eta) + (n-1)\eta F\right], \\ p(r) &= \tfrac{\rho {v_0}^2}{4n-2}\left[\tfrac{r}{r_0}\right]^{4n-2}, \\ T(r,z) &= T_\infty + (T_w - T_\infty)\Theta(\eta), \end{aligned}\right\} \tag{2.59}$$

where η is a dimensionless similarity variable defined by

$$\eta = \left[\frac{z}{r_0}\right]\left[\frac{r}{r_0}\right]^{n-1}\sqrt{\frac{v_0 r_0}{\nu}}. \tag{2.60}$$

In terms of the non-dimensional variables the governing equations reduce to:

$$H' - F = 0, \tag{2.61}$$

$$F'' - (n+1)HF' - (1-2n)F^2 - G^2 + 1 = 0, \tag{2.62}$$

$$G'' - (n+1)HG' + 2nFG = 0, \tag{2.63}$$

$$\Theta'' - Pr(n+1)H(\eta)\Theta' = 0. \tag{2.64}$$

We applied equations (2.61)-(2.64) in paper 6.

2.3.3 Unsteady flow

We adopt the same similarity transformations equations described by Watson & Wang [35] to solve the unsteady flow problem:

$$\left.\begin{aligned} u(r,z,t) &= r\Omega_0(1-\alpha t)^{-1}F(\eta), \\ v(r,z,t) &= r\Omega_0(1-\alpha t)^{-1}G(\eta), \\ w(r,z,t) &= -2\sqrt{\nu\Omega_0}(1-\alpha t)^{-\frac{1}{2}}H(\eta), \\ p(r,z,t) &= -\rho\nu\Omega_0 P(\eta)(1-\alpha t)^{-1}, \\ T(r,z,t) &= T_\infty + (T_w - T_\infty)\Theta(\eta), \end{aligned}\right\} \tag{2.65}$$

where η is the dimensionless similarity variable

$$\eta = z\sqrt{\Omega_0/\nu}(1-\alpha t)^{-\frac{1}{2}}. \tag{2.66}$$

Similarly, we assumed that the temperature $T(r,z,t)$ can be expressed as a function of the similarity variable η. Whereas, $\Omega_0(1-\alpha t)^{-1}$ is the angular velocity of the rotating disk. The term α is a constant that determines the rate of change of the angular velocity of the disk.

In terms of the non-dimensional variables defined in equations (2.65) and (2.66), the partial differential equations (2.9)-(2.13) reduce to:

$$H' - F = 0, \tag{2.67}$$

$$F'' + 2HF' - F^2 + G^2 - \hat{\alpha}[F + \frac{\eta}{2}F'] = 0, \tag{2.68}$$

$$G'' + 2HG' - 2FG - \hat{\alpha}[G + \frac{\eta}{2}G'] = 0, \tag{2.69}$$

$$P' - 4FH - 2F' + \hat{\alpha}[H + \eta F] = 0, \tag{2.70}$$

$$\Theta'' + 2PrH\Theta' - \frac{1}{2}\hat{\alpha}Pr\eta\Theta' = 0. \tag{2.71}$$

Where, $\hat{\alpha} = \alpha/\Omega_0$ denotes a non-dimensional unsteadiness parameter. We applied equations (2.67)-(2.71) in paper 4.

2.4 Boundary conditions

The boundary conditions for swirling flow above the solid surface are shown in the Figure 2.1 & Figure 2.2. The viscous fluid phase sticks to the permeable planar surface at $z = 0$, and attains a state of solid body rotation with angular velocity Ω high above the surface. In the present study, the temperature T_w of the stationary disk is constant. As $z \to \infty$ the radial velocity (u) and circumferential velocity (v) are zero as shown in the Figure 2.1 & Figure 2.2. The inviscid particle phase is shown in the Figure 2.2 to follow the motion of the fluid phase far above the solid surface for Bödewadt flow with fluid-particle suspension, where A is the dimensionless suction velocity. The corresponding boundary conditions specified in Figure 2.1 can be written as:

$$\begin{array}{llllll} F(\eta) = 0, & G(\eta) = 0, & H(\eta) = -A, & \Theta(\eta) = 1, & at & \eta = 0, \\ F(\eta) = 0, & G(\eta) = 1, & P(\eta) = 0, & \Theta(\eta) = 0, & as & \eta \to \infty. \end{array} \tag{2.72}$$

We applied the equation (2.72) in research paper 1, and the corresponding boundary conditions specified in Figure 2.2 reduce to:

$$\begin{array}{l} F(\eta) = 0, \quad G(\eta) = 0, \quad H(\eta) = -A, \qquad at \quad \eta = 0, \\ \left.\begin{array}{lll} F(\eta) = 0, & G(\eta) = 1, & P(\eta) = 1, \\ F_p(\eta) = 0, & G_p(\eta) = 1, & H_p(\eta) = H(\eta), \\ Q(\eta) = 1, & & \end{array}\right\} as \quad \eta \to \infty. \end{array} \tag{2.73}$$

We utilized the (2.73) in research papers 2 & 3.

The boundary conditions for infinite rotating disk for steady flow are shown in the Figure 2.3. There is no slip condition at the wall on a rotating disk at $z = 0$. In Figure 2.3, for unsteady flow, the relevant boundary conditions on the velocity and temperature field are taken from by Wang [35]. At $z = 0$ and $z \to \infty$ the radial velocity (u) and axial velocity (w) are zero, but circumferential velocity (v) is $r\Omega_0(1 - \alpha t)^{-1}$ at $z = 0$. The boundary conditions corresponding to the Figure 2.3 for steady and unsteady flows reduce to:

$$\begin{array}{llllll} F(\eta) = 0, & G(\eta) = 1, & H(\eta) = 0, & \Theta(\eta) = 1, & at & \eta = 0, \\ F(\eta) = 0, & G(\eta) = 0, & P(\eta) = 1, & \Theta(\eta) = 0, & as & \eta \to \infty, \end{array} \tag{2.74}$$

which we employed in research papers 4 & 5. Furthermore, the boundary conditions are expanded as follows:

$$\begin{array}{rl} u = 0, v = 0, w = Av_0\sqrt{\frac{\nu}{v_0 r_0}}\left[\frac{r}{r_0}\right]^{n-1}(n+1), T = T_w, & at \quad z = 0, \\ u = 0, v = v_0\left[\frac{r}{r_0}\right]^{2n-1}, T = T_\infty, & as \quad z \to \infty. \end{array} \tag{2.75}$$

The tangential flow (v) high above the planar surface at $z = 0$ is assumed to exhibit a power-law variation, where the power $m = 2n - 1$ denotes a prescribed parameter. The corresponding boundary conditions specified in (2.75) can be written as :

$$\begin{array}{llllll} F(\eta) = 0, & G(\eta) = 0, & H(\eta) = A, & \Theta(\eta) = 1, & at & \eta = 0, \\ F(\eta) = 0, & G(\eta) = 1, & \Theta(\eta) = 0, & as & \eta \to \infty, & \end{array} \tag{2.76}$$

which we applied in paper 6.

2.5 Numerical approach

We have solved the two-point boundary value problems (BVPs) consisting of the coupled set of ordinary differential equations subjected to the boundary conditions, using the *bvp4c* MATLAB solver, which yields very good results for the non-linear ODEs with multi-point BVPs. The finite-difference code utilizes the 3-stage Lobatto IIIa formula, which is a collocation formula. The collocation polynomial provides a C1-continuous solution that is fourth-order accurate uniformly in [a,b]. For multipoint BVPs, the solution is C1-continuous within each region, but continuity is not automatically imposed at the interfaces. On the other hand, mesh selection and error control are based on the residual of the continuous solution. Moreover, analytically the condensation factor is considered when the system of algebraic equations are formulated (see, e.g, Shampine et al. [43]).

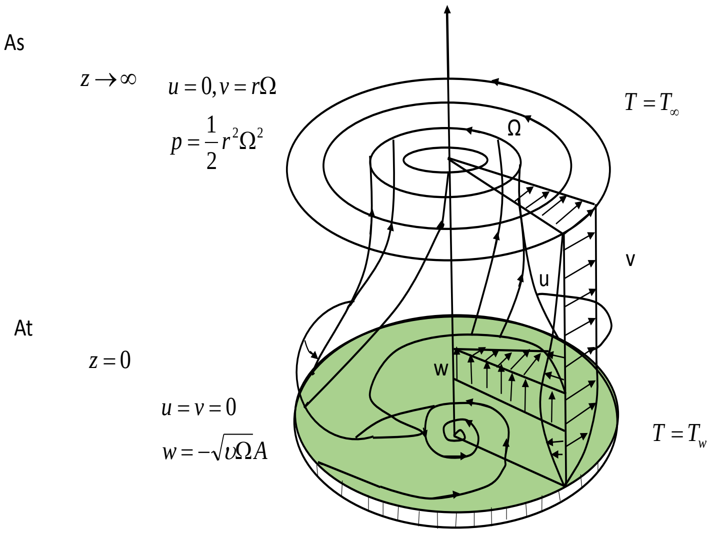

Figure 2.1: Sketch of the three-dimensional flow field set up by a steadily revolving flow high above the shaded surface. The variations of the radial (u) and circumferential (v) velocity components are indicated. The axial velocity component (w) is shown upward.

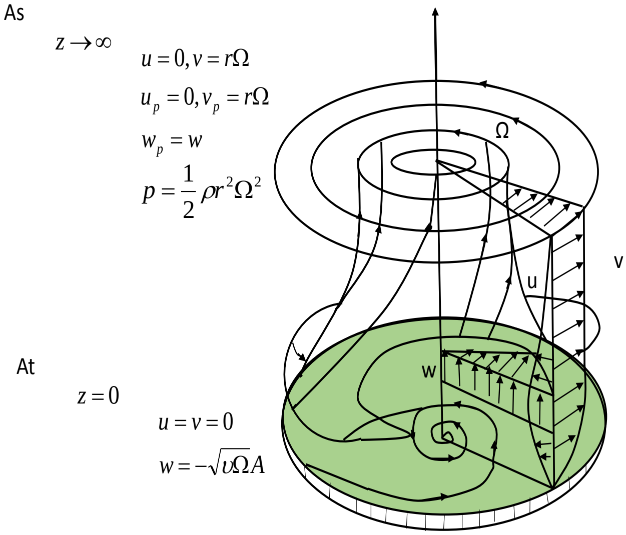
As
$z \to \infty$
$u = 0, v = r\Omega$
$u_p = 0, v_p = r\Omega$
$w_p = w$
$p = \frac{1}{2}\rho r^2 \Omega^2$
Ω
v
u
w
At
$z = 0$
$u = v = 0$
$w = -\sqrt{\upsilon\Omega} A$

Figure 2.2: Sketch of the three-dimensional flow field set up by a steadily revolving flow high above the shaded surface. The variations of the radial (u) and circumferential (v) velocity components are indicated. The axial velocity component (w) is shown upward, as in the classical Bödewadt problem [1]. In presence of strong suction, as considered herein, the axial velocity is downward.

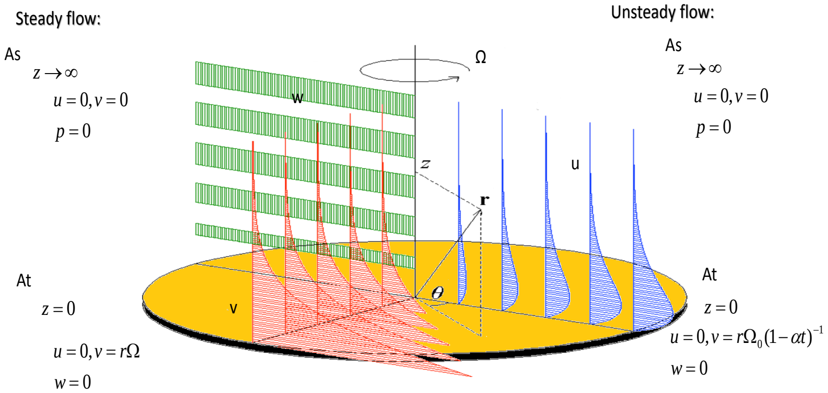
Steady flow:
As
$z \to \infty$
$u = 0, v = 0$
$p = 0$
At
$z = 0$
$u = 0, v = r\Omega$
$w = 0$
Ω
w
v
z
r
θ
u
Unsteady flow:
As
$z \to \infty$
$u = 0, v = 0$
$p = 0$
At
$z = 0$
$u = 0, v = r\Omega_0(1-\alpha t)^{-1}$
$w = 0$

Figure 2.3: Sketch of the three-dimensional flow field set up by a revolving infinite rotating disk. The variations of the radial velocity (u), circumferential velocity (v), and axial velocity (w) components are indicated. This is adopted from Imayama & Lingwood [2].

Chapter 3

Summary of research papers

3.1 List of papers

The thesis is based on and contains the following research papers.

Paper 1. M. Rahman, H. I. Andersson."On heat transfer flow in B$\ddot{o}$dewadt flow". International Journal of Heat and Mass Transfer 112 (2017) 1057-1061

Paper 2. M. Rahman, H. I. Andersson. "Revolving flow of a fluid-particle suspension with suction". Alexandria Engineering Journal, In press (2017)

Paper 3. M. Rahman, H. I. Andersson."B$\ddot{o}$dewadt flow of a fluid-particle suspension with strong suction" . Proceedings of 13th International Conference on Heat Transfer, Fluid Mechanics and Thermodynamics - HEFAT 2017, Portoroz, Slovenia, 17th-19th July (2017), pp. 59-64

Paper 4. M. Rahman, H. I. Andersson."On heat transfer in unsteady von K$\acute{a}$rm$\acute{a}$n flow". Submitted to: International Journal of Heat and Mass Transfer (2017)

Paper 5. M. Rahman, H. I. Andersson."A note on buoyancy effects in von K$\acute{a}$rm$\acute{a}$n flow over a rotating disk". Submitted to: Journal of Applied Mathematics and Physics (ZAMP), (2017)

Paper 6. M. Rahman, H. I. Andersson."Heat transfer in generalized vortex flow over a permeable surface" .International Journal of Heat and Mass Transfer 118 (2018) 1090-1097

This chapter presents a brief summary of the main findings reported in six appended paper's, showing in below flow chart.

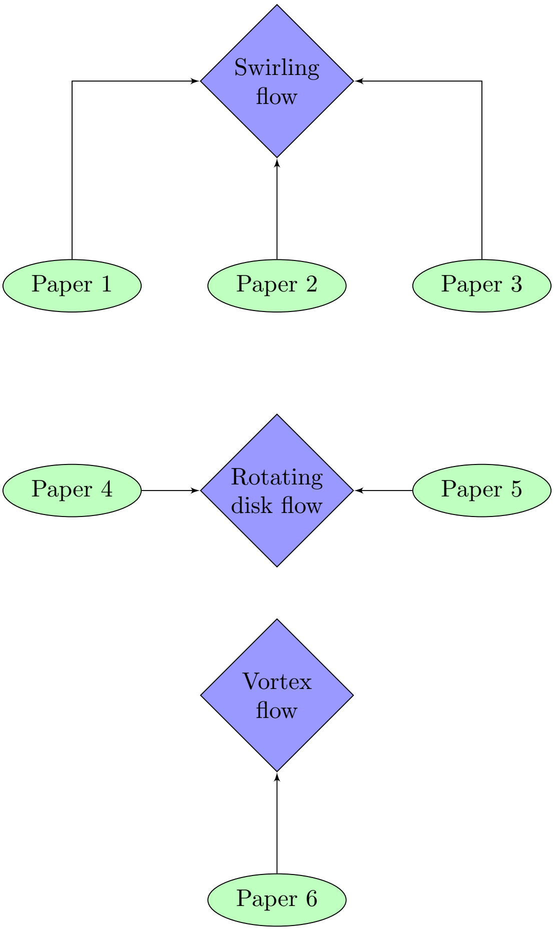
Swirling flow
Paper 1
Paper 2
Paper 3
Paper 4
Rotating disk flow
Paper 5
Vortex flow
Paper 6

Paper 1

On heat transfer in B$\ddot{o}$dewadt flow

In this paper, heat transfer in revolving B$\ddot{o}$dewadt flow above a planar surface has been considered. We have shown that a similarity solution of the thermal energy problem does not exist as long as the surface is impermeable. The failure of the existence of physically realistic similarity solutions for the thermal field is ascribed to the fact that the axial flow component is directed away from the surface. If the planar surface is porous and allows for suction, the direction of the axial flow can be reversed. Similarity solutions have been obtained for some different values of the dimensionless suction velocity A and the Prandtl number Pr. The thermal boundary layer became gradually thinner with increasing suction A and for higher Pr, thereby also increasing the heat transfer rate through the planar surface .

Paper 2 & 3

Revolving flow of a fluid-particle suspension with suction

B$\ddot{o}$dewadt flow of a fluid-particle suspension with strong suction

In paper 2 & 3, the three-dimensional revolving flow of a particle-fluid suspension above a plane surface has been considered. The flow represents an extension of the classical B$\ddot{o}$dewadt flow to a two-fluid problem. The governing equations for the two phases are coupled through an interaction force with the particle relaxation time τ as a free parameter. By means of a similarity transformation, the coupled set of non-linear ODEs becomes a two-point boundary value problem. The numerical results showed that the radial inward particle velocity increased whereas the circumferential velocity decreased by shortening τ, thereby strengthening the spiralling particle motion. These predictions are consistent with the so-called tea-cup effect, i.e. accumulation of tea leaves at the centre of the cup. On the contrary, the revolving fluid motion was reduced as a result of the particle-fluid interactions.

Paper 4

On heat transfer in unsteady Von K$\acute{a}$rm$\acute{a}$n flow

Heat transfer in revolving flow driven by a decelerating rotating disk has been considered. The well-known similarity transformation of the three-dimensional flow problem has been extended to also transform the thermal energy equation into an ordinary differential equation. An analytical solution has been derived for the temperature distribution in the vicinity of the disk. Sample solutions of the resulting two-parameter problem have been presented to illustrate the combined effects of deceleration and thermal diffusivity. One could observe that the thermal boundary layer became thinner at higher Prandtl numbers and for faster disk deceleration.

Paper 5

A note on buoyancy effects in von K$\acute{a}$rm$\acute{a}$n flow over a rotating disk

In this note the steadily revolving flow driven by a rotating disk has been considered by means of similarity analysis. Attention is paid to the pressure distribution above the disk, which has most often been ignored. We found that buoyancy lead to a substantial pressure reduction in the vicinity of the disk for Prandtl numbers below unity. At sufficiently high Grashof numbers, this buoyancy-induced pressure reduction even eliminates the excess stagnation pressure at the disk.

Paper 6

Heat transfer in generalized vortex flow over a permeable surface

In this paper, heat transfer in the thermal boundary layer beneath a generalized vortex flow has been considered. The steadily revolving flow is allowed to vary with the distance r from the symmetry axis as r^m. The governing equations for heat and momentum transport transformed exactly to a coupled set of ordinary differential equations by means of a tailor-made similarity transformation. Some different flow situations in presence of suction have been considered, including solid-body rotation $(m = +1)$ and a potential vortex $(m = -1)$. The thermal boundary layer was observed to thicken monotonically with increasing m-values, accompanied by a reduction of the heat transfer rate through the planar surface above which the flow revolves. These findings were explained as the combined influence of two different effects, namely: $i)$ a variation of the effective Prandtl number $(m+3)Pr/2$ that directly affected the thermal diffusion, whereas $ii)$ an indirect variation of the axial velocity component that affected the thermal convection.

Chapter 4

Conclusions and Future Work

Paper 1

We have shown that realistic similarity solutions of the thermal energy problem do not exist for B$\ddot{o}$dewadt flow in absence of suction $(A = 0)$. The only earlier results for pure B$\ddot{o}$dewadt flow by Sahoo et al. [24] and Turkyilmazoglu [8] are therefore not physically realistic. This explains why heat transfer in B$\ddot{o}$dewadt flow seems to have escaped the attention of the research community. If sufficient suction is applied, however, plausible solutions do exist. This phenomenon is explained by the reversal of the axial velocity component when suction is imposed. This finding is consistent with the fact that similarity solutions of the heat transfer problem associated with Von K$\acute{a}$rm$\acute{a}$n flow do exist. The thermal energy equation in that case is exactly the same as in the B$\ddot{o}$dewadt flow, but the sign of the axial velocity component H is opposite. One can therefore conjecture that solutions of the thermal problem of the Von K$\acute{a}$rm$\acute{a}$n flow ceases to exist if sufficient blowing through the rotating disk is applied, so that the axial flow direction is reversed.

It should be noted that our conclusions are valid only for the actual heat and fluid flow problem studied herein. The presence of either a magnetic field [36], partial slip [11] or stretching of the surface [8] will alter the flow field and thereby also the possible existence of similarity solutions of the thermal field. Moreover, if, for instance, viscous dissipation or ohmic heating is included in the thermal energy equation, see e.g. Sahoo [11], the situation is different and similarity solutions may exist even in absence of suction.

Similarity solutions of the heat transfer problem associated with B$\ddot{o}$dewadt flow subjected to significant suction $(A \geq 1)$ have been provided here for the first time. Increasing suction tends to make the thermal boundary layer gradually thinner and thereby increases the heat transfer rate through the solid surface. Likewise, as the relative importance of thermal diffusivity reduces for higher Prandtl numbers, the thermal boundary layer becomes gradually thinner.

Paper 2 & 3

In papers 2 & 3, the governing equations of the three-dimensional two-fluid problem have been transformed into a coupled set of ordinary differential equations by means of an exact similarity transformation. The resulting set of ODEs is a two parameter problem in terms of the dimensionless suction velocity A and the fluid-particle interaction parameter β. β is the ratio between the rotation time scale Ω^{-1} and the particle relaxation time τ. β is therefore a reciprocal Stokes number. The particles are spiralling inwards in the vicinity of the surface. The radial inward velocity $|u_p|$ increases and the circumferential velocity v_p decreases with increasing interaction parameter β, i.e. the spiralling increases with β. This phenomenon is commonly known as the tea cup effect: when the tea is stirred, tea leaves near the bottom move towards the centre of the cup and heap up. Contrary to the particle phase, the inward spiralling of the fluid phase is gradually reduced as the fluid-particle interaction parameter is increased. The circumferential flow is only modestly affected, but the surface shear stress is nevertheless increased.

Paper 4

The purpose of this paper was to show for the first time that also the heat transfer problem associated with the revolving flow driven by a decelerating rotating disk is amenable to exact similarity solutions. A similarity transformation was devised which transformed the time-dependent thermal energy equation to an ordinary differential equation. Similarity solutions have not been achieved for any other time-variations of the angular velocity of the disk, i.e. neither for a step-change, sudden start-up, or torsional oscillations.
The unsteadiness parameter $\hat{\alpha} = \alpha/\Omega_0$, which reflects the relative importance of deceleration ($\alpha < 0$) and disk rotation (Ω_0), turned out to be the controlling parameter in addition to the Prandtl number Pr. The thickness of the thermal boundary layer was found to decrease with increasing values of $-\hat{\alpha}$ and Pr. The heat transfer rate through the disk increased monotonically with increasing magnitudes of these controlling parameters. In the high-Prandtl-number limit (low diffusivity), we found that the Nusselt number varied as $\sqrt{-\hat{\alpha} Pr}$.

Paper 5

In this brief report, by invoking the usual boundary-layer approximations, the pressure gradient across the three-dimensional boundary layer on a constantly rotating disk is assumed negligible. Accordingly, the stagnation pressure on the disk becomes equal to the ambient pressure. However, we argued that the similarity solution of the flow field also solves the axisymmetric Navier-Stokes equation. In absence of buoyancy we found an analytical expression for the pressure variation normal to the disk with an excess stagnation pressure at the surface of the disk. By means of numerical integration's we showed that buoyancy leads to a substantially reduction of the pressure in the vicinity of the rotating disk for $Pr \leq 1$, whereas the buoyancy effect becomes almost negligible for larger Prandtl numbers. This pressure reduction has, however, no implications on the dynamics of the flow, but tends to eliminate the excess stagnation pressure on the disk surface. The lowering of the stagnation pressure may affect the stability of the rotating disk, as for instance in hard disk drives.

Paper 6

In this paper the heat transfer aspects of revolving vortex flow above a planar surface have been investigated. The axisymmetric fluid velocity field was first studied by Bödewadt [1] by assuming that the revolving flow was in a state of solid-body rotation, whereas others [6, 38, 39] considered power-law variations of the tangential velocity component in the far-field. Since the flow field is required in order to solve the convection-diffusion type of problem for the thermal energy, we adopted the similarity transformation used by King & Lewellen [6] and showed that also the heat transfer problem admits similarity solutions.

First, however, we computed the three-componential flow field which is needed in order to solve also the thermal boundary layer equation. The present numerical solutions shown in Section 3.1 were in excellent agreement with the earlier results by King & Lewellen [6], but deviated substantially from the results reported by Kuo [39].

In a recent paper [44] we argued that physically realistic similarity solutions for the heat transfer problem accompanying the Bödewadtt flow [1] can only be obtained in presence of suction through the planar surface. To this end we also considered surface suction herein. For a given value (-2.0) of the dimensionless suction parameter A, we observed that the actual power $m = 2n - 1$ describing the radial variation of the revolving vortex flow had a decisive effect on the thermal boundary layer. A distinct and monotonically thickening of the thermal boundary layer was observed with increasing values of the power m over the range from $m = -1$ to $m = +1$, i.e. as the revolving flow was altered from a potential vortex $(m = -1)$ to a state of solid-body rotation $(m = +1)$. The gradually increasing thermal boundary layer thickness was accompanied by a reduction of the heat transfer rate through the planar surface above which the flow revolves. These findings were explained as the combined influence of two different effects caused by the different power-law variations of the generalized vortex flow: i) a variation of the effective Prandtl number $(n + 1)Pr$ affects the thermal diffusion, whereas ii) a variation of the axial velocity field H affects the thermal convection. These distinctly different effects of $m = 2n - 1$ both alter the thermal boundary layer in the same direction.

4.1 Future work

In this present work, we focused on the fluid flow, as well as particle flow with the special focus on heat transfer. However couple of issue remains unanswered, which need to be thoroughly investigated. The following highlights few of those.

- After follow the same model already discussed in our work, we can investigate the very interesting result with consider the lift and drag force on fluid-particle suspension with suction in Bödewadt flow .

- Heat transfer can be investigated with different Prandlt numbers on fluid-particle suspension with lift and drag force together in Bödewadt flow.

- Heat transfer on steady and unsteady von K$\acute{a}$rm$\acute{a}$n flow of a fluid-particle suspension with suction and injection can be investigated with some different values of parameter $\hat{\alpha}$ and Prandtl number Pr .
- Heat transfer in B$\ddot{o}$dewadt flow of a fluid-particle suspension with suction and injection can be investigated with some different values of suction velocity A and Prandtl number Pr.

Bibliography

[1] U. Boedewadt, “Die drehströmung über festem grunde,” *ZAMM-Journal of Applied Mathematics and Mechanics/Zeitschrift für Angewandte Mathematik und Mechanik*, vol. 20, no. 5, pp. 241–253, 1940.

[2] S. Imayama, P. H. Alfredsson, and R. J. Lingwood, “On the laminar–turbulent transition of the rotating-disk flow: the role of absolute instability,” *Journal of Fluid Mechanics*, vol. 745, pp. 132–163, 2014.

[3] Y. Nakayama, *Introduction to fluid mechanics*. Butterworth-Heinemann, 1998.

[4] T. V. Kármán, “über laminare und turbulente reibung,” *ZAMM-Journal of Applied Mathematics and Mechanics/Zeitschrift für Angewandte Mathematik und Mechanik*, vol. 1, no. 4, pp. 233–252, 1921.

[5] P. Zandbergen and D. Dijkstra, “Von kármán swirling flows,” *Annual review of fluid mechanics*, vol. 19, no. 1, pp. 465–491, 1987.

[6] W. King and W. S. Lewellen, “Boundary-layer similarity solutions for rotating flows with and without magnetic interaction,” *The Physics of Fluids*, vol. 7, no. 10, pp. 1674–1680, 1964.

[7] B. Sahoo, S. Abbasbandy, and S. Poncet, “A brief note on the computation of the bödewadt flow with navier slip boundary conditions,” *Computers & Fluids*, vol. 90, pp. 133–137, 2014.

[8] M. Turkyilmazoglu, “Bödewadt flow and heat transfer over a stretching stationary disk,” *International Journal of Mechanical Sciences*, vol. 90, pp. 246–250, 2015.

[9] H. Attia, “Unsteady flow of a non-newtonian fluid above a rotating disk with heat transfer,” *International journal of heat and mass transfer*, vol. 46, no. 14, pp. 2695–2700, 2003.

[10] S. O. MacKerrell, “Stability of bödewadt flow,” *Philosophical Transactions of the Royal Society of London A: Mathematical, Physical and Engineering Sciences*, vol. 363, no. 1830, pp. 1181–1187, 2005.

[11] B. Sahoo, “Effects of slip on steady bödewadt flow and heat transfer of an electrically conducting non-newtonian fluid,” *Communications in Nonlinear Science and Numerical Simulation*, vol. 16, no. 11, pp. 4284–4295, 2011.

[12] B. Sahoo, “Steady bödewadt flow of a non-newtonian reiner-rivlin fluid,” *Differential Equations and Dynamical Systems*, vol. 20, pp. 367–376, 2012.

[13] B. Sahoo and S. Poncet, “Effects of slip on steady bödewadt flow of a non-newtonian fluid,” *Communications in Nonlinear Science and Numerical Simulation*, vol. 17, no. 11, pp. 4181–4191, 2012.

[14] L. B. Zung, “Flow induced in fluid-particle suspension by an infinite rotating disk,” *The Physics of Fluids*, vol. 12, no. 1, pp. 18–23, 1969.

[15] K. K. Sankara and L. Sarma, “On the steady flow produced in fluid-particle suspension by an infinite rotating disk with surface suction,” *International journal of engineering science*, vol. 23, no. 8, pp. 875–886, 1985.

[16] M. A. Allaham and J. Peddieson, “The flow induced by a rotating disk in a particulate suspension,” *International journal of engineering science*, vol. 31, no. 7, pp. 1025–1034, 1993.

[17] M. Turkyilmazoglu, “Magnetohydrodynamic two-phase dusty fluid flow and heat model over deforming isothermal surfaces,” *Physics of Fluids*, vol. 29, no. 1, p. 013302, 2017.

[18] A. Einstein, “Die ursache der mäanderbildung der flußläufe und des sogenannten baerschen gesetzes,” *Naturwissenschaften*, vol. 14, no. 11, pp. 223–224, 1926.

[19] H. A. Muhammad Rahman, “Bödewadt flow of a fluid-particle suspension with strong suction,” *Proceedings of 13th International Conference on Heat Transfer, Fluid Mechanics and Thermodynamics - HEFAT 2017, Portoroz, Slovenia*, vol. 212, pp. 59–64, 2017.

[20] K. Millsaps and K. Pohlhausen, “Heat transfer by laminar flow from a rotating plate,” *Journal of the Aeronautical Sciences*, vol. 19, no. 2, pp. 120–126, 1952.

[21] J. Gregg and E. Sparrow, “Heat transfer from a rotating disk to fluids of any prandtl number,” vol. 81, pp. 249–251, 1959.

[22] I. V. Shevchuk, *Convective heat and mass transfer in rotating disk systems*, vol. 45. Springer Science & Business Media, 2009.

[23] I. Shevchuk and M. Buschmann, “Rotating disk heat transfer in a fluid swirling as a forced vortex,” *Heat and mass transfer*, vol. 41, no. 12, pp. 1112–1121, 2005.

[24] B. Sahoo, R. A. Van Gorder, and H. Andersson, “Steady revolving flow and heat transfer of a non-newtonian reiner–rivlin fluid,” *International Communications in Heat and Mass Transfer*, vol. 39, no. 3, pp. 336–342, 2012.

[25] H. I. Andersson, “Comments on bvps in non-newtonian boundary-layer flow,” *Applied mathematics and computation*, vol. 182, no. 2, pp. 1714–1716, 2006.

[26] A. Pantokratoras, “A common error made in investigation of boundary layer flows,” *Applied Mathematical Modelling*, vol. 33, no. 1, pp. 413–422, 2009.

[27] I. V. Shevchuk, “Turbulent heat and mass transfer over a rotating disk for the prandtl or schmidt numbers much larger than unity: an integral method,” *Heat and mass transfer*, vol. 45, no. 10, pp. 1313–1321, 2009.

[28] P. Sibanda and O. D. Makinde, “On steady mhd flow and heat transfer past a rotating disk in a porous medium with ohmic heating and viscous dissipation,” *International Journal of Numerical Methods for Heat & Fluid Flow*, vol. 20, no. 3, pp. 269–285, 2010.

[29] A. Guha and S. Sengupta, “Non-linear interaction of buoyancy with von kármánâĂŹs swirling flow in mixed convection above a heated rotating disc,” *International Journal of Heat and Mass Transfer*, vol. 108, pp. 402–416, 2017.

[30] W. G. Cochran, “The flow due to a rotating disc,” *Mathematical Proceedings of the Cambridge Philosophical Society*, vol. 30, no. 03, pp. 365–375, 1934.

[31] M. Rogers and G. Lance, “The rotationally symmetric flow of a viscous fluid in the presence of an infinite rotating disk,” *Journal of Fluid Mechanics*, vol. 7, no. 4, pp. 617–631, 1960.

[32] M. Turkyilmazoglu, “An asymptotic investigation into the stabilization effect of suction in the rotating-disk boundary layer flow,” *Computers & Mathematics with Applications*, vol. 53, no. 5, pp. 750–759, 2007.

[33] R. Lingwood and P. H. Alfredsson, “Instabilities of the von kármán boundary layer,” *Applied Mechanics Reviews*, vol. 67, no. 3, p. 030803, 2015.

[34] C. Wang, “Exact solutions of the unsteady navier-stokes equations,” *Appl. Mech. Rev*, vol. 42, no. 11, pp. 269–282, 1989.

[35] L. T. Watson and C.-Y. Wang, “Deceleration of a rotating disk in a viscous fluid,” *The Physics of Fluids*, vol. 22, no. 12, pp. 2267–2269, 1979.

[36] G. Nath and B. Venkatachala, “The effect of suction on boundary layer for rotating flows with or without magnetic field,” *Proceedings Mathematical Sciences*, vol. 85, no. 5, pp. 332–337, 1977.

[37] B. Sahoo, S. Abbasbandy, and S. Poncet, “A brief note on the computation of the bödewadt flow with navier slip boundary conditions,” *Computers & Fluids*, vol. 90, pp. 133–137, 2014.

[38] B. Venkatachala and G. Nath, “Mass transfer effects on the generalised vortex flow over a stationary surface with or without magnetic field,” in *Indian Academy of Sciences, Proceedings(Engineering Sciences)*, vol. 3, pp. 211–223, 1980.

[39] H. Kuo, “Axisymmetric flows in the boundary layer of a maintained vortex,” *Journal of the Atmospheric sciences*, vol. 28, no. 1, pp. 20–41, 1971.

[40] F. K. Moore, “Three-dimensional boundary layer theory,” *Advances in Applied Mechanics*, vol. 4, pp. 159–228, 1956.

[41] K. Nanbu, “Vortex flow over a flat surface with suction,” *AIAA J*, vol. 9, no. 8, pp. 1642–1645, 1971.

[42] K. K. Sankara and L. Sarma, “On the steady flow produced in fluid-particle suspension by an infinite rotating disk with surface suction,” *International journal of engineering science*, vol. 23, no. 8, pp. 875–886, 1985.

[43] L. F. Shampine, J. Kierzenka, and M. W. Reichelt, “Solving boundary value problems for ordinary differential equations in matlab with bvp4c,” *Tutorial notes*, vol. 2000, pp. 437–448, 2000.

[44] H. A. Muhammad Rahman, “On heat transfer in bödewadt flow,” *Int. J. Heat Mass Transfer*, vol. 212, pp. 1057–1061, 2017.

Part II

PAPER 1

On heat transfer in Bödewadt flow

M.Rahman , H.I.Andersson

International Journal of Heat and Mass Transfer 112 (2017) 1057-1061

International Journal of Heat and Mass Transfer 112 (2017) 1057–1061

Contents lists available at ScienceDirect

International Journal of Heat and Mass Transfer

journal homepage: www.elsevier.com/locate/ijhmt

Review

On heat transfer in Bödewadt flow

Muhammad Rahman [a,b,*], Helge I. Andersson [a]

[a] Department of Energy and Process Engineering, Norwegian University of Science and Technology, Trondheim, Norway
[b] Department of Mathematics, Mirpur University of Science and Technology, Mirpur, Pakistan

ARTICLE INFO

Article history:
Received 17 January 2017
Received in revised form 3 April 2017
Accepted 7 May 2017
Available online 20 May 2017

Keywords:
Revolving flow
Bödewadt flow
Heat transfer
Similarity solutions

ABSTRACT

Heat transfer in revolving Bödewadt flow above a planar surface has been considered. We have shown that a similarity solution of the thermal energy problem does not exist as long as the surface is impermeable. The failure of the existence of physically realistic similarity solutions for the thermal field is ascribed to the fact that the axial flow component is directed away from the surface. If the planar surface is porous and allows for suction, the direction of the axial flow can be reversed. Similarity solutions have been obtained for some different values of the dimensionless suction velocity *A* and the Prandtl number *Pr*. The thermal boundary layer became gradually thinner with increasing suction *A* and for higher *Pr*, thereby also increasing the heat transfer rate through the planar surface.

© 2017 Elsevier Ltd. All rights reserved.

Contents

1. Introduction 1057
2. Mathematical model equations 1058
3. Similarities transformations 1058
4. Exact analytical solution 1058
5. Numerical approach 1059
6. Numerical results 1059
   6.1. Velocity field 1059
   6.2. Heat transfer 1060
7. Concluding remarks 1061
References 1061

1. Introduction

The steadily revolving flow of a viscous fluid above a solid surface was first studied by Bödewadt [1] who transformed the governing partial differential equations into a set of ordinary differential equations by means of the same similarity transformation as originally used by Von Karman [2] in his classical study of the swirling flow driven by a constantly rotating disk. The Bödewadt flow can be considered as a reversed Von Karman flow with the axial velocity component directed away from the planar surface rather than towards the rotating disk. However, the three velocity components in the Bödewadt flow exhibit a more complex variation than in the Von Karman flow and the Bödewadt boundary layer is substantially thicker than the corresponding Von Karman boundary layer.

In this paper we consider the heat transfer in steadily revolving Bödewadt flow. The heat transfer in this prototype flow seems to have received only negligible attention in comparison with the heat transfer in the Von Karman flow. Heat transfer in flow above a rotating disk was first studied by Millsaps & Pohlhausen [3] and Sparrow & Gregg [4], followed by many others. See, e.g., the book by Shevchuk [5]. Shevchuk and Buschmann [6], for instance, found self-similar solutions for the flow and heat transfer in a fluid co-rotating with a rotating disk with a radially varying disk temperature. One may speculate whether the lack of studies of heat transfer in Bödewadt flow is due the relatively higher complexity of the three-dimensional flow field.

---

* Corresponding author at: Department of Energy and Process Engineering, Norwegian University of Science and Technology, Trondheim, Norway.
E-mail address: muhammad.rahman@ntnu.no (M. Rahman).

http://dx.doi.org/10.1016/j.ijheatmasstransfer.2017.05.024
0017-9310/© 2017 Elsevier Ltd. All rights reserved.

The only earlier studies that we are aware of are the recent papers by Sahoo [7], Sahoo et al. [8], and Turkyilmazoglu [9]. Sahoo [7] included heat transfer analysis in his study of Bödewadt flow of an electrically conducting fluid with partial slip. Some temperature profiles were presented, but not for pure Bödewadt flow of a Newtonian fluid with no-slip at the solid surface. Sahoo et al. [8] also focussed on non-Newtonian fluid properties and the majority of their results were concerned with the flow field, but two figures showing heat transfer results also for Newtonian fluids were included. As we will see later, these results might be questionable. Even more recently, Turkyilmazoglu [9] studied the heat transfer in Bödewadt flow over a stretching but non-rotating disk. In the absence of stretching, however, his results suggested a constant temperature all across the viscous boundary layer and therefore failed to satisfy the outer boundary condition for the thermal field. In this paper heat transfer in Bödewadt flow will be revisited with the view to clarify the contradictory findings of Sahoo et al. [8] and Turkyilmazoglu [9].

2. Mathematical model equations

Let us consider the steadily revolving flow of a viscous fluid above a planar surface. In cylindrical polar coordinates (r, θ, z) the governing mass conservation, momentum and thermal energy equations become:

$$\frac{\partial}{\partial r}(ru) + \frac{\partial}{\partial z}(rw) = 0, \tag{1}$$

$$u\frac{\partial u}{\partial r} - \frac{v^2}{r} + w\frac{\partial u}{\partial z} = -\frac{1}{\rho}\frac{\partial p}{\partial r} + \nu\left[\frac{\partial^2 u}{\partial r^2} + \frac{\partial}{\partial r}\left(\frac{u}{r}\right) + \frac{\partial^2 u}{\partial z^2}\right], \tag{2}$$

$$u\frac{\partial v}{\partial r} + \frac{uv}{r} + w\frac{\partial v}{\partial z} = \nu\left[\frac{\partial^2 v}{\partial r^2} + \frac{\partial}{\partial r}\left(\frac{v}{r}\right) + \frac{\partial^2 v}{\partial z^2}\right], \tag{3}$$

$$u\frac{\partial w}{\partial r} + w\frac{\partial w}{\partial z} = -\frac{1}{\rho}\frac{\partial p}{\partial z} + \nu\left[\frac{\partial^2 w}{\partial r^2} + \frac{1}{r}\frac{\partial w}{\partial r} + \frac{\partial^2 w}{\partial z^2}\right], \tag{4}$$

$$\rho C_p\left(u\frac{\partial T}{\partial r} + w\frac{\partial T}{\partial z}\right) = k\left(\frac{\partial^2 T}{\partial r^2} + \frac{1}{r}\left(\frac{\partial T}{\partial r}\right) + \frac{\partial^2 T}{\partial z^2}\right), \tag{5}$$

where (u, v, w) are the velocity components of the fluid in the radial, circumferential and axial directions, respectively, and T is the temperature. Here, we have assumed rotational symmetry about the vertical z-axis, *i.e.*$\partial/\partial\theta = 0$. The kinematic viscosity of the fluid is ν and C_p is the specific heat at constant pressure of the fluid. k is the thermal conductivity of the fluid.

The boundary conditions are

$$\left.\begin{array}{llll} u = 0, \quad v = 0, & w = -\sqrt{\nu\Omega}A, & T = T_w, & at \quad z = 0, \\ u = 0, \quad v = r\Omega, & p = \frac{1}{2}r^2\Omega^2, & T = T_\infty, & as \quad z \to \infty, \end{array}\right\}. \tag{6}$$

Here, Ω and T_∞ are the angular velocity and temperature of the revolving fluid high above the surface, while A and T_w are the dimensionless suction velocity and temperature at the solid surface at $z = 0$. In the present study the temperature T_w of the stationary disk is constant. Shevchuk and Buschmann [6], however, allowed for a radial power-law variation of the surface temperature of a rotating disk.

3. Similarities transformations

Following Bödewadt we express the fluid velocity components and pressure as

$$\begin{aligned} u(r,z) &= r\Omega F(\eta), \\ v(r,z) &= r\Omega G(\eta), \\ w(r,z) &= \sqrt{\nu\Omega}H(\eta), \\ p(r,z) &= \rho\left(-\nu\Omega P(\eta) + \frac{1}{2}r^2\Omega^2\right), \\ T(r,z) &= T_\infty + (T_w - T_\infty)\Theta(\eta), \end{aligned} \tag{7}$$

where η is a dimensionless variable defined by

$$\eta = z\sqrt{\Omega/\nu}. \tag{8}$$

In terms of the non-dimensional variables defined by (7,8) the governing Eqs. (1)–(5) become:

$$2F + H' = 0, \tag{9}$$

$$F'' - HF' - F^2 + G^2 = 1, \tag{10}$$

$$G'' - HG' - 2FG = 0, \tag{11}$$

$$P' + 2FH - 2F' = 0, \tag{12}$$

$$\Theta'' - PrH\Theta' = 0, \tag{13}$$

where Pr is the Prandtl number, $Pr = \frac{C_p\mu_k}{k}$. The corresponding boundary conditions specified in (6) transfer to:

$$\begin{array}{lllll} F(\eta) = 0, & G(\eta) = 0, & H(\eta) = -A, & \Theta(\eta) = 1 & at \quad \eta = 0, \\ F(\eta) = 0, & G(\eta) = 1, & P(\eta) = 0, & \Theta(\eta) = 0 & as \quad \eta \to \infty. \end{array} \tag{14}$$

4. Exact analytical solution

The ODE for the thermal field (13) can be integrated twice to give the solution for the temperature profile:

$$\Theta(\eta) = 1 - \frac{I(\eta)}{I(\infty)}, \tag{15}$$

where

$$I(\eta) = \int_0^\eta exp\left[Pr\int_0^\eta Hds\right]d\eta, \tag{16}$$

and $H(\eta)$ is the axial velocity component obtained from the solution of the accompanying flow problem.

Now, $I'(\eta) = exp\left[Pr\int_0^\eta Hds\right]$ and therefore $I'(0) = 1$ so that the temperature gradient at the surface becomes:

$$\Theta'(0) = -\frac{I'(0)}{I(\infty)} = -\frac{1}{I(\infty)}. \tag{17}$$

If we for simplicity assume that the axial velocity component is constant, i.e. $H(\eta) = H_0$, the integration can be performed analytically as:

$$\begin{aligned} I(\eta) &= \int_0^\eta exp\left[Pr\int_0^\eta H_0 ds\right]d\eta = \int_0^\eta exp[PrH_0\eta]d\eta \\ &= \frac{1}{PrH_0}exp[PrH_0\eta]_0^\eta, \end{aligned} \tag{18}$$

and finally, $I(\eta) = \frac{1}{PrH_0}[exp(PrH_0\eta) - 1]$ which gives $I(\infty) = -\frac{1}{PrH_0}$ provided that $H_0 < 0$. This gives the temperature gradient $\Theta'(0) = -\frac{1}{I(\infty)} = PrH_0 < 0$. The assumption of a constant axial velocity H_0 is made here to be able to demonstrate that the sign of the temperature gradient at the surface is determined by the sign of H_0. In reality, however, the axial velocity H varies with η. Nevertheless, it was shown by Turkyilmazoglu [10] that the axial velocity component of the von Karman flow becomes constant in presence

Table 1
Effect of suction parameter A on the shear stress characteristics $F'(0)$ and $G'(0)$. Comparisons with results computed by Nath and Venkatachala [12] in their Table 1.

A	$-F'(0)$		$G'(0)$	
	Present	N & V	Present	N & V
0	0.9420	0.9420	0.7729	0.7729
0.5	0.9033	NA	1.0652	NA
1.0	0.8351	0.8350	1.3885	1.3863
2.0	0.6468	0.6462	2.1560	2.1550
3.0	0.4800	NA	3.0611	NA

of strong suction. The same tendency is likely to appear also in the Bödewadt flow.

5. Numerical approach

We solved the two-point boundary value problem consisting of the coupled set of ordinary differential Eqs. (9)–(13) subjected to the boundary conditions (14). For this purpose we have used the bvp4c MATLAB solver, which gives very good results for the nonlinear ODEs with multipoint BVPs. This finite-difference code utilizes the 3-stage Lobatto IIIa formula, that is a collocation formula and the collocation polynomial provides a C1-continuous solution that is fourth-order accurate uniformly in [a,b]. For multipoint BVPs, the solution is C1-continuous within each region, but continuity is not automatically imposed at the interfaces. Mesh selection and error control are based on the residual of the continuous solution. Analytical condensation is used when the system of algebraic equations is formed; see e.g. Shampine et al.[11]. Numerical solutions of the three-dimensional flow problem were provided by Nath and Venkatachala [12] for three different values of the suction parameter A. The comparisons in Table 1 show that the results of the present computations compare very well with their data. Moreover, the entries for $A = 0$ match exactly with the corresponding data tabulated by Turkyilmazoglu [9].

6. Numerical results

6.1. Velocity field

Computed results for the three velocity components are shown in Figs. 1–3. In absence of suction, the fluid motion well above the surface is characterized by a uniform angular velocity G, which is reduced through a viscous boundary layer in order for the fluid to adhere to the no-slip condition $G = 0$ at the solid surface. The reduction of the circumferential velocity component in the vicinity of the surface reduces the radial directed centripetal acceleration (or centrifugal force) such that the prevailing radial pressure gradient induces an inward fluid motion F. In order to assure mass conservation, this inward fluid motion gives in turn rise to an axial outward flow $H > 0$. Such a spiralling flow exists near the planar surface, although more complex variations of the velocity field are seen further away, but yet before the uniformly rotating flow conditions are reached for $\eta > 12$. This oscillatory nature of the three velocity components was reported already by Bödewadt [1] and makes the Bödewadt flow qualitatively different from the Von Karman flow. However, it is interesting to notice that these oscillations are damped and even suppressed in presence of a magnetic field (King and Lewellen [13]), partial slip (Sahoo et al. [14]) or if the disk is stretched (Turkyilmazoglu [9]). Of particular relevance for the present study is the effect of surface suction. Nath and Venkatachala [12] showed that sufficient suction through the planar surface suppressed the oscillatory nature of the three-dimensional flow field and, moreover, made the axial flow be directed in the inward direction rather than outward, as is the case in the classical Bödewadt flow.

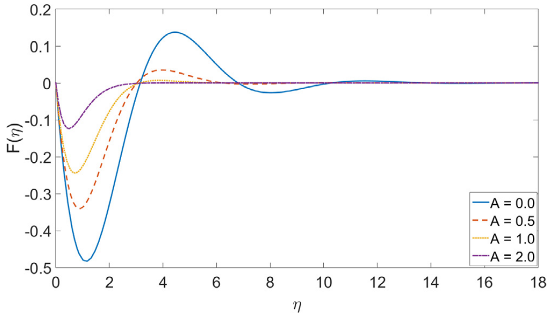

Fig. 1. Radial velocity component $F(\eta)$ for some different values of the suction parameter A.

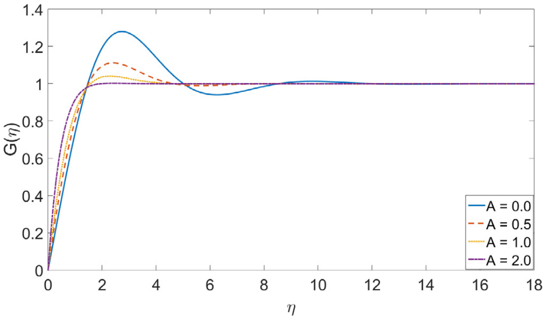

Fig. 2. Circumferential velocity component $G(\eta)$ for some different values of the suction parameter A.

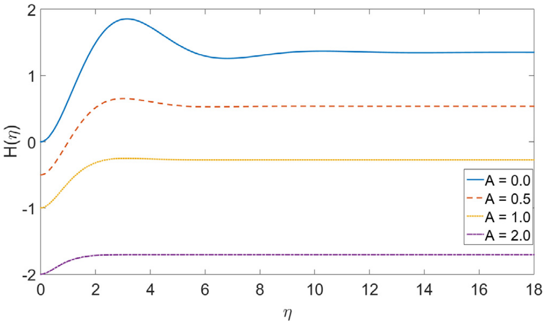

Fig. 3. Axial velocity component $H(\eta)$ for some different values of the suction parameter A.

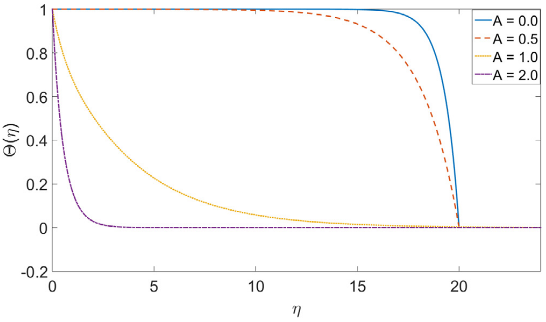

Fig. 4. Variation of temperature $\Theta(\eta)$ for some different values of suction parameter A and $Pr = 1$.

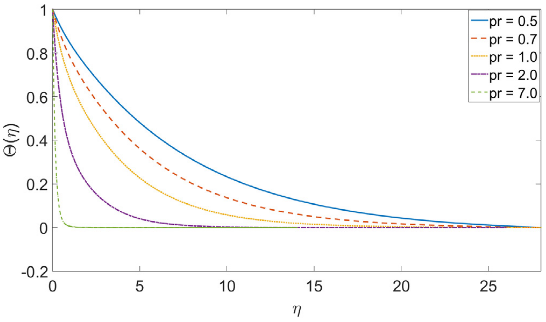

Fig. 5. Variation of temperature $\Theta(\eta)$ for some different values of Pr and $A = 1.0$.

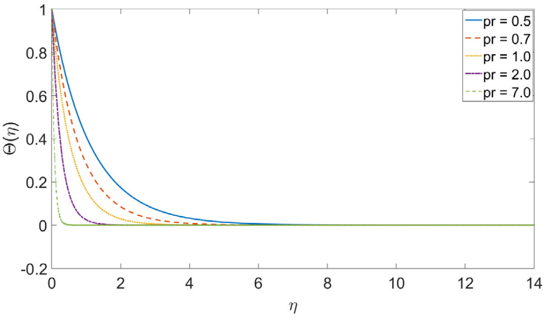

Fig. 6. Variation of temperature $\Theta(\eta)$ for some different values of Pr and $A = 2.0$.

Nath and Venkatachala [12] showed results for two different values of the suction parameter A (1.0 and 2.0) and compared these results with the pure Bödewadt case $A = 0$. Here, we have revisited the same cases and also included results with modest suction ($A = 0.5$) and stronger suction ($A = 3$). The trends observed by Nath and Venkatachala [12] are reproduced here. The radial inflow F in Fig. 1 is monotonically reduced with increasing suction and this is accompanied with a reduction of the axial flow H in Fig. 3. The direction of the axial flow is inverted when the suction rate $A \geqslant 1$, such that the fluid instead moves towards the solid surface. With modest suction, however, the fluid in the vicinity of the surface moves away from the surface, whereas the fluid further away is directed towards it such that H changes sign at about $\eta = 1$ for $A = 0.5$. The radial and tangential shear stresses are proportional with the slopes of the respective velocity profiles $F'(0)$ and $G'(0)$ given in Table 1 and compared with corresponding results reported by Nath and Venkatachala [12]. Here, we can see that while the tangential shear stress $G'(0)$ increases with A, the magnitude of the radial shear stress $-F'(0)$ decreases with increasing suction.

6.2. Heat transfer

While the three-dimensional flow field is a one-parameter problem determined by the suction parameter A, the accompanying thermal problem is a two-parameter problem in A and Pr. Computed temperature profiles for various values of A and Prandtl number $Pr = 1$ are shown in Fig. 4. These results show a remarkable effect of the suction parameter depending on whether $A \geqslant 1$ or not. The temperature profiles for $A = 0$ and $A = 0.5$ show that the temperature is constant from the surface and far beyond $\eta = 12$ before the temperature drops to zero in order to satisfy the outer boundary condition. These profiles resemble $\Theta(\eta) = 1$ seen in Fig. 3 in Turkyilmazoglu [9] for zero stretching, i.e. pure Bödewadt flow. Although all the results in Fig. 4 are solutions of the ODE which satisfy the two thermal boundary conditions, only results for $A > 1$ are physically plausible in the sense that the heat flux $-\Theta'$ far away from the surface asymptotes to zero. The auxiliary condition that $\Theta' \to 0$ as $\eta \to \infty$ is commonly overlooked in analysis of thermal boundary layers, similarly as the auxiliary conditions $F' \to 0$ and $G' \to 0$ as $\eta \to \infty$ for the momentum boundary layer; see Andersson [15] and Pantokratoras [16]. Realistic solutions are therefore obtained only in presence of sufficient suction.

From Fig. 3 we recall that the axial velocity component H changes sign from positive to negative as the suction parameter A is gradually increased. Since the only effect of the fluid flow on the thermal energy problem is through the axial velocity component $H(\eta)$, the presence of suction is likely to have a major impact on the temperature distribution. Indeed, we showed in Section 4 that if $H = H_0$ the temperature gradient $\Theta'(0) = PrH_0$ becomes negative only provided that $H_0 < 0$. This explains why we only obtain plausible solutions when sufficiently strong suction is applied, i.e. when the axial velocity turned negative everywhere. It is therefore remarkable that Shaoo et al. [8] showed temperature profiles for $Pr = 1$ in their Fig. 9 which resemble those for $A \geqslant 1$ in our Fig. 4. We believe that these results were obtained due to an unnoticed sign error in their thermal energy equation.

Table 2
Heat transfer rate $-\Theta'(0)$ at the surface.

Pr	A				
	0	0.5	1.0	2.0	3.0
0.5			0.1934	0.9239	1.4736
0.7			0.2984	1.3154	2.0713
1.0			0.4943	1.9114	2.9705
2.0			1.4013	3.9215	5.9743
7.0			6.7857	13.9633	20.9879

The slope Θ' of the four temperature profiles in Fig. 4 is negative. However, the magnitude of the slope of the physically plausible temperature variations decreases with η, whereas the unphysical profiles exhibit a gradually increasing $|\Theta'|$. A critical value A_{crit} of the dimensionless suction parameter can therefore be defined as the A-value that leads to an inflection point in the temperature profile, i.e. $\Theta'' = 0$. The second derivative of the temperature distribution can readily be obtained from the exact analytical solution given by Eqs. (15) and (16) as

$$\Theta''(\eta) = \Theta'(0) \cdot Pr \cdot H(\eta) \cdot exp\left[Pr\int_0^{\eta} Hd\eta\right]. \tag{19}$$

The critical A-value accordingly corresponds to the amount of suction $H(0) = -A$ which is just sufficient to make the axial velocity component H negative for all values of η. By means of systematic integrations of the three-dimensional flow problem we found that $A_{crit} = 0.85$.

The realistic solutions in Fig. 4 show that the adaption of the dimensionless temperature from $\Theta = 1$ at the surface to $\Theta = 0$ far above the surface occurs over a gradually shorter distance with increasing A. Stronger suction accordingly tends to make the thermal boundary layer thinner for a given value of the Prandtl number. Figs. 5 and 6 show temperature profiles for a range of Prandtl numbers for prescribed suction $A = 1$ and $A = 2$, respectively. For a given flow field, the thermal boundary layer becomes gradually thinner as Pr increases from 0.5 to 7.0. This trend is consistent with the general knowledge that the importance of thermal conduction, relative to viscous diffusion, diminishes with increasing Pr. The excess surface temperature is therefore felt only in the near vicinity of the surface for $Pr \gg 1$. In-depth discussions on high-Prandtl-number effects on the thermal boundary layer thickness and the surface heat transfer can be found in Shevchuk [5,17].

The Nusselt number Nu is a convenient non-dimensional measure of the local heat transfer rate at the surface $\eta = 0$. The Nusselt number is usually defined as $Nu = \frac{q(0)L}{k(T_w - T_\infty)} = \frac{-\partial T/\partial z|_{z=0}L}{T_w - T_\infty}$. Schevchuk & Buschmann [6] and Shevchuk [5,17] took $L = r$, which gives $Nu = -\Theta'(0)\sqrt{\Omega r^2/\nu}$. Here, however, the length scale L is taken as $\sqrt{\nu/\Omega}$ to give $Nu = -\Theta'(0)$. Nu is proportional with $-\Theta'(0)$ tabulated in Table 2 for all values of A and Pr considered herein. Here, we observe that the heat transfer increases with increasing suction and for higher Prandtl numbers.

7. Concluding remarks

We have shown that realistic similarity solutions of the thermal energy problem do not exist for Bödewadt flow in absence of suction ($A = 0$). The only earlier results for pure Bödewadt flow by Sahoo et al. [8] and Turkyilmazoglu [9] are therefore not physically realistic. This explains why heat transfer in Bödewadt flow seems to have escaped the attention of the research community. If sufficient suction is applied, however, plausible solutions do exist. This phenomenon is explained by the reversal of the axial velocity component when suction is imposed. This finding is consistent with the fact that similarity solutions of the heat transfer problem associated with Von Karman flow do exist. The thermal energy equation in that case is exactly the same as in the Bödewadt flow, but the sign of the axial velocity component H is opposite. One can therefore conjecture that solutions of the thermal problem of the Von Karman flow ceases to exist if sufficient blowing through the rotating disk is applied, so that the axial flow direction is reversed.

It should be noted that our conclusions are valid only for the actual heat and fluid flow problem studied herein. The presence of either a magnetic field [12], partial slip [7] or stretching of the surface [9] will alter the flow field and thereby also the possible existence of similarity solutions of the thermal field. Moreover, if, for instance, viscous dissipation or ohmic heating is included in the thermal energy equation, see e.g. Sahoo [7], the situation is different and similarity solutions may exist even in absence of suction.

Similarity solutions of the heat transfer problem associated with Bödewadt flow subjected to significant suction ($A \geqslant 1$) have been provided here for the first time. Increasing suction tends to make the thermal boundary layer gradually thinner and thereby increases the heat transfer rate through the solid surface. Likewise, as the relative importance of thermal diffusivity reduces for higher Prandtl numbers, the thermal boundary layer becomes gradually thinner.

References

[1] U.T. Bödewadt, Die Drehströmung *Über* festem Grunde, J. Appl. Math. Mech./Zeitschrift für Angewandte Mathematik und Mechanik 20 (1940) 241–253.
[2] Th.V. Kármán, *Über* laminare und turbulente Reibung, J. Appl. Math. Mech/Zeitschrift für Angewandte Mathematik und Mechanik 1 (1921) 233–252.
[3] K. Millsaps, K. Pohlhausen, Heat transfer by laminar flow from a rotating plate, J. Aeronaut. Sci. 19 (1952) 120–126.
[4] E.M. Sparrow, J.L. Gregg, Heat transfer from a rotating disk to fluids of any Prandtl number, J. Heat Trans. 81 (1959) 249–251.
[5] I.V. Shevchuk, Convective Heat and Mass Transfer in Rotating Disk Systems, Vol. 45, Springer Science & Business Media, 2009.
[6] I.V. Shevchuk, M.H. Buschmann, Rotating disk heat transfer in a fluid swirling as a forced vortex, Heat Mass Trans. 41 (2005) 1112–1121.
[7] B. Sahoo, Effects of slip on steady Bödewadt flow and heat transfer of an electrically conducting non-Newtonian fluid, Commun. Nonlinear Sci. Num. Simul. 16 (2011) 4284–4295.
[8] B. Sahoo, R.A. Van Gorder, H.I. Andersson, Steady revolving flow and heat transfer of a non-Newtonian Reiner-Rivlin fluid, Int. Commun. Heat Mass Trans. 39 (2012) 336–342.
[9] M. Turkyilmazoglu, Bödewadt flow and heat transfer over a stretching stationary disk, Int. J. Mech. Sci. 90 (2015) 246–250.
[10] M. Turkyilmazoglu, An asymptotic investigation into the stabilization effect of suction in the rotating-disk boundary layer flow, Comput. Math. Appl. 53 (2007) 750–759.
[11] L.F. Shampine, J. Kierzenka, M.W. Reichelt, Solving boundary value problems for ordinary differential equations in MATLAB with bvp4c, Tutorial Notes (2000) 437–448.
[12] G. Nath, B.J. Venkatachala, The effect of suction on boundary layer for rotating flows with or without magnetic field, Proceedings of the Indian Academy of Sciences-Section A, vol. 85(5), Springer India, 1977, pp. 332–337.
[13] W.S. King, W.S. Lewellen, Boundary-layer similarity solutions for rotating flows with and without magnetic interaction, Phys. Fluids 7 (1964) 1674–1680.
[14] B. Sahoo, S. Abbasbandy, S. Poncet, A brief note on the computation of the Bödewadt flow with Navier slip boundary conditions, Comput. Fluids 90 (2014) 133–137.
[15] H.I. Andersson, Comments on BVPs in non-Newtonian boundary-layer flow, Appl. Math. Comput. 182 (2006) 1714–1716.
[16] A. Pantokratoras, A common error made in investigation of boundary layer flows, Appl. Math. Model. 33 (2009) 413–422.
[17] I.V. Shevchuk, Turbulent heat and mass transfer over a rotating disk for the Prandtl or Schmidt numbers much larger than unity: an integral method, Heat Mass Trans. 45 (2009) 1313–1321.

PAPER 2

Revolving flow of a fluid-particle suspension with suction

M.Rahman , H.I.Andersson

Alexandria Engineering Journal, In press (2017)

ARTICLE IN PRESS
Alexandria Engineering Journal (2017) **xxx**, xxx–xxx

HOSTED BY
ELSEVIER

Alexandria University
Alexandria Engineering Journal
www.elsevier.com/locate/aej
www.sciencedirect.com

ORIGINAL ARTICLE

Revolving flow of a fluid-particle suspension with suction

Muhammad Rahman *, **Helge I. Andersson**

Department of Energy and Process Engineering, Norwegian University of Science and Technology, No-7491 Trondheim, Norway

Received 21 March 2017; revised 1 August 2017; accepted 23 August 2017

KEYWORDS

Revolving flow;
Bödewadt flow;
Particle-fluid suspension;
Similarity solutions;
Tea-cup effect

Abstract The three-dimensional revolving flow of a particle-fluid suspension above a plane surface is considered. The flow represents an extension of the classical Bödewadt flow to a two-fluid problem. The governing equations for the two phases are coupled through an interaction force with the particle relaxation time τ as a free parameter. By means of a similarity transformation, the coupled set of non-linear ODEs becomes a two-point boundary value problem. The numerical results show that the radial inward particle velocity increases whereas the circumferential velocity decreases by shortening τ, thereby strengthening the spiralling particle motion. These predictions are consistent with the so-called tea-cup effect, i.e. accumulation of tea leaves at the centre of the cup. On the contrary, the revolving fluid motion is reduced as a result of the particle-fluid interactions.

© 2017 Faculty of Engineering, Alexandria University. Production and hosting by Elsevier B.V. This is an open access article under the CC BY-NC-ND license (http://creativecommons.org/licenses/by-nc-nd/4.0/).

1. Introduction

The steadily revolving flow of a viscous fluid above a planar surface is commonly known as Bödewadt flow; see Bödewadt [1]. The fluid motion well above the surface is characterised by a uniform angular velocity, which is reduced through a viscous boundary layer in order for the fluid to adhere to the no-slip condition at the solid surface. The reduction of the circumferential velocity component in the vicinity of the surface reduces the radially directed centripetal acceleration (or centrifugal force) such that the prevailing radial pressure gradient induces an inward fluid motion. In order to assure mass conservation, this inward fluid motion gives in turn rise to an axial upward flow. Such a spiralling flow exists near the planar surface, although more complex variations of the velocity field have been reported further away, but yet before the uniformly rotating flow conditions are reached. The oscillatory nature of the three velocity components reported by Bödewadt [1] has been subject to criticism, but this criticism was deem unjustified by Zandbergen and Dijkstra [2]. It is interesting to notice that these oscillations are damped and even suppressed in presence of a magnetic field (King and Lewellen [3]), partial slip (Sahoo, Abbasbandy and Poncet [4]), stretching surface (Turkyilmazolgu [5]) or suction (Nath and Venkatachala [6]). With a sufficiently high suction velocity through the planar surface, the axial flow is directed in the downward direction rather than upward, as is the case in the classical Bödewadt flow. In view of its fundamental importance as a prototype swirling flow the Bödewadt flow has received renewed focus in recent years. The inviscid instability of the Bödewadt boundary layer was examined by MacKerrell [7] whereas Sahoo [8,9] and Sahoo and Poncet [10] demonstrated that also

---

* Corresponding author.
E-mail addresses: muhammad.rahman@ntnu.no (M. Rahman), helge.i.andersson@ntnu.no (H.I. Andersson).

Peer review under responsibility of Faculty of Engineering, Alexandria University.

http://dx.doi.org/10.1016/j.aej.2017.08.017
1110-0168 © 2017 Faculty of Engineering, Alexandria University. Production and hosting by Elsevier B.V.
This is an open access article under the CC BY-NC-ND license (http://creativecommons.org/licenses/by-nc-nd/4.0/).

Please cite this article in press as: M. Rahman, H.I. Andersson, Revolving flow of a fluid-particle suspension with suction, Alexandria Eng. J. (2017), http://dx.doi.org/10.1016/j.aej.2017.08.017

such revolving flows of a non-Newtonian Reiner-Rivlin fluid admit exact similarity solutions.

The swirling flow induced by a steadily rotating disk was first described by von Kármán [11]. The von Kármán flow is essentially a reversed Bödewadt flow, albeit without the oscillatory features that characterize the latter. Zung [12] studied a von Kármán flow of a fluid-particle suspension and his analysis was subsequently extended by Sankara and Sarma [13] to include surface suction and further explored by Allaham and Peddieson [14].

Studies of suspensions of small particles in a continuous medium (either gas or liquid) are of fundamental interest in fluid mechanics and yet with numerous applications like, for instance, aerosol clouds and erosion protection. Additional applications were recently pointed out by Turkyilmazolgu [15]. A daily life example is the characteristic flow-induced sedimentation of tea leaves in a flat-bottomed cup of tea, as discussed by Einstein [16] and illustrated in Fig. 1.

The aim of the present study is to adopt a similar approach as that advocated by Zung [12] to Bödewadt flow of a fluid-particle suspension. After first having shown that the governing two-phase flow equations admit similarity solutions, numerical solutions of the coupled set of non-linear ordinary differential equations will show how the particle phase is revolving along with the fluid and also how the presence of particles will affect the swirling motion of the fluid phase.

2. Mathematical model equations

Let us consider the steadily revolving flow of a fluid-particle suspension above a planar surface. In cylindrical polar coordinates (r, θ, z) the governing mass conservation and momentum equations for the fluid and particle phases become:

$$\frac{\partial}{\partial r}(ru) + \frac{\partial}{\partial z}(rw) = 0, \tag{1}$$

$$\frac{\partial}{\partial r}(r\rho_p u_p) + \frac{\partial}{\partial z}(r\rho_p w_p) = 0, \tag{2}$$

$$u\frac{\partial u}{\partial r} - \frac{v^2}{r} + w\frac{\partial u}{\partial z} = -\frac{1}{\rho}\frac{\partial p}{\partial r} + \nu\left[\frac{\partial^2 u}{\partial r^2} + \frac{\partial}{\partial r}\left(\frac{u}{r}\right) + \frac{\partial^2 u}{\partial z^2}\right] + \frac{F_r}{\rho}, \tag{3}$$

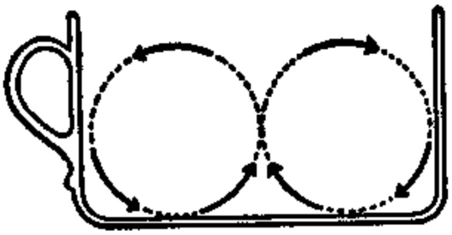

Fig. 1 Sketch of the secondary fluid motion in the vertical plane through the symmetry axis of a flat-bottomed cup of tea. The secondary motion arises due to a revolving fluid motion in the horizontal plane, caused for instance by stirring by a spoon, and sweeps the tea leaves towards the center of the cup.

$$u\frac{\partial v}{\partial r} + \frac{uv}{r} + w\frac{\partial v}{\partial z} = \nu\left[\frac{\partial^2 v}{\partial r^2} + \frac{\partial}{\partial r}\left(\frac{v}{r}\right) + \frac{\partial^2 v}{\partial z^2}\right] + \frac{F_\theta}{\rho}, \tag{4}$$

$$u\frac{\partial w}{\partial r} + w\frac{\partial w}{\partial z} = -\frac{1}{\rho}\frac{\partial p}{\partial z} + \nu\left[\frac{\partial^2 w}{\partial r^2} + \frac{1}{r}\frac{\partial w}{\partial r} + \frac{\partial^2 w}{\partial z^2}\right] + \frac{F_z}{\rho}, \tag{5}$$

$$u_p\frac{\partial u_p}{\partial r} - \frac{v_p^2}{r} + w_p\frac{\partial u_p}{\partial z} = -\frac{1}{\rho_p}\frac{\partial p}{\partial r} - \frac{F_r}{\rho_p}, \tag{6}$$

$$u_p\frac{\partial v_p}{\partial r} + \frac{u_p v_p}{r} + w_p\frac{\partial v_p}{\partial z} = -\frac{F_\theta}{\rho_p}, \tag{7}$$

$$u_p\frac{\partial w_p}{\partial r} + w_p\frac{\partial w_p}{\partial z} = -\frac{1}{\rho_p}\frac{\partial p}{\partial z} - \frac{F_z}{\rho_p}, \tag{8}$$

where (u, v, w) and (u_p, v_p, w_p) are the velocity components of the fluid and particle phases in the radial, circumferential and axial directions, respectively. Here, we have assumed rotational symmetry about the vertical z-axis, i.e. $\partial/\partial\theta = 0$. The kinematic viscosity of the fluid is ν and the densities of the fluid and particle phases are ρ and ρ_p. The above set of governing equations is the same as that considered by Zung [12] and Sankara and Sarma [13] for swirling von Kármán flow of a fluid-particle suspension above a steadily rotating disk, except that the a priori unknown pressure p was assigned only to the fluid phase. In the present study, however, the pressure gradients are shared between the two phases in proportion to their density ratio. This alternative formulation was suggested by Allaham and Peddeison [14] but not adopted in their subsequent calculations. In the present problem, however, it is essential to include pressure gradient terms also in the particle-phase equations of motion. Indeed, a radial pressure gradient is required to balance the centripetal acceleration in the far field in Eq. (6).

Particle-fluid interactions are accounted for by means of the following force components

$$F_r = \rho_p(u_p - u)/\tau, \tag{9}$$

$$F_\theta = \rho_p(v_p - v)/\tau, \tag{10}$$

$$F_z = \rho_p(w_p - w)/\tau, \tag{11}$$

included in the fluid phase equations and their negative counterparts in the particle phase equations. These expressions represent force per volume and are based on the assumption of a linear drag law, i.e. Stokes drag, where τ

$$\tau = m/6\pi\mu a, \tag{12}$$

is the relaxation time of a single spherical particle with mass $m$and radius a immersed in a fluid with dynamic viscosity $\mu = \rho\nu$. The viscous fluid phase sticks to the permeable planar surface at $z = 0$ and attains a state of solid body rotation with angular velocity Ω high above the surface:

$$\left.\begin{array}{llll} u = 0, & v = 0, & w = -\sqrt{\nu\Omega}A & at \quad z = 0 \\ u = 0, & v = r\Omega, & p = \frac{1}{2}\rho r^2\Omega^2 & as \quad z \to \infty \end{array}\right\}, \tag{13}$$

where $A \geqslant 0$ is a dimensionless suction velocity. The inviscid particle phase can be assumed to follow the motion of the fluid phase far above the solid surface, i.e.

Please cite this article in press as: M. Rahman, H.I. Andersson, Revolving flow of a fluid-particle suspension with suction, Alexandria Eng. J. (2017), http://dx.doi.org/10.1016/j.aej.2017.08.017

$$\begin{aligned} &u_p = u = 0, \quad v_p = v = r\Omega, \\ &w_p = w, \qquad \rho_p = \rho, \qquad \mathit{for}\ z \to \infty. \end{aligned} \tag{14}$$

3. Similarity transformation and resulting ODEs

The two-phase flow that arises above the planar surface can be characterized by the length scale $\sqrt{v/\Omega}$, the time scale Ω^{-1} and the velocity scale $\sqrt{v\Omega}$. We can therefore introduce the same dimensionless similarity variables used already by von Kármán [11] and Bödewadt [1]:

$$\eta = z\sqrt{\Omega/v}. \tag{15}$$

The same similarity transformations are used for the fluid phase velocities and pressure:

$$\begin{aligned} &u(r,z) = r\Omega F(\eta), \\ &v(r,z) = r\Omega G(\eta), \\ &w(r,z) = \sqrt{v\Omega}H(\eta), \\ &p(r,z) = \rho\left(-v\Omega P(\eta) + \tfrac{1}{2}r^2\Omega^2\right). \end{aligned} \tag{16}$$

The latter pressure transformation was not required in Bödewadt's original approach which was based on the boundary layer approximations which imply that the pressure is constant all across the boundary layer. The variables characterizing the particle phase can be recast into dimensionless forms by means of the transformation used for von Kármán flow by Sankara and Sarma [13]:

$$\begin{aligned} &u_p(r,z) = r\Omega F_p(\eta), \\ &v_p(r,z) = r\Omega G_p(\eta), \\ &w_p(r,z) = \sqrt{v\Omega}H_p(\eta), \\ &\rho_p(r,z) = \rho Q(\eta), \end{aligned} \tag{17}$$

where Q is the ratio between the densities of the two phases. The governing set of partial differential Eqs. (1)–(8) transforms into a set of ordinary differential equations:

$$2F + H' = 0, \tag{18}$$

$$Q'H_p + QH_p' + 2QF_p = 0, \tag{19}$$

$$F'' - HF' - F^2 + G^2 + \beta Q(F_p - F) = 1, \tag{20}$$

$$G'' - HG' - 2FG + \beta Q(G_p - G) = 0, \tag{21}$$

$$P' = -2FH + 2F' - \beta Q(H_p - H), \tag{22}$$

$$F_p'H_p + F_p^2 - G_p^2 + \beta(F_p - F) = -1/Q, \tag{23}$$

$$G_p'H_p + 2F_pG_p + \beta(G_p - G) = 0, \tag{24}$$

$$QH_p'H_p + \beta Q(H_p - H) = P' \tag{25}$$

where the prime denotes differentiation with respect to the similarity variable η. The accompanying boundary conditions (13) and (14) transform into:

$$F(\eta) = 0, \quad G(\eta) = 0, \quad H(\eta) = -A, \qquad at \quad \eta = 0,$$

$$\left.\begin{aligned} &F(\eta) = 0, \quad G(\eta) = 1, \quad P(\eta) = 1, \\ &F_p(\eta) = 0, \quad G_p(\eta) = 1, \quad H_p(\eta) = H(\eta), \\ &Q(\eta) = 1. \end{aligned}\right\} as \quad \eta \to \infty. \tag{26}$$

The resulting two-fluid flow problem now depends only on two dimensionless parameters, namely the suction parameter A and the interaction parameter $\beta = 1/\Omega\tau$ where τ was introduced in Eq. (12). The ratio between a particle time scale and a fluid time scale, e.g. τ/Ω^{-1}, is often referred to as a Stokes number. The single-phase Bödewadt flow with suction is recovered in the particular case when the interaction parameter $\beta = 0$.

4. Numerical integration technique

Our primary interest is in the flow field. The pressure gradient P' can therefore be eliminated from the axial components of the fluid and particle equations to give

$$H_p' = \left(2F' - 2\beta Q(H_p - H) - 2FH\right)/H_pQ. \tag{27}$$

We have used the bvp4c MATLAB solver, which gives very good results for the non-linear ODEs with multipoint BVPs. This finite-difference code utilizes the 3-stage Lobatto IIIa formula, that is a collocation formula and the collocation polynomial provides a C1-continuous solution that is fourth-order accurate uniformly in [a,b]. For multipoint BVPs, the solution is C1-continuous within each region, but continuity is not automatically imposed at the interfaces. Mesh selection and error control are based on the residual of the continuous solution. Analytical condensation is used when the system of algebraic equations is formed; see Shampine et al. [17]. The coupled set of non-linear ODEs are integrated for $A = 2.0$ and some different values of β.

For the particular parameter value $\beta = 0$, the two-point boundary value problem defined in Section 3 simplifies since the particle phase decouples from the fluid phase. In our recent paper [18], results for this single-phase flow compared excellently with earlier results provided by Nath and Venkatachala [6] for some different values of the dimensionless suction velocity $A = 0, 1,$ and 2.

For non-zero values of the interaction parameter β, the fluid phase momentum equations are coupled to the particle phase momentum equations through interaction force terms. Although our numerical integration approach worked perfectly well for $\beta = 0$, we were unable to obtain converged numerical solutions for $\beta > 0$ in absence of suction ($A = 0$). We first computed some sample solutions for $A = 3$ (Rahman and Andersson [19]). In the present paper we instead consider $A = 2$ after first having validated the computational accuracy by comparisons with the results obtained by Nath and Venkatachala [6].

Allaham and Peddieson [14] mentioned that numerical solutions of particulate von Kármán flow driven by an impermeable disk did not exist for some parameter combinations, but also that no such restrictions were found when suction was imposed. It is well known that Bödewadt flow over an impermeable surface, i.e. $A = 0$, is more complex than the corresponding Kármán flow. The three velocity components exhibit an oscillatory behaviour and the Bödewadt boundary layer is substantially thicker than the von Kármán boundary layer. In presence of suction, however, the Bödewadt boundary layer becomes substantially thinner and the oscillatory behaviour vanishes. For these reasons, numerical solutions are more readily obtained.

Please cite this article in press as: M. Rahman, H.I. Andersson, Revolving flow of a fluid-particle suspension with suction, Alexandria Eng. J. (2017), http://dx.doi.org/10.1016/j.aej.2017.08.017

5. Results and discussions

We are primarily interested in particle-fluid interactions in the three-dimensional flow field. We therefore considered five different values of the particle-fluid interaction parameter β in the range from 0.2 to 2.0. The suction parameter A was kept constant and equal to 2.0. This particular parameter value was chosen since Nath and Venkatachala [6] considered the same albeit without a particle phase.

We can see from Fig. 2 that the radial inward flow is reduced in the presence of particles and this reduction increases with β. This is caused by the interaction force F_r which is positive since $u_p > u$ everywhere except in the near vicinity of the surface. It is noteworthy that also the particle phase flows towards the symmetry axis. Contrary to u, however, u_p does not obey no-slip at the surface. This gives rise to a change-of-sign of the slip velocity $u_p - u$ next to the surface and thereby a reversal of F_r. The thickness of the thin near-wall layer with $F_r < 0$ increases from about 0.2 to $0.4\sqrt{v/\Omega}$ as β increases from 0.2 to 2.0.

The particle velocity u_p in Fig. 3 is radially inward and increases in magnitude all the way towards the surface. This inward motion strengthens monotonically with increasing interaction parameter β, primarily due to a reduction of the circumferential particle velocity v_p. The gradual reduction of the magnitude of the centripetal acceleration in Eq. (6) is partly compensated by an increasing magnitude of the convection $u_p \partial u_p / \partial r = 1/2 \partial u_p^2 / \partial r < 0$.

The interaction parameter β has an almost negligible effect on the circumferential fluid velocity v in Fig. 4 which reduces monotonically from that of solid body rotation $v = r\Omega$ to no-slip $v = 0$ at the surface. The circumferential slip velocity $v_p - v$ becomes inevitably positive in the viscous boundary layer since the particle velocity v_p is neither affected by viscous forces nor obeys no-slip. The circumferential interaction force F_θ on the fluid phase is thus positive and slightly increases v with increasing β, whereas the corresponding reaction force on the particle phase $-F_\theta < 0$ and therefore tends to enhance the deceleration of the particle motion with increasing β, as one can observe in Fig. 5.

The fluid phase flows axially towards the surface, i.e. $w < 0$, as can be seen in Fig. 6. This opposite flow direction compared

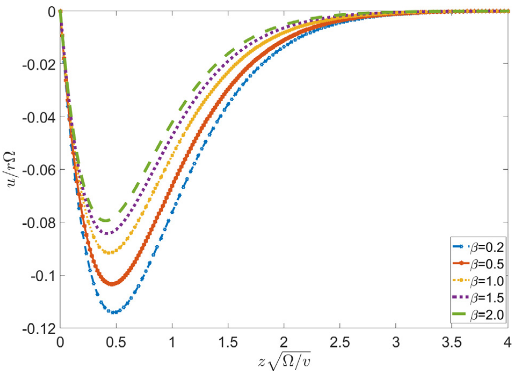

Fig. 2 Radial fluid velocity component $F = u/r\Omega$ for some different values of the interaction parameter β.

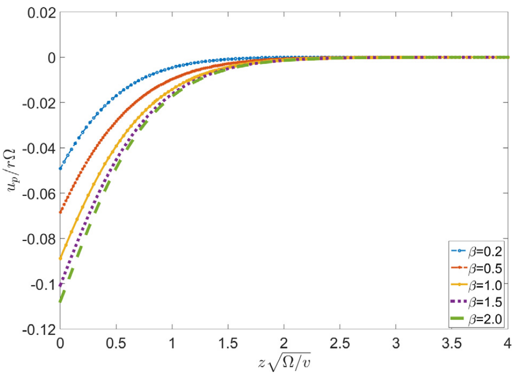

Fig. 3 Radial particle velocity component $F_p = u_p/r\Omega$ for some different values of the interaction parameter β.

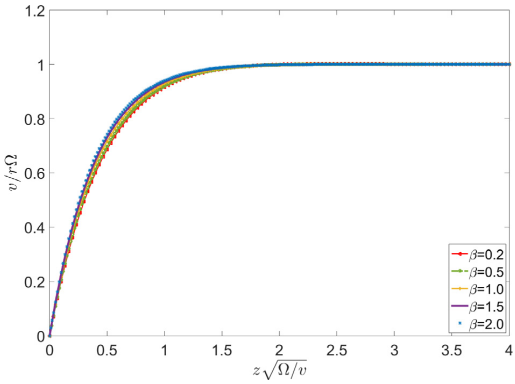

Fig. 4 Circumferential fluid velocity component $G = v/r\Omega$ for some different values of the interaction parameter β.

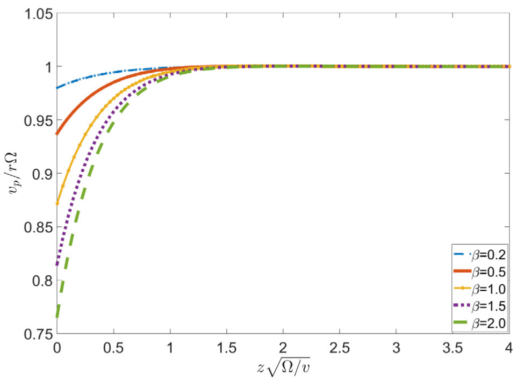

Fig. 5 Circumferential particle velocity component $G_p = v_p/r\Omega$ for some different values of the interaction parameter β.

Please cite this article in press as: M. Rahman, H.I. Andersson, Revolving flow of a fluid-particle suspension with suction, Alexandria Eng. J. (2017), http://dx.doi.org/10.1016/j.aej.2017.08.017

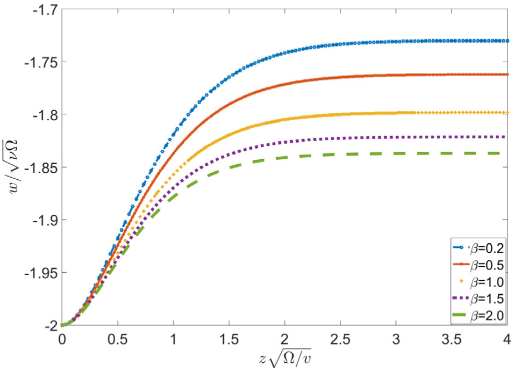

Fig. 6 Axial fluid velocity component $H = w/\sqrt{v\Omega}$ for some different values of the interaction parameter β.

to that in classical Bödewadt flow ($w > 0$) is due the surface suction. The magnitude of the downward flow can be seen to increase from that beyond $\eta = z\sqrt{\Omega/v} \approx 2$ where solid-body rotation prevails through the viscous boundary layer until $w/\sqrt{v\Omega} = -2.0$ at the surface $z = 0$. The interaction force F_z is generally positive since the slip velocity $w_p - w > 0$ (compare Figs. 6 and 7). The axial convection is $w_p \partial w_p/\partial z = 1/2\partial w_p^2/\partial z$ is partially balanced by the negative reaction force $-F_z$ in the particle Eq. (8). However, the dimensionless pressure P decreases monotonically upwards, i.e. $P' < 0$, as seen in Fig. 8. This variation gives rise to a positive pressure gradient $\partial p/\partial z$ in the axial direction, i.e. a pressure force that acts towards the surface and thus tends to support the axial motion towards the surface.

The relative density Q, i.e. the ratio between the particle and fluid densities ρ_p/ρ, is a variable quantity that has been obtained as an integral part of the numerical solution of the present two-fluid flow problem. The Q-profiles in Fig. 9 show that the particle density ρ_p is some 10% lower than the fluid density near the surface but increases to match ρ outside of the viscous boundary layer.

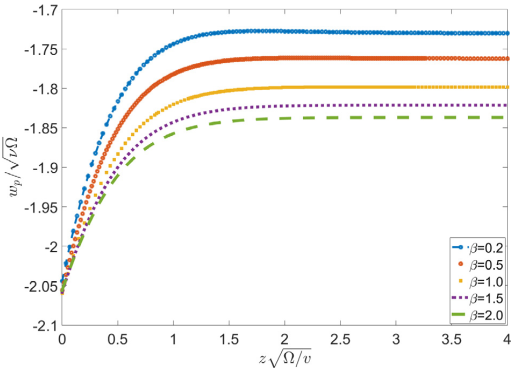

Fig. 7 Axial particle velocity component $H_p = w_p/\sqrt{v\Omega}$ for some different values of the interaction parameter β.

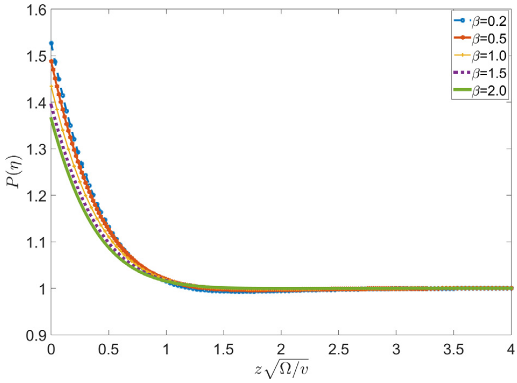

Fig. 8 Pressure P for some different values of the interaction parameter β.

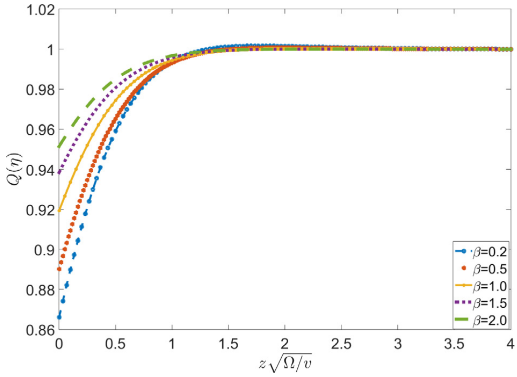

Fig. 9 Ratio of particle and fluid densities $Q = \rho_p/\rho$ for some different values of the interaction parameter β.

Let us finally look at the motion of the particle phase in the limit as $\beta \to 0$ if $\rho_p = \rho$. The horizontal velocity components become $u_p = 0$ and $v_p = r\Omega$, i.e. the radial component vanishes and the linearly increasing circumferential velocity makes the centripetal acceleration exactly balance the radial pressure force in Eq. (6).

The boundary layer characteristics obtained from the numerical solutions are given in Table 1. For the fluid phase: $-F'(0), G'(0), -H(\infty)$. For the particle phase: $-F_p(0), G_p(0), -H_p(0)$.

We learned from Table 1 that:

- The magnitude of the slope of the radial velocity $F'(0)$ decreases with increasing fluid-particle interactions.
- The slope of the circumferential fluid velocity $G'(0)$ increases with increasing β (not clearly visible in Fig. 4).
- The magnitude of the downward fluid velocity $-H(\infty)$ is slightly increased from 1.73 to 1.84 with increasing β.
- The circumferential particle velocity $G_p(0)$ decreases from 0.98 to 0.77 as β increases from 0.2 to 2.0.
- The inward radial particle velocity $-F_p(0)$ more than doubles from about 0.05 to 0.11 as β is increased.

Please cite this article in press as: M. Rahman, H.I. Andersson, Revolving flow of a fluid-particle suspension with suction, Alexandria Eng. J. (2017), http://dx.doi.org/10.1016/j.aej.2017.08.017

Table 1 Flow characteristics for suction parameter $A = 2.0$.

β	$-F'(0)$	$-F_p(0)$	$G_p(0)$	$G'(0)$	$-H_p(0)$	$-H(\infty)$
0.2	0.6136	0.0492	0.9815	2.2165	2.0443	1.7301
0.5	0.5770	0.0685	0.9373	2.3038	2.0559	1.7622
1.0	0.5396	0.0889	0.8716	2.4342	2.0599	1.7983
1.5	0.5192	0.1008	0.8149	2.5453	2.0585	1.8213
2.0	0.5082	0.1078	0.7661	2.6402	2.0559	1.8370

6. Concluding remarks

In this study we adopted the mathematical model of mass and momentum transport in two-fluid systems used earlier for von Kármán flow by Zung [12] and Sankara and Sarma [13]. In the Bödewadt flow, however, it was essential to include pressure force terms in the particle phase momentum equations in order to balance the centripetal acceleration in Eq. (6) in the far field.

- The governing equations of the three-dimensional two-fluid problem have been transformed into a coupled set of ordinary differential equations by means of an exact similarity transformation.
- The resulting set of ODEs is a two parameter problem in terms of the dimensionless suction velocity A and the fluid-particle interaction parameter β.
- β is the ratio between the rotation time scale Ω^{-1} and the particle relaxation time τ. β is therefore a reciprocal Stokes number.
- The particles are spiralling inwards in the vicinity of the surface. The radial inward velocity $|u_p|$ increases and the circumferential velocity v_p decreases with increasing interaction parameter β, i.e. the spiralling increases with β. This phenomenon is commonly known as the tea cup effect: when the tea is stirred, tea leaves near the bottom move towards the centre of the cup and heap up.
- Contrary to the particle phase, the inward spiralling of the fluid phase is gradually reduced as the fluid-particle interaction parameter is increased. The circumferential flow is only modestly affected, but the surface shear stress is nevertheless increased.

References

[1] U.T. Bödewadt, Die Drehströmung Über festem Grunde, J. Appl. Math. Mech./Zeitschrift für Angewandte Mathematik und Mechanik 20 (1940) 241–253.

[2] P.J. Zandbergen, D. Dijkstra, Von Kármán swirling flows, Annu. Rev. Fluid Mech. 19 (1987) 465–491.

[3] W.S. King, W.S. Lewellen, Boundary-layer similarity solutions for rotating flows with and without magnetic interaction, Phys. Fluids 7 (1964) 1674–1680.

[4] B. Sahoo, S. Abbasbandy, S. Poncet, A brief note on the computation of the Bödewadt flow with Navier slip boundary conditions, Comput. Fluids 90 (2014) 133–137.

[5] M. Turkyilmazoglu, Bödewadt flow and heat transfer over a stretching stationary disk, Int. J. Mech. Sci. 90 (2015) 246–250.

[6] G. Nath, B.J. Venkatachala, The effect of suction on boundary layer for rotating flows with or without magnetic field, Proc. Indian Acad. Sci.-Section A 85 (1977) 332–337.

[7] S.O. MacKerrell, Stability of Bödewadt flow, Philos. Trans. Roy. Soc. London A: Math. Phys. Eng. Sci. 363 (2005) 1181–1187.

[8] B. Sahoo, Effects of slip on steady Bödewadt flow and heat transfer of an electrically conducting non-Newtonian fluid, Commun. Nonlinear Sci. Numer. Simul. 16 (2011) 4284–4295.

[9] B. Sahoo, Steady Bödewadt flow of a non-Newtonian Reiner-Rivlin fluid, Diff. Equ. Dyn. Syst. 20 (2012) 367–376.

[10] B. Sahoo, S. Poncet, Effects of slip on steady Bödewadt flow of a non-Newtonian fluid, Commun. Nonlinear Sci. Numer. Simul. 17 (2012) 4181–4191.

[11] Th V. Kármán, Über laminare und turbulente Reibung, J. Appl. Math. Mech./Zeitschrift für Angewandte Mathematik und Mechanik 1 (1921) 233–252.

[12] L.B. Zung, Flow induced in fluid-particle suspension by infinite rotating disk, Phys. Fluids 12 (1969) 18–23.

[13] K.K. Sankara, L.V.K.V. Sarma, On the steady flow produced in fluid-particle suspension by an infinite rotating disk with surface suction, Int. J. Eng. Sci. 23 (1985) 875–886.

[14] M.A. Allaham, J. Peddieson, The flow induced by a rotating disk in a particulate suspension, Int. J. Eng. Sci. 31 (1993) 1025–1034.

[15] M. Turkyilmazoglu, Magnetohydrodynamic two-phase dusty fluid flow and heat model over deforming isothermal surfaces, Phys. Fluids 29 (2017) 013302.

[16] A. Einstein, Die Ursache der Manderbildung der Flusslufe und des sogenannten Baerschen Gesetzes, Die Naturwissenschaften 14 (1926) 223–224.

[17] L.F. Shampine, J. Kierzenka, M.W. Reichelt, Solving boundary value problems for ordinary differential equations in MATLAB with bvp4c, Tut. Notes (2000) 437–448.

[18] M. Rahman, H.I. Andersson, On heat transfer in Bödewadt flow, Int. J. Heat Mass Transfer 112 (2017) 1057–1061.

[19] M. Rahman, H.I. Andersson, Bödewadt flow of a fluid-particle suspension with strong suction, in: Proceedings of 13th International Conference on Heat Transfer, Fluid Mechanics and Thermodynamics – HEFAT 2017, Portoroz, Slovenia, 17th–19th July 2017, pp. 59-64.

Please cite this article in press as: M. Rahman, H.I. Andersson, Revolving flow of a fluid-particle suspension with suction, Alexandria Eng. J. (2017), http://dx.doi.org/10.1016/j.aej.2017.08.017

PAPER 3

B*ö*dewadt flow of a fluid-particle suspension with strong suction

M.Rahman , H.I.Andersson

Proceedings of 13th International Conference on Heat Transfer, Fluid Mechanics and Thermodynamics - HEFAT 2017, Portoroz, Slovenia, 17th-19th July (2017), pp. 59-64

BÖDEWADT FLOW OF A FLUID-PARTICLE SUSPENSION WITH STRONG SUCTION

Muhammad Rahman* and Helge I. Andersson
*Author for correspondence
Department of Energy and Process Engineering,
Norwegian University of Science and Technology-NTNU
Trondheim, 7491,
Norway,
E-mail: muhammad.rahman@ntnu.no

ABSTRACT

The three-dimensional revolving flow of a particle-fluid suspension above a plane surface has been considered. The flow represents an extension of the classical Bödewadt flow to a two-fluid problem. The governing equations for the two phases are coupled through an interaction force with the particle relaxation time τ as a free parameter. By means of a similarity transformation, the coupled set of non-linear ODEs becomes a two-point boundary value problem. The numerical results showed that the radial inward particle velocity increased whereas the circumferential velocity decreased by shortening τ, thereby strengthening the spiralling particle motion. On the contrary, the fluid motion was reduced as a result of the particle-fluid interactions.

NOMENCLATURE

A	[-]	Suction parameter
a	[m]	Particle radius
F	[-]	Radial velocity
G	[-]	Circumferential velocity
H	[-]	Axial velocity
m	[kg]	Particle mass
P	[-]	Pressure
p	$[N/m^2]$	Pressure
Q	[-]	Ratio between the densities
r	[m]	Radial coordinate
u,v,w	[m/s]	Cylindrical polar velocity components for fluid phase
u_p,v_p,w_p	[m/s]	Cylindrical polar velocity components for particle phase
z	[m]	Axial coordinate

Special characters

β	[-]	Reciprocal Stokes number
η	[-]	Dimensionless similarity variable
θ	[rad]	Circumferential coordinate
μ	$[N.s/m^2]$	Dynamic viscosity
ν	$[m^2/s]$	Kinematic viscosity
ρ	$[kg/m^3]$	Density of the fluid
τ	[s]	Relaxation time
Ω	[1/s]	Angular velocity

Subscripts

p	Particle
r	Radial direction
z	Axial direction
θ	Circumferential direction

INTRODUCTION

The steadily revolving flow of a viscous fluid above a planar surface is commonly known as Bödewadt flow; see Bödewadt [1]. The fluid motion well above the surface is characterised by a uniform angular velocity, which is reduced through a viscous boundary layer in order for the fluid to adhere to the no-slip condition at the solid surface. The reduction of the circumferential velocity component in the vicinity of the surface reduces the radially directed centripetal acceleration (or centrifugal force) such that the prevailing radial pressure gradient induces an inward fluid motion. In order to assure mass conservation, this inward fluid motion gives in turn rise to an axial upward flow. Such a spiralling flow exists near the planar surface, although more complex variations of the velocity field have been reported further away, but yet before the uniformly rotating flow conditions are reached. The oscillatory nature of the three velocity components reported by Bödewadt [1] has been subject to criticism, but this criticism was deem unjustified by Zandbergen and Dijkstra [2]. It is interesting to notice that these oscillations are damped and even suppressed in presence of a magnetic field (King and Lewellen [3]), partial slip (Sahoo, Abbasbandy and Poncet [4]) or suction (Nath and Venkatachala [5]). With a sufficiently high suction velocity through the planar surface, the axial flow is directed in the downward direction rather than upward, as is the case in the classical Bödewadt flow. In view of its fundamental importance as a prototype swirling flow the Bödewadt flow has received renewed focus in recent years. The inviscid instability of the Bödewadt boundary layer was examined by MacKerrell [6] whereas Sahoo [7] and Sahoo and Poncet [8] demonstrated that also such revolving flows of a non-Newtonian Reiner-Rivlin fluid admit exact similarity solutions.

The swirling flow induced by a steadily rotating disk was first described by von Kármán [9]. The von Kármán flow is essentially a reversed Bödewadt flow, albeit without the oscillatory features that characterize the latter. Zung [10] studied a von Kármán flow of a fluid-particle suspension and his analysis was subsequently extended by Sankara and Sarma [11] to include surface suction and further explored by Allaham and Peddieson [12].

The aim of the present study is to adopt a similar approach as that advocated by Zung [10] to Bödewadt flow of a fluid-particle suspension. After first having shown that the governing two-phase flow equations admit similarity solutions, numerical solutions of the coupled set of non-linear ordinary differential equations will show how the particle phase is revolving along with the fluid and also how the presence of particles will affect the swirling motion of the fluid phase.

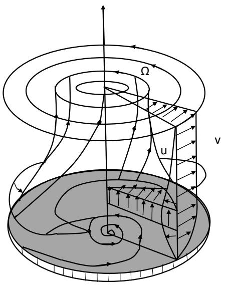

Figure 1. Sketch of the three-dimensional flow field set up by a steadily revolving flow high above the shaded surface. The variations of the radial (u) and circumferential (v) velocity components are indicated. The axial velocity component is upward, as in the classical B*ö*dewadt problem [1]. In presence of strong suction, as considered herein, the axial velocity is downward.

MATHEMATICAL MODEL EQUATIONS

Consider the steadily revolving flow of a fluid-particle suspension above a planar surface. In cylindrical polar coordinates (r,θ,z) the governing mass conservation and momentum equations for the fluid and particle phases become:

$$\frac{\partial}{\partial r}(ru)+\frac{\partial}{\partial z}(rw)=0, \tag{1}$$

$$\frac{\partial}{\partial r}(r\rho_p u_p)+\frac{\partial}{\partial z}(r\rho_p w_p)=0, \tag{2}$$

$$u\frac{\partial u}{\partial r}-\frac{v^2}{r}+w\frac{\partial u}{\partial z}=-\frac{1}{\rho}\frac{\partial p}{\partial r}+\nu\left[\frac{\partial^2 u}{\partial r^2}+\frac{\partial}{\partial r}\left(\frac{u}{r}\right)+\frac{\partial^2 u}{\partial z^2}\right]+\frac{F_r}{\rho}, \tag{3}$$

$$u\frac{\partial v}{\partial r}+\frac{uv}{r}+w\frac{\partial v}{\partial z}=\nu\left[\frac{\partial^2 v}{\partial r^2}+\frac{\partial}{\partial r}\left(\frac{v}{r}\right)+\frac{\partial^2 v}{\partial z^2}\right]+\frac{F_\theta}{\rho}, \tag{4}$$

$$u\frac{\partial w}{\partial r}+w\frac{\partial w}{\partial z}=-\frac{1}{\rho}\frac{\partial p}{\partial z}+\nu\left[\frac{\partial^2 w}{\partial r^2}+\frac{1}{r}\frac{\partial w}{\partial r}+\frac{\partial^2 w}{\partial z^2}\right]+\frac{F_z}{\rho}, \tag{5}$$

$$u_p\frac{\partial u_p}{\partial r}-\frac{v_p^2}{r}+w_p\frac{\partial u_p}{\partial z}=-\frac{1}{\rho_p}\frac{\partial p}{\partial r}-\frac{F_r}{\rho_p}, \tag{6}$$

$$u_p\frac{\partial v_p}{\partial r}+\frac{u_p v_p}{r}+w_p\frac{\partial v_p}{\partial z}=-\frac{F_\theta}{\rho_p}, \tag{7}$$

$$u_p\frac{\partial w_p}{\partial r}+w_p\frac{\partial w_p}{\partial z}=-\frac{1}{\rho_p}\frac{\partial p}{\partial z}-\frac{F_z}{\rho_p}, \tag{8}$$

where $(u,\ v,\ w)$ and $(u_p,\ v_p,\ w_p)$ are the velocity components of the fluid and particle phases in the radial, circumferential and axial directions, respectively. Here, we have assumed rotational symmetry about the vertical z-axis, $i.e.\partial/\partial\theta=0$. The kinematic viscosity of the fluid is ν and the densities of the fluid and particle phases are ρ and ρ_p. The above set of governing equations is the same as that considered by Zung [10] and Sankara and Sarma [11] for swirling von K*á*rm*á*n flow of a fluid-particle suspension above a steadily rotating disk, except that the a priori unknown pressure p was assigned only to the fluid phase. In the present study, however, the pressure gradients are shared between the two phases in proportion to their density ratio. This alternative formulation was suggested by Allaham and Peddeison [12] but not adopted in their subsequent calculations. In the present problem, however, it is essential to include pressure gradient terms also in the particle-phase equations of motion. Indeed, a radial pressure gradient is required to balance the centripetal acceleration in the far field in equation (6).

Particle-fluid interactions are accounted for by means of the following force components

$$F_r=\rho_p(u_p-u)/\tau, \tag{9}$$

$$F_\theta=\rho_p(v_p-v)/\tau, \tag{10}$$

$$F_z=\rho_p(w_p-w)/\tau, \tag{11}$$

included in the fluid phase equations and their negative counterparts in the particle phase equations. These expressions represent force per volume and are based on the assumption of a linear drag law, i.e. Stokes drag, where τ

$$\tau=m/6\pi\mu a, \tag{12}$$

is the relaxation time of a single spherical particle with mass m and radius a immersed in a fluid with dynamic viscosity $\mu=\rho\nu$.

The Stokes force defined in equations (9)-(11) represents a pragmatic way to account for fluid-particle interactions. The linear drag law assumes that the fluid is viscous and the particles are small. The relative velocity between fluid and particles, i.e. the slip velocity, should be sufficiently small to make the Reynolds number based on the slip velocity smaller than unity. These assumptions can be realistic for instance for dust particles in air and sand particles in water.

The viscous fluid phase sticks to the permeable planar surface at $z=0$ and attains a state of solid body rotation with angular velocity Ω high above the surface:

$$\left.\begin{array}{llll} u=0,\ v=0, & w=\sqrt{\nu\Omega}A & at & z=0 \\ u=0,\ v=r\Omega,\ p=\frac{1}{2}\rho r^2\Omega^2 & & as & z\to\infty \end{array}\right\}, \tag{13}$$

where $A \leq 0$ is a dimensionless suction velocity. The inviscid particle phase can be assumed to follow the motion of the fluid phase far above the solid surface, i.e.

$$\left.\begin{array}{ll} u_p=u=0, & v_p=v=r\Omega, \\ w_p=w, & \rho_p=\rho, \end{array}\right\} \ for\ z\to\infty. \tag{14}$$

It is noteworthy that the boundary conditions (14) for the particle phase are imposed only far above the solid surface. Allaham and Peddieson [12] considered the possibility of including viscous effects also in the particle equations. If so, the particle equations would become of second-order and no-slip conditions should be imposed at the solid surface. In the present study, however, we follow the way paved by Zung [10] and Sankara and Sarma [11] and viscous terms have been ignored in the particle equations. The equations (6)-(8) are first-order PDEs and the boundary conditions (14) suffice and make the problem well-posed.

SIMILARITY TRANSFORMATION AND RESULTING ODEs

The two-phase flow that arises above the planar surface can be characterized by the length scale $\sqrt{\nu/\Omega}$, the time scale Ω^{-1} and the velocity scale $\sqrt{\nu\Omega}$. One can therefore introduce the same dimensionless similarity variables as used already by von Kármán [9] and Bödewadt [1]:

$$\eta = z\sqrt{\Omega/\nu}. \tag{15}$$

The same similarity transformations are used for the fluid phase velocities and pressure:

$$\begin{array}{c} u(r,z)=r\Omega F(\eta), \\ v(r,z)=r\Omega G(\eta), \\ w(r,z)=\sqrt{\nu\Omega}H(\eta), \\ p(r,z)=\rho(-\nu\Omega P(\eta)+\frac{1}{2}r^2\Omega^2). \end{array} \tag{16}$$

The latter pressure transformation was not required in Bödewadt's original approach which was based on the boundary layer approximations. That assumption implies that the pressure is constant all across the boundary layer.

The variables characterizing the particle phase can be recast into dimensionless forms by means of the transformation used by Sankara and Sarma [11]:

$$\begin{array}{c} u_p(r,z)=r\Omega F_p(\eta), \\ v_p(r,z)=r\Omega G_p(\eta), \\ w_p(r,z)=\sqrt{\nu\Omega}H_p(\eta), \\ \rho_p(r,z)=\rho Q(\eta), \end{array} \tag{17}$$

where Q is the ratio between the densities of the two phases. The governing set of partial differential equations (1)-(8) transforms into a set of ordinary differential equations:

$$2F+H'=0, \tag{18}$$

$$Q'H_p+QH_p{}'+2QF_p=0, \tag{19}$$

$$F''-HF'-F^2+G^2+\beta Q(F_p-F)=1, \tag{20}$$

$$G''-HG'-2FG+\beta Q(G_p-G)=0, \tag{21}$$

$$P'=-2FH+2F'-\beta Q(H_p-H), \tag{22}$$

$$F_p{}'H_p+F_p^2-G_p^2+\beta(F_p-F)=-1/Q, \tag{23}$$

$$G_p{}'H_p+2F_pG_p+\beta(G_p-G)=0, \tag{24}$$

$$QH_p{}'H_p+\beta Q(H_p-H)=P', \tag{25}$$

where the prime denotes differentiation with respect to the similarity variable η. The accompanying boundary conditions (13)-(14) transform into:

$$F(\eta)=0,\ G(\eta)=0,\ H(\eta)=A, \quad at\ \eta=0,$$

$$\left.\begin{array}{l} F(\eta)=0,\ \ G(\eta)=1, \quad P(\eta)=1, \\ F_p(\eta)=0,\ G_p(\eta)=1,\ H_p(\eta)=H(\eta), \\ Q(\eta)=1. \end{array}\right\} as \quad \eta\to\infty. \tag{26}$$

The resulting two-fluid flow problem now depends only on two dimensionless parameters, namely the suction parameter A and the interaction parameter $\beta = 1/\Omega\tau$ where τ was introduced in equation (12). The ratio between a particle time scale and a fluid time scale, e.g. $\tau/\Omega^{-1} = \beta^{-1}$, is often referred to as a Stokes number.

NUMERICAL INTEGRATION TECHNIQUE

The primary interest is in the flow field. The pressure gradient P' can therefore be eliminated from the axial components of the fluid and particle equations to give

$$H_p{}' = \left(2F' - 2\beta Q(H_p - H) - 2FH\right)/H_pQ. \qquad (27)$$

The bvp4c MATLAB solver, which gives very good results for non-linear ODEs with multipoint BVPs, has been used. This finite-difference code utilizes the 3-stage Lobatto IIIa formula, that is a collocation formula and the collocation polynomial provides a C1-continuous solution that is fourth-order accurate uniformly in [a,b]. For multipoint BVPs, the solution is C1-continuous within each region, but continuity is not automatically imposed at the interfaces. Mesh selection and error control are based on the residual of the continuous solution. Analytical condensation is used when the system of algebraic equations is formed; see Shampine et al.[13].

The coupled set of non-linear ODEs are integrated for $A = -3.0$ and some different values of β. Suction [5], as well as the presence either of surface slip [4] or a magnetic force field [3], tends to stabilize the revolving flow with respect to the oscillating behaviour of the three velocity components reported already by Bödewadt [1]. This is the likely reason why it turned out to be difficult to perform the present computations without suction, i.e. for $A = 0$.

RESULT AND DISCUSSIONS

The primarily interest is in particle-fluid interactions in the three-dimensional flow field. Four different values of the particle fluid interaction parameter β in the range from 0.3 to 4.0 have therefore been considered. The suction parameter A was kept constant and equal to -3.0. This particular parameter value is 50% higher than the strongest suction considered by Nath and Venkatachala [5] albeit without a particle phase.

One can see from Figure 2 that the radial inward flow is reduced in the presence of particles and this reduction increases with β . This is caused by the interaction force F_r which is positive since $u_p > u$ everywhere except in the near vicinity of the surface. It is noteworthy that also the particle phase flows towards the symmetry axis. The particle velocity u_p in Figure 3 is radially inward and increases in magnitude all the way towards the surface. This inward motion strengthens monotonically with increasing interaction parameter β. Contrary to u, however, u_p does not obey no-slip at the surface. This gives rise to a change-of-sign of the slip velocity $u_p - u$ next to the surface and thereby a reversal of the radial force F_r defined in equation (9). The slip velocity presented in Fig 4 shows that the thickness of the near-wall layer with $F_r < 0$ increases from about 0.03 to $0.2\sqrt{\nu/\Omega}$ as β increases from 0.3 to 4.0.

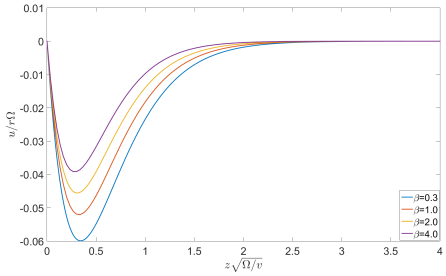

Figure 2. Radial fluid velocity component $F = u/r\Omega$ for some different values of the interaction parameter β.

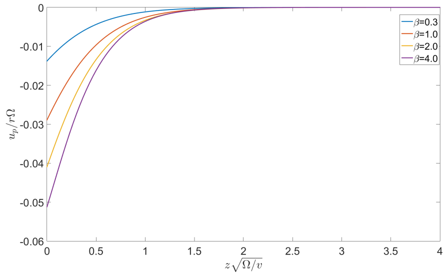

Figure 3. Radial particle velocity component $F_p = u_p/r\Omega$ for some different values of the interaction parameter β.

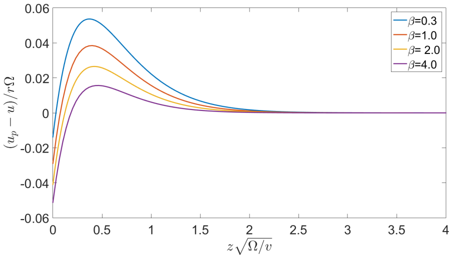

Figure 4. Difference between the particle and fluid velocities $F_p - F$ for some different values of the interaction parameter β.

The interaction parameter β has an almost negligible effect on the circumferential fluid velocity v in Figure 5 which reduces monotonically from that of solid body rotation $v = r\Omega$ to no-slip $v = 0$ at the surface. The circumferential slip velocity $v_p - v$ becomes inevitably positive in the viscous boundary layer since the particle velocity v_p is neither affected by viscous forces nor obeys no-slip. The circumferential interaction force F_θ on the fluid phase is positive, whereas the reaction force on the particle phase $-F_\theta < 0$ and therefore tends to enhance the deceleration of the particle motion with increasing β, as one can observe in Figure 6.

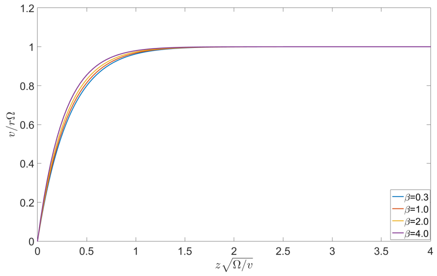

Figure 5. Circumferential fluid velocity component $G = v/r\Omega$ for some different values of the interaction parameter β.

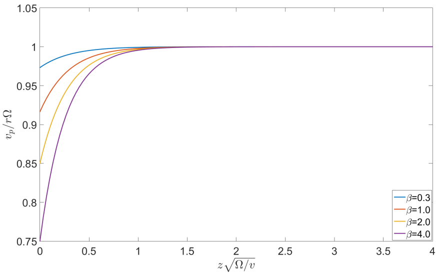

Figure 6. Circumferential particle velocity component $G_p = v_p/r\Omega$ for some different values of the interaction parameter β.

The fluid phase flows axially towards the surface, i.e. $w < 0$, as can be seen in Figure 7. This opposite flow direction compared to that in classical Bödewadt flow $(w > 0)$ is due the strong surface suction. The magnitude of the downward flow can be seen to increase from that beyond $\eta = z\sqrt{\Omega/\nu} \approx 2$ where solid-body rotation prevails through the viscous boundary layer until $w/\sqrt{\nu\Omega} = -3.0$ at the surface $z = 0$. The interaction force F_z is generally positive since the slip velocity $w_p - w > 0$ (compare Figs 7 and 8). The axial convection is $w_p\partial w_p/\partial z = 1/2\partial w_p^2/\partial z$ is partially balanced by the negative reaction force $-F_z$ in the particle equation (8). However, the dimensionless pressure P decreases monotonically upwards, i.e. $P' < 0$. This variation gives rise to a positive pressure gradient in the axial direction, i.e. a pressure force that acts towards the surface and thus tends to support the axial motion towards the surface.

The relative density Q, i.e. the ratio between the particle and fluid densities ρ_p/ρ, is a variable quantity that has been obtained as an integral part of the numerical solution of the flow problem. The Q-profiles in Figure 9 show that the particle density ρ_p is only a few percent lower than the fluid density near the surface but increases to match ρ outside of the viscous boundary layer.

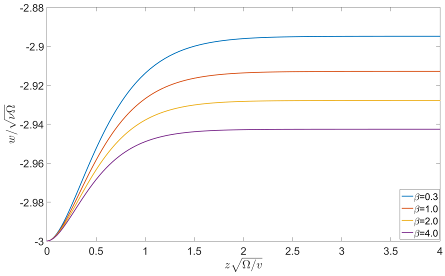

Figure 7. Axial fluid velocity component $H = w/\sqrt{\nu\Omega}$ for some different values of the interaction parameter β.

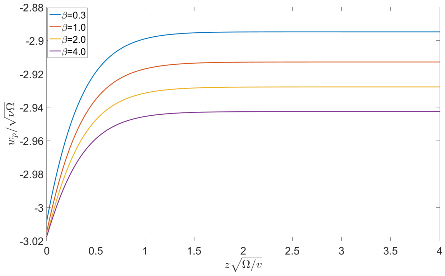

Figure 8. Axial particle velocity component $H_p = w_p/\sqrt{\nu\Omega}$ for some different values of the interaction parameter β.

Let us finally look at the motion of the particle phase in the limit as $\beta \to 0$ if $\rho_p = \rho$. The horizontal velocity components become $u_p = 0$ and $v_p = r\Omega$, i.e. the radial component vanishes and the linearly increasing circumferential velocity makes the centripetal acceleration exactly balance the radial pressure force.

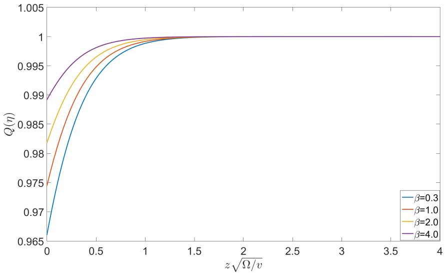

Figure 9. Ratio of particle and fluid densities $Q = \rho_p/\rho$ for some different values of the interaction parameter β.

Some primary boundary layer characteristics obtained from the numerical solutions are given in Table 1. For the fluid phase:$-F'(0)$, $G'(0), -H(\infty)$. For the particle phase: $-F_p(0)$, $G_p(0)$, $-H_p(0)$. The following observations can be made from the tabulated results. The magnitude of the slope of the radial velocity $F'(0)$ decreases with increasing fluid-particle interactions. The slope of the circumferential fluid velocity $G'(0)$ increases with increasing β (not clearly visible in Figure 5). The magnitude of the downward fluid velocity $-H(\infty)$ is slightly increased from 2.8948 to 2.9426 with increasing β . The circumferential particle velocity $G_p(0)$ decreases from 0.9732 to 0.7501 as β increases from 0.3 to 4.0. The inward radial particle velocity $-F_p(0)$ increases from about 0.0138 to 0.0512 as β is increased.

Table 1. Flow characteristics for suction parameter $A = -3.0$.

β	$-F'(0)$	$-F_p(0)$	$G_p(0)$	$G'(0)$	$-H_p(0)$	$-H(\infty)$
0.3	0.4547	0.0138	0.9732	3.1441	3.0008	2.8948
1.0	0.4156	0.0289	0.9165	3.3142	3.0145	2.9129
2.0	0.3853	0.0409	0.8501	3.5125	3.0173	2.9278
4.0	0.3607	0.0512	0.7501	3.8098	3.0174	2.9426

CONCLUDING REMARKS

The present study adopted a two-fluid approach to model the presence of solid particles in a viscous carrier fluid. The particles have been treated as a continuous solid phase modelled by the Eulerian partial differential equations (6)-(8). Alternatively, the particles could have been treated as individual point-particles and modelled by Lagrangian ordinary differential equations (one set of ODEs for each and every particle), as described for instance by Zhao et al. [14].

The governing equations of the three-dimensional two-fluid problem have been transformed into a coupled set of ordinary differential equations by means of an exact similarity transformation. The resulting set of ODEs is a two parameter problem in terms of the dimensionless suction velocity A and the fluid-particle interaction parameter β. Here, β is the ratio between the rotation time scale Ω^{-1} and the particle relaxation time τ. β is therefore a reciprocal Stokes number.

The particles are spiralling inwards in the vicinity of the surface. The radial inward velocity $|u_p|$ increases and the circumferential velocity v_p decreases with increasing interaction parameter β, i.e. the spiralling increases with β. This phenomenon is commonly known as the tea cup effect: when the tea is stirred, tea leaves near the bottom move towards the centre of the cup and heap up. Contrary to the particle phase, the inward spiralling of the fluid phase is gradually reduced as the fluid-particle interaction parameter is increased. The circumferential flow is only modestly affected, but the surface shear stress is nevertheless increased.

REFERENCES

[1] Bödewadt, U. T. "Die Drehströmung Über festem Grunde." Journal of Applied Mathematics and Mechanics/Zeitschrift für Angewandte Mathematik und Mechanik 20. (1940): 241-253.

[2] Zandbergen, P. J., and D. Dijkstra. "Von Kármán swirling flows." Annual Review of Fluid Mechanics 19. (1987): 465-491.

[3] King, W. S., and W.S.Lewellen. "Boundary-layer similarity solutions for rotating flows with and without magnetic interaction." Physics of Fluids 7. (1964): 1674-1680.

[4] Sahoo, B., Abbasbandy, S., Poncet, S. A brief note on the computation of the Bödewadt flow with Navier slip boundary conditions. Computers Fluids, 90. (2014): 133-137.

[5] Nath, G., and B. J. Venkatachala. "The effect of suction on boundary layer for rotating flows with or without magnetic field." Proceedings of the Indian Academy of Sciences-Section A. 85. (1977): 332-337.

[6] MacKerrell, S.O. "Stability of Bödewadt flow." Philosophical Transactions of the Royal Society of London A: Mathematical, Physical and Engineering Sciences 363. (2005): 1181-1187.

[7] Sahoo, B. "Steady Bödewadt flow of a non-Newtonian Reiner-Rivlin fluid." Differential Equations and Dynamical Systems 20. (2012): 367-376.

[8] Sahoo, B., and S.Poncet. "Effects of slip on steady Bödewadt flow of a non-Newtonian fluid." Communications in Nonlinear Science and Numerical Simulation 17. (2012): 4181-4191.

[9] Kármán, Th V. "Über laminare und turbulente Reibung." Journal of Applied Mathematics and Mechanics/Zeitschrift für Angewandte Mathematik und Mechanik 1. (1921): 233-252.

[10] L.B Zung. "Flow induced in fluid-particle suspension by infinite rotating disk." Physics of Fluids, 12. (1969): 18-23.

[11] Sankara, K.K., and L. V. K. V. Sarma. "On the steady flow produced in fluid-particle suspension by an infinite rotating disk with surface suction." International Journal of Engineering Science 23. (1985): 875-886.

[12] Allaham, M.A., and J.Peddieson. "The flow induced by a rotating disk in a particulate suspension." International Journal of Engineering Science 31. (1993): 1025-1034.

[13] Shampine, L.F., J.Kierzenka, and M.W. Reichelt. "Solving boundary value problems for ordinary differential equations in MATLAB with bvp4c." Tutorial notes (2000): 437-448.

[14] Zhao, L.H., H.I. Andersson and J.J.J. Gillissen. "Turbulence modulation and drag reduction by spherical particles". Physics of Fluids 22. (2010) 081702.

PAPER 4

On heat transfer in unsteady von K$\acute{a}$rm$\acute{a}$n flow

M.Rahman , H.I.Andersson

Submitted to: International Journal of Heat and Mass Transfer, (2017)

On heat transfer in unsteady Von K*á*rm*á*n flow

Muhammad Rahman*, Helge I.Andersson

Department of Energy and Process Engineering,
Norwegian University of Science and Technology, Trondheim, Norway

---

Abstract

Heat transfer in revolving flow driven by a decelerating rotating disk has been considered. The well-known similarity transformation of the three-dimensional flow problem has been extended to also transform the thermal energy equation into an ordinary differential equation. An analytical solution has been derived for the temperature distribution in the vicinity of the disk. Sample solutions of the resulting two-parameter problem have been presented to illustrate the combined effects of deceleration and thermal diffusivity. One could observe that the thermal boundary layer became thinner at higher Prandtl numbers and for faster disk deceleration.

Keywords: `Heat transfer; Similarity solutions; Decelerating disk flow; High-Pr asymptote.`

---

1. Introduction

The fluid flow induced by a steadily rotating disk was first considered by von K*á*rm*á*n [1] who devised an ingenious similarity transformation, by means of which the axisymmetric Navier-Stokes equations were transformed into a set of ordinary differential equations (ODEs). While von K*á*rm*á*n [1] obtained approximate solutions for the three velocity components by means of the momentum integral method approach, more accurate solutions were obtained by Cochran [2] and Rogers & Lance [3]; see also the review article by Zandbergen & Dijkstra [4]. The accompanying heat transfer problem was first studied by Millsaps & Pohlhausen [5] and Sparrow & Gregg [6], followed by several others.

A prerequisite for steady-state solutions to exist is that the disk is rotating steadily with a constant angular velocity Ω_0. Unsteady flows induced by a time-varying angular velocity $\Omega(t)$ of the disk has also received considerable attention in the past, for instance by consideration of a step-change in Ω, an impulsively start-up from rest, and a torsionally oscillating disk. A particularly attractive case is a decelerating disk for which the angular velocity Ω decreases inversely proportional to time, i.e. $\Omega(t) = \Omega_0(1-\alpha t)^{-1}$ where α is a constant measured in sec^{-1} which discriminates between an accelerating $(\alpha > 0)$ and a decelerating $(\alpha < 0)$ disk. Similarity solutions of the unsteady Navier-Stokes equations are rare (see the review by Wang [7]), but Watson & Wang [8] nevertheless obtained a transformation which exactly transformed the time-dependent Navier-Stokes equations to ODEs in the similarity variable. A particularly peculiar observation made by Watson & Wang [8] was that the fluid in the vicinity of the disk rotates faster rather than slower than the disk for a sufficiently fast deceleration of the disk. One may wonder if and how these circumstances may affect the temperature distribution in the fluid and, in particular, the heat transfer between the decelerating disk and the fluid.

The aim of the present paper is to investigate the unsteady heat transfer from an isothermal disk. Such time-dependent problems were studied for instance by Attia [9, 10], who solved a system of partial differential equations in terms of a modified axial coordinate and time. Here, however, we will first demonstrate that the heat transfer in the unsteady flow that results from a decelerating disk can be obtained in terms of the same similarity variable as that introduced by Watson & Wang [8]. Numerical solutions of the resulting ODEs will be presented for different values of the unsteadiness parameter α/Ω_0 and Prandtl number Pr.

2. Mathematical Model Equations

The full equations governing unsteady mass, momentum, and thermal energy conservation in cylindrical polar coordinates (r,θ,z) are:

$$\frac{\partial}{\partial r}(ru)+\frac{\partial}{\partial z}(rw)=0, \tag{1}$$

$$\frac{\partial u}{\partial t}+u\frac{\partial u}{\partial r}-\frac{v^2}{r}+w\frac{\partial u}{\partial z}=-\frac{1}{\rho}\frac{\partial p}{\partial r}+\nu\left[\frac{\partial^2 u}{\partial r^2}+\frac{\partial}{\partial r}\left(\frac{u}{r}\right)+\frac{\partial^2 u}{\partial z^2}\right], \tag{2}$$

---

*Corresponding author

Email address: `muhammad.rahman@ntnu.no` (Muhammad Rahman)

$$\frac{\partial v}{\partial t}+u\frac{\partial v}{\partial r}+\frac{uv}{r}+w\frac{\partial v}{\partial z}=\nu\left[\frac{\partial^2 v}{\partial r^2}+\frac{\partial}{\partial r}\left(\frac{v}{r}\right)+\frac{\partial^2 v}{\partial z^2}\right], \quad (3)$$

$$\frac{\partial w}{\partial t}+u\frac{\partial w}{\partial r}+w\frac{\partial w}{\partial z}=-\frac{1}{\rho}\frac{\partial p}{\partial z}+\nu\left[\frac{\partial^2 w}{\partial r^2}+\frac{1}{r}\frac{\partial w}{\partial r}+\frac{\partial^2 w}{\partial z^2}\right], \quad (4)$$

$$\rho C_p\left(\frac{\partial T}{\partial t}+u\frac{\partial T}{\partial r}+w\frac{\partial T}{\partial z}\right)=k\left(\frac{\partial^2 T}{\partial r^2}+\frac{1}{r}\frac{\partial T}{\partial r}+\frac{\partial^2 T}{\partial z^2}\right), \quad (5)$$

where symmetry about the z-axis, i.e. $\partial/\partial\theta=0$, has been assumed. Here, (u, v, w) are the velocity components in the radial, circumferential and axial directions, respectively, and p and T are the pressure and temperature in the fluid. The density ρ, the kinematic viscosity ν, the thermal conductivity k, and the specific heat at constant pressure C_p are constant properties of the Newtonian fluid.

The relevant boundary conditions on the velocity and temperature field are:

$$\left.\begin{array}{ll} u=0, v=r\Omega_0(1-\alpha t)^{-1}, w=0, T=T_w, & at \quad z=0, \\ u=0, v=0, p=0, T=T_\infty, & as \quad z\to\infty, \end{array}\right\}. \quad (6)$$

Here, $\Omega_0(1-\alpha t)^{-1}$ and T_w are the angular velocity and temperature of the rotating disk, while T_∞ is the temperature infinitely far away from the disk. The constant α determines the rate of change of the angular velocity of the disk. For accelerating disks, i.e. $\alpha>0$, the expression for the time-dependent boundary condition for the circumferential velocity v at the disk is well-posed only for relatively short times, i.e. $t<\alpha^{-1}$.

3. Similarities Transformations

The velocity and temperature governed by the partial differential equations (1)-(5) are functions of r, z, and t. Here, we adopt the same similarity transformations as those used by Watson & Wang [8] to solve the unsteady flow problem:

$$\begin{aligned} u(r,z,t)&=r\Omega_0(1-\alpha t)^{-1}F(\eta), \\ v(r,z,t)&=r\Omega_0(1-\alpha t)^{-1}G(\eta), \\ w(r,z,t)&=-2\sqrt{\nu\Omega_0}(1-\alpha t)^{-\frac{1}{2}}H(\eta), \\ p(r,z,t)&=-\rho\nu\Omega_0 P(\eta)(1-\alpha t)^{-1}, \\ T(r,z,t)&=T_\infty+(T_w-T_\infty)\Theta(\eta), \end{aligned} \quad (7)$$

where η is the dimensionless similarity variable

$$\eta=z\sqrt{\Omega_0/\nu}(1-\alpha t)^{-\frac{1}{2}}. \quad (8)$$

Similarly, we have also assumed that the temperature $T(r,z,t)$ can be expressed as a function only of the similarity variable η. In terms of the non-dimensional variables defined in equations (7) and (8), the governing partial differential equations (1)-(5) transform to:

$$H'-F=0, \quad (9)$$

$$F''+2HF'-F^2+G^2-\hat{\alpha}[F+\frac{\eta}{2}F']=0, \quad (10)$$

$$G''+2HG'-2FG-\hat{\alpha}[G+\frac{\eta}{2}G']=0, \quad (11)$$

$$P'-4FH-2F'+\hat{\alpha}[H+\eta F]=0, \quad (12)$$

$$\Theta''+2PrH\Theta'-\frac{1}{2}\hat{\alpha}Pr\eta\Theta'=0. \quad (13)$$

Here, $\hat{\alpha}=\alpha/\Omega_0$ is a non-dimensional unsteadiness parameter and Pr is the Prandtl number $Pr=C_p\mu/k$. The boundary conditions (6) transform to:

$$\begin{array}{llllll} F(\eta)=0, & G(\eta)=1, & H(\eta)=0, & \Theta(\eta)=1, & at & \eta=0, \\ F(\eta)=0, & G(\eta)=0, & P(\eta)=1, & \Theta(\eta)=0, & as & \eta\to\infty, \end{array} \quad (14)$$

The similarity transformations (7), (8) are equivalent with those used by Watson & Wang [8] and the resulting set of ODEs for the velocity field (9)-(12) is therefore the same as their transformed equations. The purpose of the present paper, however, is to extend their work to also include heat transfer analysis. Attia [9, 10] studied heat transfer in transient flow caused by a suddenly imposed rotation of a disk. By means of the same similarity variable $\eta=z\sqrt{\Omega_0/\nu}$ as originally used by von K*á*rm*á*n [1], he transformed the governing equations for the heat and fluid flow problem to a set of partial differential equations in η and t. Attia [9, 10] neglected the effect of thermal diffusion in the radial direction in the thermal energy equation, i.e. the two first terms on the right-hand side of equation (5). These terms are retained herein for the sake of generality, but vanish exactly when we assume the temperature field $T(r,z,t)$ to be independent of r in accordance with the similarity transformation (7, 8).

4. Analytical Solution For The Temperature Field

The ODE (13) for the thermal field can be integrated twice to give the solution for the temperature profile:

$$\Theta(\eta)=1-\frac{I(\eta)}{I(\infty)}, \quad (15)$$

where

$$I(\eta)=\int_0^\eta\left\{exp\left[-2Pr\int_0^t Hds+\frac{1}{4}\hat{\alpha}Prt^2\right]\right\}dt, \quad (16)$$

and $H(\eta)$ is the axial velocity component obtained from the solution of the accompanying flow problem. Now, with $I'(\eta)=exp\left[-2Pr\int_0^\eta Hds+\frac{1}{4}\hat{\alpha}Pr\eta^2\right]$ and therefore $I'(0)=1$ the temperature gradient at the surface of the disk becomes:

$$\Theta'(0)=-\frac{I'(0)}{I(\infty)}=-\frac{1}{I(\infty)}. \quad (17)$$

The Nusselt number is usually defined as $Nu = hL/k$ where the length scale L can be taken as $L(t) = \sqrt{\frac{\nu}{\Omega(t)}} = \sqrt{\frac{\nu}{\Omega_0}}(1-\alpha t)^{\frac{1}{2}}$ and the heat transfer coefficient h is defined in terms of the heat flux q at the rotating disk as $h = \frac{q(0)}{T_w - T_\infty} = \frac{-k\partial T/\partial z|_{z=0}}{T_w - T_\infty}$. The Nusselt number therefore becomes

$$Nu = -\Theta'(0). \tag{18}$$

For high Prandtl numbers, the temperature adjustment will occur deep inside the momentum boundary layer where all other effects than the viscous stress are negligible in equation (10), i.e. $F'' = 0$. Therefore $F(\eta) = \eta F'(0)$ which satisfies the no-slip boundary condition $F(0) = 0$. From the mass conservation equation (9) we accordingly obtain that

$$H(\eta) = \int_0^\eta F(s)ds = \int_0^\eta F'(0)sds = \frac{1}{2}F'(0)\eta^2, \tag{19}$$

satisfying the impermeability boundary condition $H(0) = 0$. This gives the solution

$$I(\eta) = \int_0^\eta \left\{ exp\left[-\frac{1}{3}PrF'(0)t^3 + \frac{1}{4}\hat{\alpha}Prt^2 \right] \right\} dt, \tag{20}$$

in the high-Pr limit. This solution depends both on Pr and $\hat{\alpha}$, but the $\hat{\alpha}$-dependence is likely to dominate for t-values $\ll 1$. Therefore, we get from the above that:

$$I(\infty) = \int_0^\infty \left\{ exp\left[\frac{1}{4}\hat{\alpha}Prt^2 \right] \right\} dt = \sqrt{\frac{\pi}{-\hat{\alpha}Pr}}, \tag{21}$$

so that we finally obtain the temperature variation:

$$\Theta(\eta) = 1 - \sqrt{\frac{-\hat{\alpha}Pr}{\pi}} \int_0^\eta \left\{ exp\left[\frac{1}{4}\hat{\alpha}Prt^2 \right] \right\} dt, \tag{22}$$

for sufficiently high Prandtl numbers.

5. Numerical Approach

We solved the two-point boundary value problem consisting of the coupled set of ordinary differential equations (9)-(13) subjected to the boundary conditions (14). For this purpose we have used the bvp4c MATLAB solver, which gives very good results for the non-linear ODEs with multipoint BVPs. This finite-difference code utilizes the 3-stage Lobatto IIIa formula, that is a collocation formula and the collocation polynomial provides a C1-continuous solution that is fourth-order accurate uniformly in [a,b]. For multipoint BVPs, the solution is C1-continuous within each region, but continuity is not automatically imposed at the interfaces. Mesh selection and error control are based on the residual of the continuous solution. Analytical condensation is used when the system of algebraic equations is formed; see Shampine et al.[11] for further details. Although our interest is in solutions of the thermal problem, we rely on accurate solutions of the fluid flow problem. Watson & Wang [8] showed that the existence of a momentum boundary layer on the rotating disk is possible only when $\hat{\alpha} < 0$, i.e. when the disk is decelerating. They presented numerical solutions for eight different values of the unsteadiness parameter in the range $0 \leq -\hat{\alpha} \leq 20$ for decelerating rotation. This parameter range was recently extended up to $\hat{\alpha} = -100$ by Hussain et al. [12]. Here, we have recomputed the three-dimensional flow field for six of the eight parameter values considered by Watson & Wang [8]. The comparison made in Table 1 shows that the present computational method closely reproduce the earlier reported results for the flow field.

Table 1: Effect of unsteadiness parameter $\hat{\alpha}$ on the flow characteristics $F'(0)$, $G'(0)$ and $H(\infty)$. Comparisons with results computed by Watson and Wang [8] in their Table 1.

$\hat{\alpha}$	$F'(0)$		$G'(0)$		$H(\infty)$	
	present	W & W	present	W & W	present	W & W
0	0.5102	0.510225	-0.6159	-0.615917	0.4420	0.4417
-0.5	0.6141	0.614283	-0.4284	-0.428406	0.4255	0.4255
-1.0	0.7198	0.719787	-0.2366	-0.236575	0.4177	0.4177
-2.0	0.9315	0.931507	0.1550	0.154981	0.4096	0.4096
-5.0	1.5626	1.562797	1.3608	1.360850	0.4005	0.4006
-10	2.5981	2.600801	3.4134	3.413860	0.3950	0.3957

6. Results and Disscussion

The variation of the radial velocity component $F(\eta)$ in Figure 1 shows that the momentum boundary layer becomes thinner and more pronounced for increasing magnitudes of $\hat{\alpha}$. The circumferential velocity component $G(\eta)$ in Figure 2 shows that the fluid next to the disk rotates slower than the disk as long as the magnitude of the unsteadiness parameter $\hat{\alpha}$ is small, i.e. similarly as for the case of a steadily rotating disk $\hat{\alpha} = 0$. When $\hat{\alpha} < -1.606699$ (according to Watson & Wang [8]), however, the fluid in the vicinity of the disk rotates faster than the disk. This puzzling observation first reported by Watson & Wang [8] is probably a result of the fast deceleration of the disk, whereas the inertia of the adjacent fluid layer enables the fluid to maintain its angular momentum for a longer while.

The distinct thinning of the boundary layer with increasing negative $\hat{\alpha}$ can also be seen for the axial velocity component $H(\eta)$ in Figure 3. Here, the asymptotic value $H(\infty)$ far from the disk represents the suction velocity required in order for the axial inflow to balance the radially-directed flow away from the axis of rotation. The reduction of $H(\infty)$ with increasing deceleration suggests that although the peak of the radial velocity F increases with increasing deceleration, as seen in Figure 1, the associated flow rate in the radial direction, i.e. $\int_0^\infty F(\eta)d\eta$, decreases. This is a direct consequence of the transformed mass conservation equation (9), which upon integration gives that $\int_0^\infty F(\eta)d\eta = \int_0^\infty H' d\eta = H(\infty)$ since $H(0) = 0$. The data in Table 1 shows that the suction velocity $H(\infty)$ has been reduced by ca 10 percent as the deceleration rate $-\hat{\alpha}$ has increased from 0 to 10. According to the results computed by Hussain et al. [12], this reduction continues as $-\hat{\alpha}$ is further increased.

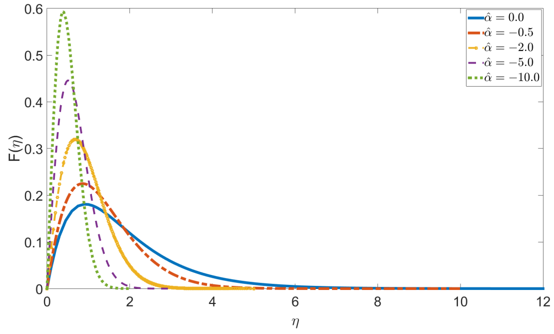

Figure 1: Radial velocity component $F(\eta)$ for some different values of the unsteadiness parameter $\hat{\alpha}$.

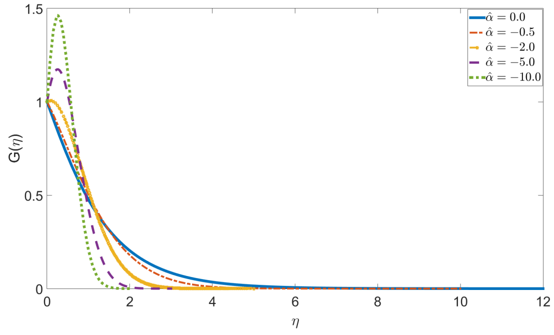

Figure 2: Circumferential velocity component $G(\eta)$ for some different values of the unsteadiness parameter $\hat{\alpha}$.

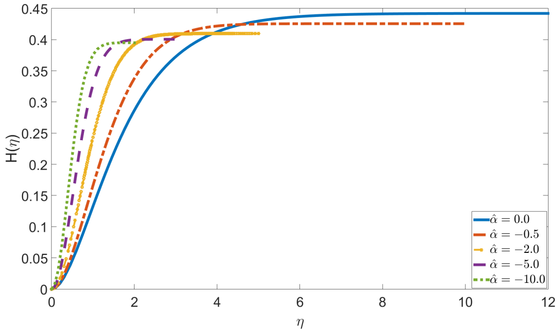

Figure 3: Axial velocity component $H(\eta)$ for some different values of the unsteadiness parameter $\hat{\alpha}$.

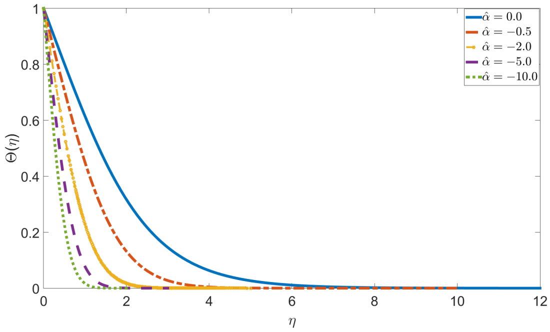

Figure 4: Variation of temperature $\Theta(\eta)$ for different values of unsteadiness parameter $\hat{\alpha}$ with $Pr = 1$.

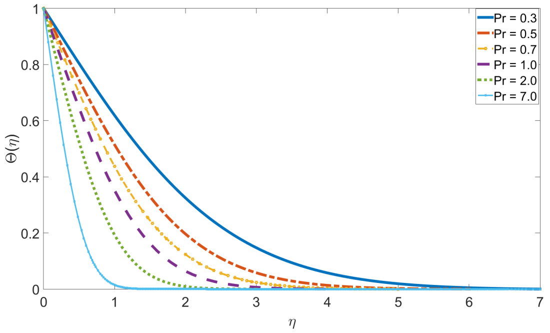

Figure 5: Variation of temperature $\Theta(\eta)$ for different Prandtl numbers and $\hat{\alpha} = -1.0$.

While the similarity problem for the fluid flow depends only on the unsteadiness parameter $\hat{\alpha}$, the accompanying heat transfer problem is a two-parameter problem in $\hat{\alpha}$ and Pr. Numerical solutions have been obtained for six different Prandtl numbers Pr in the range from 0.3 to 7.0. The results presented in Figure 4 show how the temperature $\Theta(\eta)$ decreases monotonically from the disk and outwards for $Pr = 1.0$. The thermal boundary layer extends to about $\eta \approx 6$ for the steadily rotating disk ($\hat{\alpha} = 0$), but the thickness of the thermal boundary layer becomes significantly thinner as the disk decelerates faster and faster.

An objective measure of the dimensionless thickness of the thermal boundary layer is η_δ defined as the η-value at which the dimensionless temperature has decreased to 1 percent of its value at the disk, i.e. $\Theta(\eta_\delta) = 0.01$. Values for η_δ are provided in Table 2. The same variation with increasing unsteadiness as observed in Figure 4 and the same dependence on the Prandtl number as seen in Figure 5 are found for all parameter combinations. The corresponding penetration depth is:

$$\delta_T = \eta_\delta \sqrt{\nu/\Omega_0}(1-\alpha t)^{1/2} = \eta_\delta \sqrt{\nu/\Omega(t)}. \tag{23}$$

This expression shows that the temperature of the isothermally heated disk is felt deeper into the ambient fluid as time goes on.

Table 2: Dimenssionless boundary layer thickness η_δ

$Pr\backslash\hat{\alpha}$	0	-0.5	-1.0	-2.0	-5.0	-10.0
0.3	11.333	7.287	5.500	4.050	2.600	1.800
0.5	9.933	5.407	4.200	3.167	2.100	1.500
0.7	8.067	4.407	3.467	2.633	1.767	1.267
1.0	6.133	3.563	2.833	2.178	1.467	1.100
2.0	3.700	2.407	1.944	1.511	1.033	0.733
7.0	1.867	1.289	1.044	0.822	0.567	0.400

The gradual thinning of the thermal boundary layer inevitably leads to a substantially enhanced heat transfer rate at the disk. The data in Table 3 show that the magnitude of $\Theta'(0)$, and thereby the Nusselt number, increases almost by a factor 5 as the deceleration increases from $\hat{\alpha} = 0$ to $\hat{\alpha} = -10$. The temperature profiles $\Theta(\eta)$ for the unsteadiness parameter $\hat{\alpha} = -1$ in Figure 5 show how the temperature adapts from the disk temperature $\Theta(0) = 1$ to the asymptotic limit $\Theta \to 0$ for $\eta \gg 1$ and how this adaption depends on the Prandtl number. As the thermal diffusivity reduces for higher Pr, the excess disk temperature is felt in a gradually thinner and thinner layer. The data for the temperature gradient in Table 3 show that the deceleration of the rotating disk has almost the same effect on the heat transfer rate in the low-Pr range as for $Pr > 1$. For high Prandtl numbers, in particular, the Nusselt number varies $\propto \sqrt{-\hat{\alpha} Pr}$ according to the high-Pr limit (21). This implies that a doubling of the unsteadiness parameter has the same effect on the heat transfer rate as a doubling of the Prandtl number.

Table 3: Heat transfer rate $-\Theta'(0)$ at the surface.

$Pr\backslash\hat{\alpha}$	0	-0.5	-1.0	-2.0	-5.0	-10.0
0.3	0.1940	0.3145	0.3953	0.5159	0.7656	1.0548
0.5	0.2640	0.4151	0.5161	0.6690	0.9861	1.3512
0.7	0.3234	0.4950	0.6125	0.7919	1.1656	1.5963
1.0	0.3963	0.5927	0.7311	0.9439	1.3892	1.9034
2.0	0.5653	0.8268	1.0184	1.3164	1.9441	2.6705
7.0	0.9818	1.4537	1.8095	2.3667	3.5429	4.9040

The similarity transformation introduced in eqs (7)-(8) applies for disks rotating with an angular velocity $\Omega_0(1-\alpha t)^{-1}$. In the present paper we have only been concerned with decelerating disks, i.e. $\alpha < 0$, for which flow field results were obtained by Watson & Wang [8] for $0 \leqslant -\hat{\alpha} \leqslant 20$ and later by Hussain et al. [12] for even faster decelerations up to $\hat{\alpha} = -100$. In an accompanying paper [13], the same authors presented results also for slowly accelerating disks up to $\hat{\alpha} = +3$. The latter study seems to contradict the analysis of the asymptotic behaviour by Watson & Wang [8], who concluded that a boundary layer existed on the disk only if $\alpha \leqslant 0$ .The shape of the profiles for the radial and circumferential velocity components presented by Hussain et al. [13] suggests that the finite interval on which the ODEs were integrated was somewhat too narrow. This common failure leads to truncated velocity profiles which fail to approach the ambient flow conditions asymptotically, as pointed out by Pantokratoras [14].

By means of the similarity transformation (7),(8), not only the three-dimensional fluid flow problem but also the accompanying thermal problem transformed into ODEs. Whereas the dependent variables depend on r, z, and t, the variations of F, G, H, P and Θ depend only on the similarity variable η, albeit with $\hat{\alpha}$ as a parameter. This is indeed a major advantage of a succesful similarity transformation. The numerical integration of the resulting set of ODEs (9)-(13) requires boundary conditions only at $\eta = 0$ and as $\eta \to \infty$, e.g. as specified in eq. (14). The computed solutions are therefore formally valid at all times $t \geqslant 0$ and for all $r \geqslant 0$. The expressions for the similarity solutions (7) are therefore valid also at $t = 0$. Similarly, these solutions are also formally valid at any location all the way from the axis of rotation $r = 0$ to an arbitrarily large distance away from the axis of rotation. However, in spite of the mathematical validity of the solutions for any r-value, the flow will eventually be unstable at sufficiently high values of the local Reynolds number $r^2\Omega/\nu$, typically of the order $2 \cdot 10^5$ [15], beyond which transition to turbulence will occour and the similarity solutions are no longer physically realistic.

7. Concluding Remarks

The purpose of this paper was to show for the first time that also the heat transfer problem associated with the revolving flow driven by a decelerating rotating disk is amenable to exact similarity solutions. A similarity transformation was devised which transformed the time-dependent thermal energy equation to an ordinary differential equation. Similarity solutions have not been achieved for any other time-variations of the angular velocity of the disk, i.e. neither for a step-change, sudden start-up, or torsional oscillations.

Let us recall that the present similarity solution is an exact solution of the unsteady Navier-Stokes and thermal energy equations (2)-(5), i.e. without invoking the boundary layer approximations. The terms accounting for radial diffusion of momentum and thermal energy are not assumed negligibly small, but vanish exactly as a consequence of the chosen similarity transformation.

The unsteadiness parameter $\hat{\alpha} = \alpha/\Omega_0$, which reflects the relative importance of deceleration ($\alpha < 0$) and disk rotation (Ω_0), turned out to be the controlling parameter in addition to the Prandtl number Pr. The thickness of the thermal boundary layer was found to decrease with increasing values of $-\hat{\alpha}$ and Pr. The heat transfer rate through the disk increased monotonically with increasing magnitudes of these controlling parameters. In the high-Prandtl-number limit (low diffusivity), we found that the Nusselt number varied as $\sqrt{-\hat{\alpha}Pr}$.

8. References

[1] Kármán, Th V. "*Über* laminare und turbulente Reibung." Journal of Applied Mathematics and Mechanics/Zeitschrift für Angewandte Mathematik und Mechanik 1 (1921): 233-252.

[2] Cochran, W. G. "The flow due to a rotating disc." Mathematical Proceedings of the Cambridge Philosophical Society. 30 (1934) 365-375.

[3] Rogers, M. H., and G. N. Lance. "The rotationally symmetric flow of a viscous fluid in the presence of an infinite rotating disk." Journal of Fluid Mechanics 7 (1960): 617-631.

[4] Zandbergen, P. J., and D. Dijkstra. "Von Kármán swirling flows." Annual Review of Fluid Mechanics 19 (1987): 465-491.

[5] Millsaps, K., and K. Pohlhausen. "Heat transfer by laminar flow from a rotating plate." Journal of the Aeronautical Sciences 19 (1952): 120-126.

[6] E. M. Sparrow and Gregg, J. L. "Heat transfer from a rotating disk to fluids of any Prandtl number." ASME Journal of Heat Transfer, 81 (1959): 249-251.

[7] Wang, C. Y. "Exact solutions of the unsteady Navier-Stokes equations." ASME Applied Mechanics Review 42 (1989): 269-282.

[8] Watson, L. T., and C. Y. Wang. "Deceleration of a rotating disk in a viscous fluid." The Physics of Fluids 22 (1979): 2267-2269.

[9] Attia, H. A. "Transient flow of a conducting fluid with heat transfer due to an infinite rotating disk." International Communications in Heat and Mass Transfer 28 (2001): 439-448.

[10] Attia, H. A. "Unsteady flow of a non-Newtonian fluid above a rotating disk with heat transfer." International Journal of Heat and Mass Transfer 46 (2003): 2695-2700.

[11] Shampine, L.F., J.Kierzenka, and M.W. Reichelt. "Solving boundary value problems for ordinary differential equations in MATLAB with bvp4c." Tutorial notes (2000): 437-448.

[12] Hussain, S. Ahmad. F., Shafique, M. & Hussain S. "Numerical solution for the deceleration of a rotating disk in a viscous fluid." International Journal of Emerging Technology and Advanced Engineering 3 (2013): 718-725.

[13] Hussain, S., Ahmad, F., Shafique, M., and Hussain, S., Numerical solution for accelerated rotating disk in a viscous fluid, Applied Mathematics, 4 (2013): 899-902.

[14] Pantokratoras, A., A common error made in investigation of boundary layer flows, Applied Mathematical Modelling, 33 (2009): 413-422.

[15] Shevchuk, I.V., Modelling of Convective Heat and Mass Transfer in Rotating Flows, Springer (2016).

PAPER 5

A note on buoyancy effects in von Kármán flow over a rotating disk

M.Rahman , H.I.Andersson

Submitted to: Journal of Applied Mathematics and Physics(ZAMP), (2017)

A note on buoyancy effects in von K$\acute{a}$rm$\acute{a}$n flow over a rotating disk

Muhammad Rahman* and Helge I.Andersson

Abstract. The steadily revolving flow driven by a rotating disk has been considered by means of similarity analysis. Attention is paid to the pressure distribution above the disk, which has most often been ignored. We found that buoyancy lead to a substantial pressure reduction in the vicinity of the disk for Prandtl numbers below unity. At sufficiently high Grashof numbers, this buoyancy-induced pressure reduction even eliminates the excess stagnation pressure at the disk.

Keywords. Swirling flow; Buoyancy; Similarity solutions; Boundary layer theory.

1. Introduction

The steadily revolving motion of a viscous fluid driven solely by a rotating disk in an otherwise quiescent and unbounded ambient has evolved into a canonical flow problem in fluid mechanics. The problem was first formulated by von K$\acute{a}$rm$\acute{a}$n [1] by means of the axisymmetric Navier-Stokes equations. He moreover devised an ingenious similarity transformation which elegantly transformed the governing partial differential equations (PDEs) to a set of ordinary differential equations (ODEs). The review article by Zandbergen & Dijkstra [2] provided a comprehensive survey of the vast attention devoted to the von K$\acute{a}$rm$\acute{a}$n swirling flow. Throughout the century that has elapsed since von K$\acute{a}$rm$\acute{a}$n's work appeared, the vast majority of investigations have been concerned solely with various aspects of the mathematical problem formulation and the resulting three-componential velocity field. However, von K$\acute{a}$rm$\acute{a}$n [1] pointed out that also the associated pressure field can be obtained from an ODE that results from the axial momentum equation as soon as the velocity field has been determined, but the pressure variation over the rotating disk was neither addressed by von K$\acute{a}$rm$\acute{a}$n [1] nor by Zandbergen & Dijkstra [2]. This is likely due to the fact that the von K$\acute{a}$rm$\acute{a}$n flow is often considered as a three-dimensional boundary layer flow, in which the pressure gradient across the boundary layer is negligible.

A variety of different extensions of the classical von *Kármán* flow problem have been made over the years. The effect of partial slip at the surface of the rotating disk has been studied for instance by Arikoglu & Ozkol [3], Andersson & Rousselet [4] and Sahoo [5]. Sahoo [5] also considered the influence of non-Newtonian rheology and adopted the Reiner-Rivlin fluid model, whereas Ahmadpour & Sadeghy [6] and Griffiths [7] more recently examined von *Kármán* flows of Bingham and Carreau fluids, respectively.

The heat transfer problem accompanying the von *Kármán* flow was apparently first studied by Millsaps & Pohlhausen [8] and Sparrow & Gregg [9]. Only recently, however, buoyancy was included in analyses of von *Kármán* swirling flows by Sibanda & Makinde [10] and Guha & Sengupta [11] by solving ODEs and PDEs, respectively.

The aim of this brief report is to study the effects of buoyancy on the fluid flow problem by means of similarity analysis and, in particular, to explore how the pressure field is affected by buoyancy (parameterized by the Grashof number) and also the Prandtl number.

2. Problem formulation

Let u, v, and w be the velocity components in cylindrical polar coordinates r, θ, z, respectively, with the origin of the z-axis at the centre of the impermeable disk. By assuming steadiness and axisymmetry, von *Kármán* [1] showed that the mass conservation equation and the three components of the Navier-Stokes equation transformed to:

$$H' + 2F = 0, \tag{1}$$

$$F'' - HF' - F^2 + G^2 = 0, \tag{2}$$

$$G'' - HG' - 2FG = 0, \tag{3}$$

$$P' = -H'' + HH', \tag{4}$$

in terms of the non-dimensional axial coordinate $\eta = z\sqrt{\Omega/\nu}$ where Ω is the angular velocity of the rotating disk and $\nu = \mu/\rho$ is the kinematic viscosity of the fluid. The dimensionless velocity components F, G, H and pressure P are defined as:

$$u(r,z) = r\Omega F(\eta), \tag{5}$$

$$v(r,z) = r\Omega G(\eta), \tag{6}$$

$$w(z) = \sqrt{\nu\Omega}H(\eta), \tag{7}$$

$$p(z) = -\rho\nu\Omega P(\eta). \tag{8}$$

The three-componential velocity field $u(r,z), v(r,z)$, and $w(z)$ can be obtained from the ODEs (1)-(3) subject to the five boundary conditions

$$F(0) = 0, \quad G(0) = 1, \quad H(0) = 0, \quad at \quad \eta = 0, \tag{9a}$$

$$F(\eta) = 0, \quad G(\eta) = 0, \quad as \qquad \eta \to \infty, \tag{9b}$$

regardless of the axial component of the momentum equation (4). While von Kármán [1] originally employed an approximate integral method, accurate numerical solutions have been provided by many others without any consideration of the pressure field. Rogers & Lance [12], however, pointed out that the pressure distribution can be found by direct integration of equation (4). Here, when the integration is subjected to the far-field boundary condition

$$P(\eta) = 1, \quad as \qquad \eta \to \infty, \tag{9c}$$

we obtain

$$P(\eta) = 2F + \frac{1}{2}H^2 - \frac{1}{2}H(\infty)^2 + 1. \tag{10}$$

This analytical solution shows that the stagnation pressure at the disk

$$P_0 = P(0) = 1 - \frac{1}{2}H(\infty)^2, \tag{11}$$

depends on the rate $H(\infty)$ at which fluid is drawn axially towards the disk from the ambient.

In order to study the influence of buoyancy on the swirling flow problem, the temperature distribution $T(z)$ is required. Therefore, by including also the thermal energy equation in the analysis, the axial momentum equation (4) should be replaced by

$$P' = -H'' + HH' - Gr\Theta, \tag{12}$$

where the last term is due to buoyancy accounted for by means of the Boussinesq approximation. The dimensionless temperature Θ is defined as

$$\Theta(\eta) = \frac{T(z) - T_\infty}{T_0 - T_\infty}, \tag{13}$$

and obtained by integration of the transformed thermal energy equation:

$$\Theta'' - PrH\Theta' = 0, \tag{14}$$

subjected to the boundary conditions

$$\Theta(0) = 1, \quad \Theta(\eta) \to 0 \quad as \qquad \eta \to \infty. \tag{15}$$

The thermal properties of the fluid β, k and C_p are parameterized in terms of a Grashof number and the Prandtl number as

$$Gr = \beta g(T_0 - T_\infty)/\sqrt{\nu\Omega^3} \quad and \quad Pr = \mu C_P/k. \tag{16}$$

The Grashof number is positive if the disk is heated ($T_0 > T_\infty$).

The relevant system of ODEs can be solved as two-point boundary value problems. For this purpose we have used the bvp4c MATLAB solver, which gives very good results for the non-linear ODEs with multipoint BVPs. This finite-difference code utilizes the 3-stage Lobatto IIIa formula, that is a collocation formula and the collocation polynomial provides a C1-continuous solution that is fourth-order accurate uniformly in [a,b]. For multipoint BVPs, the solution is C1-continuous within each region, but continuity is not automatically imposed at the interfaces. Mesh selection and error control are based on the residual of the continuous solution. Analytical condensation is used when the system of algebraic equations is formed; see Shampine et al.[13]. We recently used the same numerical approach to integrate the two-point boundary-value problem associated with revolving Bödewadt flow [14].

3. Presentation of results

First of all, the three-componential velocity field was computed by numerical integration of eqs.(1)-(3) subject to the five boundary conditions (9a,9b). The results in Figure 1 reproduce earlier results of the same flow problem and the typical flow features are seen: the shear-driven motion (G) in the azimuthal direction decays rapidly with the distance η from the rotating disk. The centrifugal force associated with the circulating motion induces a radially directed outward flow ($F > 0$), which is compensated by an axial flow ($H < 0$) towards the disk.

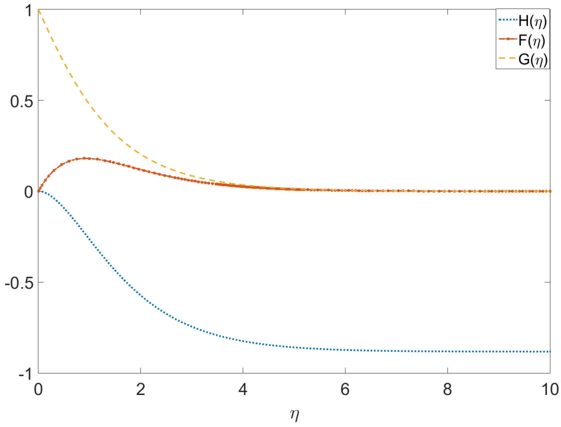

FIGURE 1. Variation of the three dimensionless velocity components $F(\eta), G(\eta)$, and $H(\eta)$ above the rotating disk.

Next, the thermal energy equation (14) subject to the two boundary conditions (15) was integrated for two Prandtl numbers, namely $Pr = 0.7$ and 7.0, representative of air and water, respectively. The temperature distributions shown in Figure 2 are consistent with earlier results of the same problem. In particular, the temperature of the fluid in the vicinity of the disk adjusts to the ambient temperature over a considerably shorter distance for the higher Prandtl number.

Finally, with access to the axial velocity $H(\eta)$ from Figure 1 and the temperature $\Theta(\eta)$ from Figure 2, the pressure is obtained by integration of the axial momentum equation (12). The pressure distributions obtained for some different Grashof numbers are shown for the two different Prandtl numbers in Figure 3(a,b). In absence of buoyancy ($Gr = 0$) we observe that the pressure increases almost monotonically from the ambient $P = 1.0$ to $P(0) \approx 0.60$.

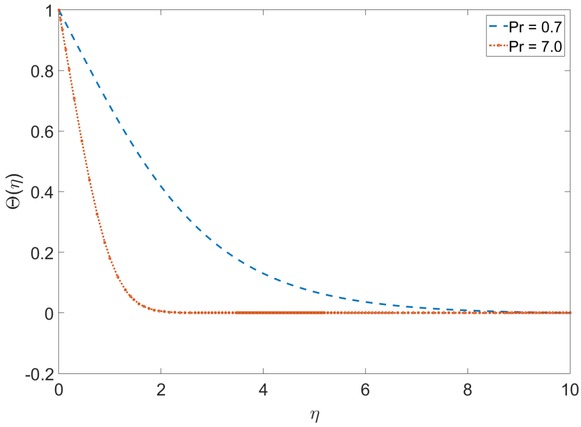

FIGURE 2. Variation of the dimensionless temperature $\Theta(\eta)$ above the rotating disk for two different Prandtl numbers.

Here, the minus sign in the equation (8) of the dimensionless pressure P should be recalled.

The effect of buoyancy is to make the pressure decrease in the vicinity of the rotating disk, before the pressure rapidly increases in a thin layer next to the surface of the disk, as seen in Figure 3 for $Pr = 0.7$. This effect becomes more pronounced for higher Grashof numbers and gradually reduces the surface pressure. At the highest Grashof number $Gr = 0.20$, the surface pressure even exceeds unity, thereby eliminating the excess stagnation pressure. The data in Table 1 shows a 70% increase of $P(0)$ with increasing buoyancy for $Pr = 0.7$. At the higher Prandtl number $Pr = 7.0$, on the other hand, the influence of buoyancy on the pressure distributions in Figure 3 and on the surface pressure in Table 1 is substantially reduced.

TABLE 1. Surface pressure $P(0)$ at the rotating disk for different Grashof and Prandtl numbers.

$Pr\backslash Gr$	0.0	0.05	0.10	0.15	0.20
0.7	0.6108	0.7145	0.8183	0.9220	1.0258
7.0	0.6108	0.6410	0.6712	0.7014	0.7316

4. Discussion

In absence of buoyancy, an axial pressure force P' is required to balance advection HH' and viscous diffusion H'' of axial momentum in accordance with equation (4). However, an additional and negative pressure force is required to balance the positive buoyancy force $Gr\Theta$ in equation (12). This explains why the dimensionless pressure $P(\eta)$ rises in the vicinity of the disk, namely

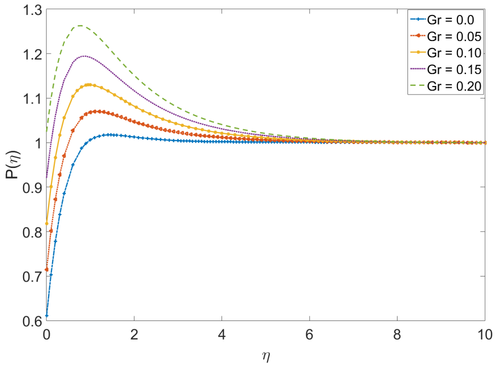

(a) Prandtl number $Pr = 0.7$;

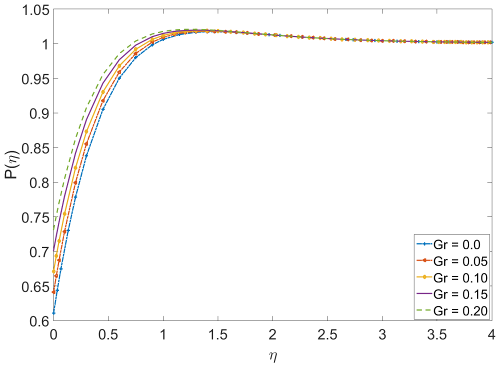

(b) Prandtl number $Pr = 7.0$;

FIGURE 3. Variation of the dimensionless pressure $P(\eta)$ above the rotating disk for some different Grashof numbers.

in order to add a negative contribution to P'. The temperature adjusts to the ambient temperature over a substantially shorter distance than over which the momentum diffuses for $Pr \gg 1$, as seen in Figure 2. For $Pr = 7$ the buoyancy force tends to vanish beyond $\eta \approx 1$ and the influence of buoyancy on the pressure distribution is therefore significantly reduced and confined to a thin layer next to the disk.

The influence of buoyancy on the von K*á*rm*á*n flow was recently studied by Sibanda & Makinde [10], who at the same time also considered effects of a magnetic field, ohmic heating, viscous dissipation and permeability. The axial momentum equation considered by Sibanda & Makinde[10] was the same as our equation (12), even though their dimensionless pressure was defined as in eq. (8), but without the minus sign. In the far-field they forced all three velocity components to zero, without any physical justification. They did unfortunately not deal explicitly with the pressure field, but presented results for the axial velocity component $H(\eta)$ which showed a number of unexpected behaviours. For example, finite values of $H'(0)$ were reported in their Table 1, but these are clearly in conflict with the no-slip condition $F(0) = 0$ in eq. (9a) since mass conservation (1) requires that $F(0) = -\frac{1}{2}H'(0)$. Furthermore, their figure 8 shows that H is dependent on Gr although the temperature only enters into the equation for the axial velocity equation. Indeed, we argue that the three-componential flow problem can be solved without consideration of equation (12). The resulting flow field will therefore be unaffected by the Grashof number, as seen in Figure 1.

A frequently overlooked fact is that terms which are normally neglected in the Navier-Stokes equations by invoking the high-Re boundary layer approximation vanish identically for all Reynolds numbers provided the assumptions inherent in von Kármáns similarity transformation, namely that $u(r,z), v(r,z)$, and $w(z)$, are adopted. The results shown in Figure 1 can therefore be believed to be valid for an arbitrarily high Re provided that the flow remains laminar. Very recently, however, Guha & Sengupta [11] provided results of an extensive study of the von Kármán flow by solving the full axisymmetric Navier-Stokes equations. Based on their numerical solutions of the governing PDEs, they identified three different regimes and demonstrated that similarity solutions based on the assumptions $u(r,z), v(r,z)$, and $w(z)$ become valid at a large non-dimensional radius $\Re$ defined as $\Re = r/\sqrt{\nu/\Omega} = \sqrt{\Omega r^2/\nu} = \sqrt{Re}$, typically when $\Re > 75$.

5. Concluding remarks

By invoking the usual boundary-layer approximations, the pressure gradient across the three-dimensional boundary layer on a constantly rotating disk is assumed negligible. Accordingly, the stagnation pressure on the disk becomes equal to the ambient pressure. However, we argued that the similarity solution of the flow field also solves the axisymmetric Navier-Stokes equation. In absence of buoyancy we found an analytical expression for the pressure variation normal to the disk with an excess stagnation pressure at the surface of the disk. By means of numerical integrations we showed that buoyancy leads to a substantially reduction of the pressure in the vicinity of the rotating disk for $Pr \leq 1$, whereas the buoyancy effect becomes almost negligible for larger Prandtl numbers. This pressure reduction has, however, no implications on the dynamics of the flow, but tends to eliminate the excess stagnation pressure on the disk surface. The lowering of the stagnation pressure may affect the stability of the rotating disk, as for instance in hard disk drives.

References

[1] von Kármán, T., 1921. "*Über* laminare und turbulente Reibung," Journal of Applied Mathematics and Mechanics/Zeitschrift für Angewandte Mathematik und Mechanik, 1(4), pp.233-252.

[2] Zandbergen, P.J. and Dijkstra, D., 1987. "Von Kármán swirling flows. Annual Review of Fluid Mechanics," 19(1), pp.465-491.

[3] Arikoglu, A. and Ozkol, I., 2005, "Analysis for slip flow over a single free disk with heat transfer," ASME J. Fluids Eng., 127, pp. 624-627.

[4] Andersson, H.I. and Rousselet, M., 2006, "Slip flow over a lubricated rotating disk," Int. J. Heat Fluid Flow, 27, pp. 329-335.

[5] Sahoo, B., 2009, "Effects of partial slip, viscous dissipation and Joule heating on Von $K\acute{a}rm\acute{a}n$ flow and heat transfer of an electrically conducting non-Newtonian fluid," Commun. Non-Linear Sci Numer. Simulat. 14, pp. 2982-2998.

[6] Ahmadpour, A. and Sadeghy, K., 2013, "Swirling flow of Bingham fluids above a rotating disk: an exact solution," J. Non-Newtonian Fluid Mech., 197, pp. 41-47.

[7] Griffiths, P.T., 2015, "Flow of a generalized Newtonian fluid due to a rotating disk," J. Non-Newtonian Fluid Mech., 221, pp. 9-17.

[8] Millsaps, K. and Pohlhausen, K., 1952. "Heat transfer by laminar flow from a rotating plate," Journal of the Aeronautical Sciences, 19(2), pp.120-126.

[9] Gregg, J.L. and Sparrow, E.M., 1959. "Heat transfer from a rotating disk to fluids of any Prandtl number," ASME J. Heat Trans., 81, pp. 249-251.

[10] Sibanda, P. and Makinde, O.D., 2010. "On steady MHD flow and heat transfer past a rotating disk in a porous medium with ohmic heating and viscous dissipation," International Journal of Numerical Methods for Heat & Fluid Flow, 20(3), pp.269-285.

[11] Guha, A. and Sengupta, S., 2017. "Non-linear interaction of buoyancy with von $K\acute{a}rm\acute{a}n$'s swirling flow in mixed convection above a heated rotating disc," International Journal of Heat and Mass Transfer, 108, pp.402-416.

[12] Rogers, M.H. and Lance, G.N., 1960. "The rotationally symmetric flow of a viscous fluid in the presence of an infinite rotating disk," Journal of Fluid Mechanics, 7(4), pp.617-631.

[13] Shampine, L.F., Kierzenka, J. and Reichelt, M.W., 2000. "Solving boundary value problems for ordinary differential equations in MATLAB with bvp4c," Tutorial notes, pp.437-448.

[14] Rahman, M. and Andersson, H.I., 2017, "On heat transfer in $B\ddot{o}$dewadt flow," Int. J. Heat Mass Transfer, 112, pp. 1057-1061.

Muhammad Rahman*
Department of Energy and Process Engineering,
Norwegian University of Science and Technology,
Postal code 7491,
Trondheim, Norway
e-mail: `muhammad.rahman@ntnu.no`

Helge I.Andersson
Department of Energy and Process Engineering,
Norwegian University of Science and Technology,
Postal code 7491,
Trondheim, Norway
e-mail: `helge.i.andersson@ntnu.no`

PAPER 6

Heat transfer in generalized vortex flow over a permeable surface

M.Rahman , H.I.Andersson

International Journal of Heat and Mass Transfer 118 (2018) 1090-1097

International Journal of Heat and Mass Transfer 118 (2018) 1090–1097

Contents lists available at ScienceDirect

International Journal of Heat and Mass Transfer

journal homepage: www.elsevier.com/locate/ijhmt

Heat transfer in generalized vortex flow over a permeable surface

Muhammad Rahman *, Helge I. Andersson

Department of Energy and Process Engineering, Norwegian University of Science and Technology, Trondheim, Norway

ARTICLE INFO

Article history:
Received 22 June 2017
Received in revised form 15 September 2017
Accepted 13 November 2017

Keywords:
Thermal boundary layer
Generalized vortex flow
Three-dimensional flow
Heat transfer
Similarity solutions

ABSTRACT

Heat transfer in the thermal boundary layer beneath a generalized vortex flow has been considered. The steadily revolving flow is allowed to vary with the distance r from the symmetry axis as r^m. The governing equations for heat and momentum transport transformed exactly to a coupled set of ordinary differential equations by means of a tailor-made similarity transformation. Some different flow situations in presence of suction have been considered, including solid-body rotation $(m = +1)$ and a potential vortex $(m = -1)$. The thermal boundary layer was observed to thicken monotonically with decreasing m-values, accompanied by a reduction of the heat transfer rate through the planar surface above which the flow revolves. These findings were explained as the combined influence of two different effects, namely: (i) a variation of the effective Prandtl number $(m + 3)Pr/2$ that directly affected the thermal diffusion, whereas (ii) an indirect variation of the axial velocity component affected the thermal convection.

© 2017 Elsevier Ltd. All rights reserved.

1. Introduction

Bödewadt [1] considered the steadily revolving flow of a viscous fluid above an impermeable solid surface. The fluid far above the planar surface was assumed to be in a state of rigid-body rotation so that the tangential velocity component v increased linearly with the distance r from the axis of rotation. The presence of viscous shear stresses inevitably slowed down the revolving fluid motion in the viscous boundary layer adjacent to the surface. A resulting imbalance between the radial pressure gradient and the centrifugal force gave rise to a velocity component directed towards the axis of rotation. Finally, to secure mass conservation, an axial flow away from the surface arose and a three-dimensional boundary layer flow was established. The effects of alternative boundary conditions at the planar surface have been examined by Nath and Venkatachala [2], Sahoo et al. [3] and Turkyilmazoglu [4]. They considered suction, partial slip, and stretching, respectively.

The classical Bödewadt flow problem was later generalized by King and Lewellen [5] who assumed the tangential velocity to vary as $v \sim r^m$ where m is dimensionless constant. They were partly concerned with the effect of the parameter m and partly with the effect of a magnetic body-force term on the fluid motion. Their study was extended by Venkatachala and Nath [6] to also include effects of suction through the surface. The generalized Bödewadt flow was also considered as a part of an extensive paper by Kuo [7] focused on tornado-like vortices. In addition to the conventional no-slip conditions at the solid surface, Kuo [7] also allowed for partial surface slip. This was referred to as a geophysical boundary condition.

It was suggested by Moore [8] that the generalized Bödewadt flow does not admit similarity solutions for $m = -1$, i.e. when the revolving flow behaves as a potential vortex. The non-existence of similarity solutions was later proved by King and Lewellen [5]. However, as demonstrated by Nanbu [9] and Venkatachala and Nath [6], similarity solutions do exist in the presence of suction through the surface.

The aim of the present paper is to investigate for the first time the heat transfer between a generalized Bödewadt flow and the planar surface above which the fluid revolves. We recently demonstrated that realistic similarity solutions of the thermal energy equation do not exist for the classical Bödewadt flow above an impermeable surface [10]. In presence of sufficent suction, however, the thermal boundary layer problem allowed for realistic similarity solutions. In order to extend the thermal analysis to generalized Bödewadt flows, accurate solutions of the three-componential velocity field are required. To this end we revisit the work by King and Lewellen [5] and Kuo [7] to first obtain the revolving flow field over an impermeable surface. Subsequently, distributed suction will be introduced, similarly as in the study by Venkatachala and Nath [6]. Finally, similarity solutions of the thermal energy equation will be provided for some different revolving flows, including solid-body rotation $(m = +1)$ and potential vortex flow $(m = -1)$, and for some different Prandtl numbers.

---

* Corresponding author.
E-mail address: muhammad.rahman@ntnu.no (M. Rahman).

https://doi.org/10.1016/j.ijheatmasstransfer.2017.11.061
0017-9310/© 2017 Elsevier Ltd. All rights reserved.

2. Problem formulation and solution approach

2.1. Mathematical model equations

Let us consider the steadily revolving flow of a viscous fluid above a planar surface. In cylindrical polar coordinates (r,θ,z) the governing mass conservation, momentum and thermal energy equations become:

$$\frac{\partial}{\partial r}(ru)+\frac{\partial}{\partial z}(rw)=0, \tag{1}$$

$$u\frac{\partial u}{\partial r}-\frac{v^2}{r}+w\frac{\partial u}{\partial z}=-\frac{1}{\rho}\frac{\partial p}{\partial r}+\nu\left[\frac{\partial^2 u}{\partial r^2}+\frac{\partial}{\partial r}\left(\frac{u}{r}\right)+\frac{\partial^2 u}{\partial z^2}\right], \tag{2}$$

$$u\frac{\partial v}{\partial r}+\frac{uv}{r}+w\frac{\partial v}{\partial z}=\nu\left[\frac{\partial^2 v}{\partial r^2}+\frac{\partial}{\partial r}\left(\frac{v}{r}\right)+\frac{\partial^2 v}{\partial z^2}\right], \tag{3}$$

$$u\frac{\partial w}{\partial r}+w\frac{\partial w}{\partial z}=-\frac{1}{\rho}\frac{\partial p}{\partial z}+\nu\left[\frac{\partial^2 w}{\partial r^2}+\frac{1}{r}\frac{\partial w}{\partial r}+\frac{\partial^2 w}{\partial z^2}\right], \tag{4}$$

$$\rho C_p\left(u\frac{\partial T}{\partial r}+w\frac{\partial T}{\partial z}\right)=k\left(\frac{\partial^2 T}{\partial r^2}+\frac{1}{r}\left(\frac{\partial T}{\partial r}\right)+\frac{\partial^2 T}{\partial z^2}\right), \tag{5}$$

where (u,v,w) are the velocity components of the fluid in the radial, tangential and axial directions, respectively, and T is the temperature. Here, we have assumed rotational symmetry about the vertical z-axis, $i.e.\partial/\partial\theta=0$. The kinematic viscosity of the fluid is ν. C_p is the specific heat at constant pressure of the fluid. k is the thermal conductivity of the fluid.

This set of coupled partial differential equations (PDEs) are the same as those governing the heat and momentum transport in the von Karman flow driven by a steadily rotating disk and the Bödewadt flow caused by revolving fluid in solid-body rotation above a planar surface. In this paper, however, we are concerned with a generalized vortex flow which includes the classical Bödewadt flow [1] only as a special case. The boundary conditions are therefore given as

$$\begin{aligned}&u=0, v=0,\quad w=Av_0\sqrt{\frac{\nu}{v_0r_0}}\left[\frac{r}{r_0}\right]^{n-1}(n+1), T=T_w,\quad at\quad z=0,\\&u=0, v=v_0\left[\frac{r}{r_0}\right]^{2n-1}, T=T_\infty,\quad as\quad z\to\infty,\end{aligned} \tag{6}$$

The tangential flow v high above the planar surface at $z=0$ is assumed to exhibit a power-law variation where the power $m=2n-1$ is a prescribed parameter. In the present study we also allow for suction through the surface. The suction velocity $w(r,0)$ varies as r^{n-1} and $A<0$ is a dimensionless suction parameter. The temperature varies from T_w at the surface to T_∞ in the vortex flow high above the surface.

By means of the usual boundary layer approximations, namely that $w\ll u,\ v$ and $\partial/\partial z\gg\partial/\partial r$, the system of Eqs. (1)–(5) simplifies to:

$$\frac{\partial}{\partial r}(ru)+\frac{\partial}{\partial z}(rw)=0, \tag{7}$$

$$u\frac{\partial u}{\partial r}-\frac{v^2}{r}+w\frac{\partial u}{\partial z}=-\frac{1}{\rho}\frac{\partial p}{\partial r}+\nu\left[\frac{\partial^2 u}{\partial z^2}\right], \tag{8}$$

$$u\frac{\partial v}{\partial r}+\frac{uv}{r}+w\frac{\partial v}{\partial z}=\nu\left[\frac{\partial^2 v}{\partial z^2}\right], \tag{9}$$

$$\frac{\partial p}{\partial z}=0. \tag{10}$$

$$\rho C_p\left(u\frac{\partial T}{\partial r}+w\frac{\partial T}{\partial z}\right)=k\frac{\partial^2 T}{\partial z^2}, \tag{11}$$

still subjected to the boundary conditions defined in Eq. (6). Here, Eq. (10) simply states that the pressure p remains constant across the three-dimensional boundary layer.

2.2. Generalized similarity transformation

In view of the generalized boundary conditions in Eq. (6), we now proceed and define the similarity transformations:

$$\begin{aligned}u(r,z)&=-v_0\left[\frac{r}{r_0}\right]^{2n-1}F(\eta),\\v(r,z)&=v_0\left[\frac{r}{r_0}\right]^{2n-1}G(\eta),\\w(r,z)&=v_0\sqrt{\frac{\nu}{v_0r_0}}\left[\frac{r}{r_0}\right]^{n-1}[(n+1)H(\eta)+(n-1)\eta F],\\p(r)&=\frac{\rho v_0^2}{4n-2}\left[\frac{r}{r_0}\right]^{4n-2},\\T(r,z)&=T_\infty+(T_w-T_\infty)\Theta(\eta),\end{aligned} \tag{12}$$

where η is a dimensionless similarity variable defined by

$$\eta=\left[\frac{z}{r_0}\right]\left[\frac{r}{r_0}\right]^{n-1}\sqrt{\frac{v_0r_0}{\nu}}. \tag{13}$$

In terms of the non-dimensional variables the governing equations become:

$$H'-F=0, \tag{14}$$

$$F''-(n+1)HF'-(1-2n)F^2-G^2+1=0, \tag{15}$$

$$G''-(n+1)HG'+2nFG=0, \tag{16}$$

$$\Theta''-Pr(n+1)H(\eta)\Theta'=0, \tag{17}$$

where Pr is the Prandtl number, $Pr=\rho\nu C_p/k$. The corresponding boundary conditions specified in (6) transform to:

$$\begin{aligned}&F(\eta)=0,\quad G(\eta)=0,\quad H(\eta)=A,\quad \Theta(\eta)=1\quad at\quad \eta=0,\\&F(\eta)=0,\quad G(\eta)=1,\quad \Theta(\eta)=0\quad as\quad \eta\to\infty.\end{aligned} \tag{18}$$

By means of the transformation defined in Eq. (12), the PDEs in Eqs. (7)–(11) transform exactly into a set of coupled non-linear ordinary differential equations (ODEs) subjected to the seven appropriate boundary conditions (18). This constitutes a three-parameter problem in terms of the power-law parameter $n=(m+1)/2$, the suction parameter A and the Prandtl number Pr.

2.3. Numerical approach

We solved the two-point boundary value problem consisting of the coupled set of ordinary differential Eqs. (14)–(17) subjected to the boundary conditions (18). For this purpose we have used the bvp4c MATLAB solver, which gives very good results for the nonlinear ODEs with multipoint BVPs. This finite-difference code utilizes the 3-stage Lobatto IIIa formula, that is a collocation formula and the collocation polynomial provides a C1-continuous solution that is fourth-order accurate uniformly in [a,b]. For multipoint BVPs, the solution is C1-continuous within each region, but continuity is not automatically imposed at the interfaces. Mesh selection and error control are based on the residual of the continuous solution. Analytical condensation is used when the system of algebraic equations is formed. See Shampine et al. [11] for further details.

Two-point boundary value problems in terms of coupled ODEs are frequently occurring in the field of heat and fluid flow. Bödewadt [1] used power-series expansions to obtain numerical solutions for the boundary layer driven by the upper fluid being in solid-body rotation, i.e. $n = 1$. The more accurate shooting methods [12] became popular a half century ago. Some difficulties with shooting methods were pointed out by Kafoussias and Williams [13]. Venkatachala and Nath [6] instead used a finite-difference method in combination with an iterative Newton's method. More recently, Rahimi-Gorji et al. [14] advocated the use of a Galerkin method to solve their two-point boundary-value problem. Each of these and other methods have their own strengths and weaknesses. Numerical solutions of the problem dealt with in the present study, i.e. Eqs. (14)–(18), could have been obtained also by means of any other method aimed to solve such problems.

3. Results and discussions

3.1. Velocity profiles in the viscous boundary layer

Profiles of the radial, tangential and axial velocity components are plotted in Figs. 1–3, respectively. The computed results are compared with the velocity profiles tabulated by Kuo (Table 3) for $n = 1$ and $n = 0.75$. The first observation that can be made is that the present results exhibit an almost perfect agreement with the data from Kuo for $n = 1$, i.e. for the classical Bödewadt flow. The main flow characteristics, as summarized in the Introduction, are evident, as well as the oscillatory variations of the three velocity components.

Another important observation seen from Figs. 1–3 is that both the amplitude and wavelength of the oscillations increase as n decreases. The peaks of the radial and tangential velocity components are higher for $n = 0.75$ than for $n = 1$. The axial flow away from surface is increased, and this increase is much more pronounced in the present study than suggested by Kuo's results. Although the trends of the variations of all the three velocity components are the same, particularly large deviations are seen for the axial velocity component H in Fig. 3. In spite of the close agreement with Kuo's results for $n = 1$, the present velocity profiles deviate substantially from Kuo's results for $n = 0.75$.

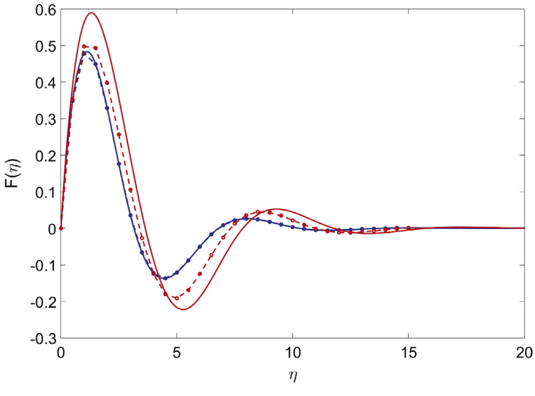

Fig. 1. Radial velocity component $F(\eta)$ for $n = 1$ (blue) and $n = 0.75$ (red). Present computations (continuous lines) compared with corresponding results (broken lines) from Table 3 in Kuo [7]. The surface is impermeable ($A = 0$). (For interpretation of the references to color in this figure legend, the reader is referred to the web version of this article.)

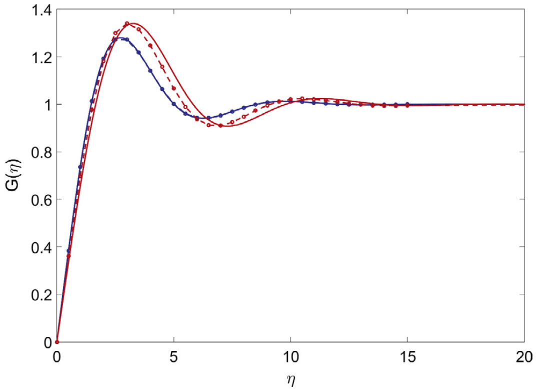

Fig. 2. Tangential velocity component $G(\eta)$ for $n = 1$ (blue) and $n = 0.75$ (red). Present computations (continuous lines) compared with corresponding results (broken lines) from Table 3 in Kuo [7]. The surface is impermeable ($A = 0$). (For interpretation of the references to color in this figure legend, the reader is referred to the web version of this article.)

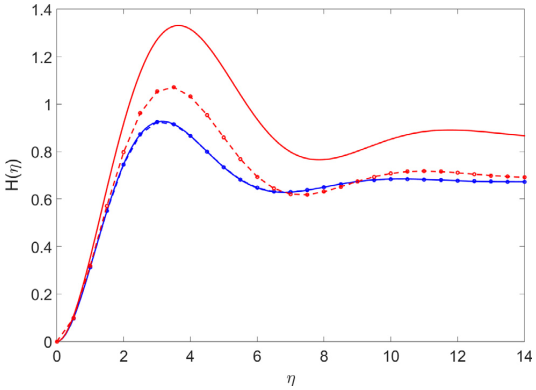

Fig. 3. Axial velocity component $H(\eta)$ for $n = 1$ (blue) and $n = 0.75$ (red). Present computations (continuous lines) compared with corresponding results (broken lines) from Table 3 in Kuo [7]. The surface is impermeable ($A = 0$). (For interpretation of the references to color in this figure legend, the reader is referred to the web version of this article.)

The most essential boundary layer characteristics are given in Table 1 and compared with corresponding data from Kuo [7] as well as with earlier results by King and Lewellen [5] for $n = 1.0$, 0.75 and 0.5. The numerical values obtained in the present study are fairly different from the results provided by Kuo [7]. This is to be expected in view of the substantial deviations between the velocity profiles seen in Figs. 1–3. However, the data deduced from the present computations closely agree with the earlier data tabulated by King and Lewellen [5]. This close agreement supports the reliability of the present computations.

The thickness of the boundary layer increases as n is reduced and the viscous influence extends far above the surface when $n \ll 1$. This behaviour makes the numerical integration of the governing ODEs gradually more cumbersome. Although the numerical solution for $n = 0.5$ satisfied the formal boundary condition (18) for the velocity components, the slope of the computed profiles did not decay properly to zero, as required by the auxiliary far-field conditions F', G', and $H' \to 0$ as $\eta \to \infty$. The entries for $n = 0.5$ in Table 1 are therefore not considered to be trustworthy.

Table 1
Boundary layer characteristics $F'(0), G'(0)$ and $H(\infty)$ in absence of suction $(A = 0)$. Present results compared with data from Kuo [7] (Tables 1 and 3), and King and Lewellen [5], (Table 1). Note that $n = (m+1)/2$. The present numerical solution for $n = 0.5$ is not considered as physically realistic.

n	m	$F'(0)$			$G'(0)$			$H(\infty)$		
		Present	Kuo	K&L	Present	Kuo	K&L	Present	Kuo	K&L
1.0	1.0	0.9420	0.9419	0.942	0.7729	0.7729	0.773	0.6747	0.67473	0.674
0.75	0.5	1.0202	0.9494	1.022	0.6749	0.7249	0.673	0.8662	0.69629	0.868
0.50	0	1.1970	1.0065	1.201	0.4464	0.5307	0.443	1.6657	0.82000	1.390

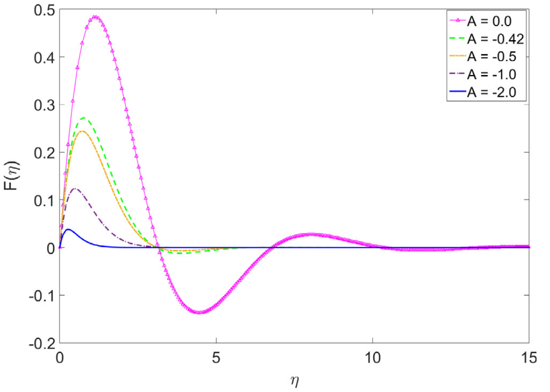

Fig. 4. Radial velocity component $F(\eta)$ for some different values of the suction parameter $A(n = 1)$.

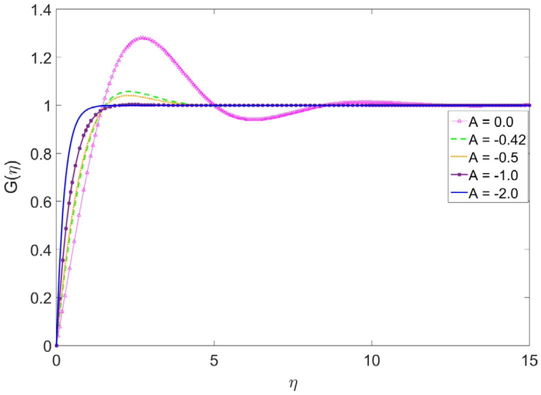

Fig. 5. Tangential velocity component $G(\eta)$ for some different values of the suction parameter $A(n = 1)$.

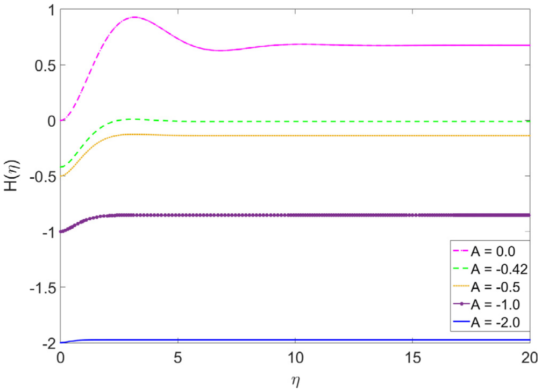

Fig. 6. Axial velocity component $H(\eta)$ for some different values of the suction parameter $A(n = 1)$.

The only results without a magnetic field and in absence of suction that are shown by Venkatachala and Nath [6] are those in their Fig. 4 for $m = 0$ and $m = 1$. The rather extreme undulations of all three velocity components for $m = 0 (n = 0.5)$ are apparently not realistic. This is probably consistent with our observed difficulties associated with the integration of the ODEs for n-values considerably smaller than 0.75.

We now proceed to examine the effect of suction through the surface. Let us first consider the effect of suction on the classical Bödewadt flow $(n = m = 1)$. The effect of suction on the Bödewadt flow is already known from Nath and Venkatachala [2] to damp the oscillatory nature of the velocity profiles, to reduce the radial velocity, and to make the viscous boundary layer thinner. The ondulatory nature of the velocity components parallel with the surface, i.e. $F(\eta)$ and $G(\eta)$ in Figs. 4 and 5, is indeed reduced and eventually vanishes with increasing suction. The viscous boundary layer adjacent to the surface becomes gradually thinner as suction increases. It is particularly noteworthy that the axial velocity component $H(\eta)$ shown in Fig. 6, which is positive and thereby directed upwards in absence of suction $(A = 0)$, changes sign if sufficient suction is applied. Characteristics from the present computations are compared with numerical results from Nath and Venkatachala [2] in Table 2. A close agreement with their data for $A = -0.5$ and -1.0 can be seen. Here, we have also computed results for $A = -2.0$.

In order to focus on the influence of the parameter n (or $m = 2n - 1$) which characterizes the revolving flow high above the surface, only strong suction $A = -2.0$ is considered in the remaining figures. The three velocity components are shown in Figs. 7–9 for several different values of the power-law parameter n. It is first of all noteworthy the presence of suction enables us to solve the two-point boundary value problem for significantly lower n-values than in absence of suction.

Now we can see that the reduction of n tends to make the viscous boundary layer thicker, just as in absence of suction. The peak of the radial velocity $F(\eta)$ in Fig. 7 increases monotonically as n is reduced from 1. The suction through the planar surface at $\eta = 0$ reverts the direction of the axial velocity H so that the flow is directed downwards, i.e. $H < 0$ in Fig. 9, rather than upwards as in Fig. 3. However, the downward velocity $-H(\infty)$ above the viscous boundary layer reduces as n is reduced below 1. The difference between the axial down flow at infinity and the suction velocity, i.e. $H(\infty) - H(0)$, needs to be supplied by the radially directed inward flow ($u < 0$ since $F > 0$). Since the latter increases as n is reduced, also $H(\infty) - H(0)$ is increased. This is a direct consequence of mass conservation $H' = F$ (14), or, equivalently, $H(\infty) - H(0) = \int_0^\infty F d\eta$.

The characteristics in Table 3 show that the radial skin friction $F'(0)$ increases and the tangential skin friction $G'(0)$ decreases with

Table 2
Boundary layer characteristics $F'(0), G'(0)$ and $H(\infty)$ for $n = 1$ in presence of suction $A = -2.0$. The present results are compared with data from Nath and Venkatachala [2], (Table 1). Note that their suction parameter a corresponds to $A = -2.0$ in the present work.

$-A$	$F'(0)$		$G'(0)$		$-H(\infty)$	
	Present	N & V	Present	N & V	Present	N & V
0	0.9420	0.9420	0.7729	0.7729	−0.6747	NA
0.5	0.8351	0.8350	1.3885	1.3863	0.1361	NA
1.0	0.6468	0.6462	2.1560	2.1550	0.8518	NA
2.0	0.3698	NA	4.0276	NA	1.9736	NA

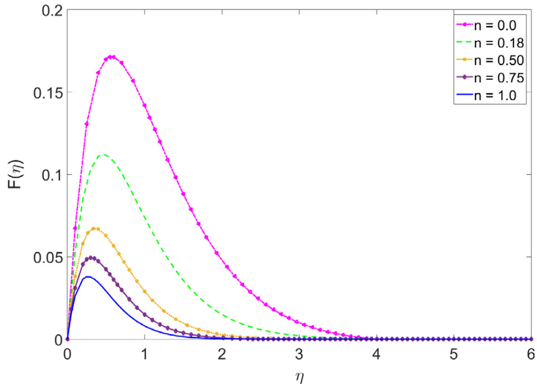

Fig. 7. Radial velocity component $F(\eta)$ for some different n-values in the range from 1 to 0 in presence of suction $(A = -2.0)$.

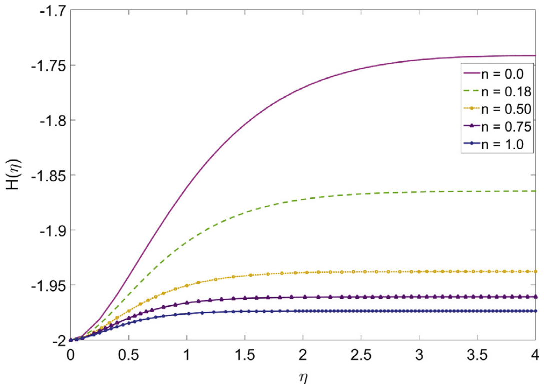

Fig. 9. Axial velocity component $H(\eta)$ for some different n-values in the range from 1 to 0 in presence of suction $(A = -2.0)$.

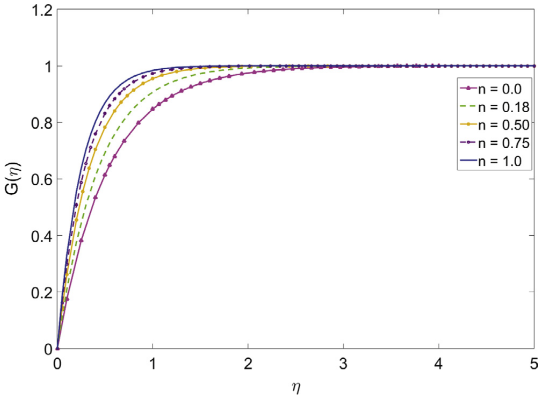

Fig. 8. Tangential velocity component $G(\eta)$ for some different n-values in the range from 1 to 0 in presence of suction $(A = -2.0)$.

decreasing n-values. This leads to a modest reduction of the axial flow in the far-field. While only a very modest vertical fluid acceleration takes place for $n = 1$, an enhanced acceleration towards the permeable surface is required for $n = 0$.

Let us recall the apparent consensus that similarity solutions of the boundary layer flow problem for $n = 0 (m = -1)$ exist only in presence of suction [5,7,9]. When sufficient suction is applied, similarity solutions do exist, for which velocity profiles and boundary layer characteristics are now shown in Figs. 7–9 and Table 3, respectively. It is remarkable, though, that Venkatachala and Nath [6] presented velocity profiles even for $n = 0$ in absence of suction in their Fig. 4(a, b, c), even though they argued in the introduction to their paper that solutions exist only in presence of a certain amount of suction. However, the strongly oscillating behaviour of their velocity components is cleary unphysical, thereby supporting the prevailing view that such similarity solutions are non-existing.

3.2. Temperature profiles in the thermal boundary layer

The thermal energy Eq. (17) subjected to the two temperature boundary conditions in Eq. (18) was first solved for the case when the external flow is in solid-body rotation, i.e. $n = m = 1$. The temperature profiles in Fig. 10 are of two qualitatively different types. Physically realistic profiles are obtained for $A = -0.5$ and below. These profiles exhibit the auxiliary asymptotes $\Theta \to 0$ and $\Theta' \to 0$ as $\eta \to \infty$. In absence of suction, however, the solution for $A = 0$ correctly satisfies the two boundary conditions for the temperature, but fails to satisfy the auxiliary requirement that $\Theta' \to 0$ as $\eta \to \infty$, i.e. that the heat flux has to vanish outside of the thermal boundary layer. This essential issue was addressed in our recent paper [10], in which the failure to obtain physically realistic similarity solutions was ascribed to the sign of the axial velocity component H.

Various temperature profiles for the particular flow field $n = m = 1$ and $A = -2.0$ are shown in Fig. 11 for different Prandtl numbers. The thermal boundary layer is gradually thinning as the Prandtl number increases, i.e. as the thermal diffusivity reduces, and the surface temperature is eventually felt only in the close vicinity of $z = 0 (\eta = 0)$. The inevitable consequence of this trend is that the magnitude of the heat transfer rate through the surface $\Theta'(0)$ increases significantly as the Prandtl number increases from 0.3 to 7.0.

Our ultimate goal is to explore the impact on the temperature field in the thermal boundary layer from the variation of the revolving flow in the far field. Temperature profiles for some different power-law variations of the tangential velocity v are shown in Fig. 12 in presence of strong suction $(A = -2.0)$ and

Table 3
Boundary layer characteristics $F'(0), G'(0)$ and $H(\infty)$ in presence of suction $A = -2.0$. Note that $n = (m+1)/2$.

n	m	$F'(0)$	$G'(0)$	$H(\infty)$
1.0	1.0	0.3698	4.0276	–1.9736
0.75	0.50	0.4216	3.5285	–1.9609
0.50	0	0.4916	3.0253	–1.9378
0.18	–0.64	0.6362	2.3598	–1.8644
0.0	-1	0.7952	1.9400	–1.7416

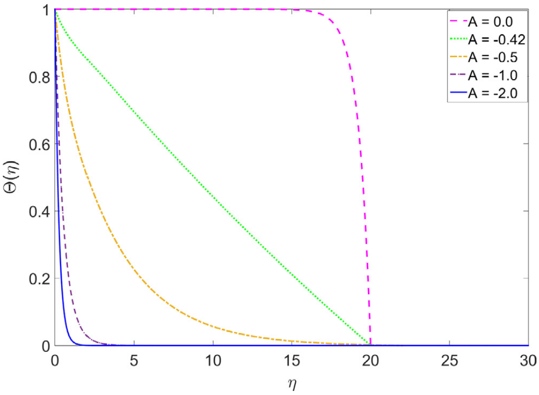

Fig. 10. Variation of temperature $\Theta(\eta)$ for the same values of the suction parameter A as for the flow field in Figs. 4–6. The flow in the far-field is in solid-body rotation $(n = m = 1)$ and the Prandtl number $Pr = 1$.

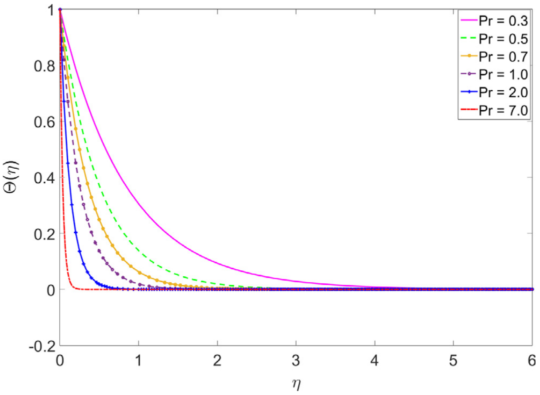

Fig. 11. Variation of temperature $\Theta(\eta)$ for some different Prandtl numbers. The flow in the far-field is in solid-body rotation $(n = m = 1)$ and subjected to strong suction $A = -2.0$.

Prandtl number $Pr = 1$. Even though the kinematic and thermal properties of the fluid are fixed, one can observe that the thermal boundary layer gradually thickens as the power n is reduced from $n = 1$ (solid-body rotation) to $n = 0$ (potential vortex). The monotonic thickening of the thermal boundary layer with decreasing n-values is accompanied by a gradually reducing slope of the temperature profiles. One can therefore infer that the heat transfer rate through the surface is significantly lower when the ambient flow is a potential vortex than is the case when the external flow is in solid-body rotation.

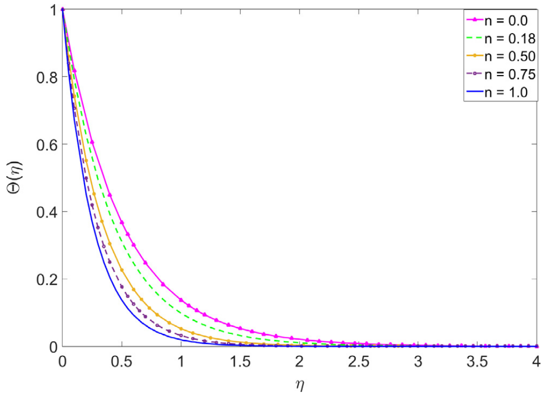

Fig. 12. Variation of temperature $\Theta(\eta)$ for differently revolving far-field flows $v \sim r^m$ with the power m in the range from $m = +1$ (solid-body rotation $n = 1$) to $m = -1$ (potential vortex $n = 0$). Strong suction $A = -2.0$ and Prandtl number $Pr = 1$.

Inspection of the thermal energy Eq. (17) shows that the effective diffusion coefficient is $[(n+1)Pr]^{-1}$. Thus, for a given fluid (i.e. Pr fixed), the thermal diffusion is twice as high for the case of a potential vortex $(n = 0)$ than if the far-field is in a state of solid-body rotation $(n = 1)$. The higher effective Prandtl number associated with the larger values of n suggests that the thermal boundary layer becomes thinner with increasing n-values. This is indeed consistent with the observations that can be made from Fig. 12.

The actual variation of the tangential flow has no other direct influence on the thermal boundary layer. How the tangential velocity v varies with r has, however, a substantial effect on the radial velocity component u, as can be seen in Fig. 7 where the peak velocity is monotonically reduced with increasing n. Ultimately, the radially-directed fluid motion is coupled to the axial flow w through the mass conservation constraint (1). Indeed, Fig. 9 shows that the magnitude of H increases with increasing n-values. This, in turn, promotes thermal convection $w\partial T/\partial z$ in the axial direction and thereby also tends to make the thermal boundary layer thinner. The indirect effect of n caused by alterations of the boundary layer flow therefore adds to the direct effect of n due to the n-dependent effective Prandtl number.

A particularly important parameter in heat transfer analysis is the Nusselt defined as

$$Nu = \frac{q(0)L}{k(T_w - T_\infty)} = \frac{-\partial T/\partial z|_{z=0} L}{T_w - T_\infty} = -\Theta'(0)\left[\frac{r}{r_0}\right]^{n-1}\sqrt{\frac{v_0 r_0}{\nu}}, \qquad (19)$$

where $q(0)$ is the rate of heat transfer through the surface at $z = 0$ and L is a representative length scale, for instance $L = r_0$. The Nusselt number is accordingly proportional with the dimensionless heat transfer rate reported in Table 4. Here, we have included results for some different values of the suction parameter A. The strongest suction $A = -2.0$ corresponds with the temperature profiles already shown in Fig. 12. In view of the quantitative results in Table 4, we conclude that the heat transfer rate is twice as high when the ambient flow is in solid-body rotation $(n = 1)$ as if the ambient flow is a potential vortex $(n = 0)$. The same trends are seen also for intermediate suction, but it is noteworthy that the heat transfer rate is even more strongly dependent on the type of revolving flow than for $A = -2.0$.

No results are available for the case with an impermeable surface $(A = 0)$ even though similarity solutions for the velocity field do exist in absence of suction for n-values about unity, as shown

Table 4
Heat transfer rate $-\Theta'(0)$ for differently revolving far-field flows $v \sim r^m$ with the power m in the range from $m = +1$ (solid-body rotation $n = 1$) to $m = -1$ (potential vortex $n = 0$). Prandtl number $Pr = 1$.

$n \setminus A$	0	−0.5	−1.0	−2.0
1.0	NA	0.4960	1.9114	3.9872
0.75	NA	0.2544	1.6336	3.4833
0.50	NA	0.2460	1.3309	2.9771
0.0	NA	0.0696	0.2843	1.9400

in Figs. 4–6 for $n = 1$. Nevertheless, the accompanying thermal problem does not admit physically realistic solutions. Although a solution may satisfy the two temperature boundary conditions (18), the temperature field does not asymptote properly to enable a gradually vanishing heat transfer rate q (see Fig. 10). We ascribe this phenomenon to the change-of-sign of the axial velocity component. According to the velocity profiles shown in Fig. 6 (for $n = 1$), the axial velocity component H remains negative only when $A \leqslant -0.42$. This is therefore a prerequisite for solutions of the thermal problem to exist [10].

The aim of our investigation has been to provide heat transfer analysis of the thermal aspects of the viscous boundary layer that develops underneath a generalized vortex flow. For the sake of simplicity, we considered the particular case of an isothermal revolving flow with temperature T_∞ above a planar surface with constant temperature T_w. The fluid motion in the three-dimensional boundary layer is driven by the revolving flow which is characterized by a circulating motion determined by the power-law variation $v \sim r^{2n-1}$ of the tangential velocity. Note that the radial velocity vanishes far above the surface $(u \to 0)$, whereas the axial velocity w approaches an a priori unknown value. At the surface $z = 0$, above which the flow revolves, the two velocity components parallel with the surface, i.e. u and v, are both zero in order to satisfy the no-slip condition. However, the surface is considered to be permeable and thus allows for either blowing or suction. The velocity component w normal to the surface is assumed to vary as r^{n-1} (i.e. as $r^{(m-1)/2}$) with the distance r from the symmetry axis. This particular r-dependence was chosen with the view to successfully transform the governing PDEs (7)–(11) to the set of ODEs (14)–(17). The surface boundary condition for w is expressed in terms of the dimensionless constant A such that positive and negative A-values correspond to blowing and suction, respectively, whereas $A = 0$ represents an impermeable surface.

4. Concluding remarks

The heat transfer aspects of revolving vortex flow above a planar surface have been investigated. The axisymmetric fluid velocity field was first studied by Bödewadt [1] by assuming that the revolving flow was in a state of solid-body rotation, whereas others [5–7] considered power-law variations of the tangential velocity component in the far-field. Since the flow field is required in order to solve the convection–diffusion type of problem for the thermal energy, we adopted the similarity transformation used by King and Lewellen [5] and showed that also the heat transfer problem admits similarity solutions.

First, however, we computed the three-componential flow field which is needed in order to solve also the thermal boundary layer equation. The present numerical solutions shown in Section 3.1 were in excellent agreement with the earlier results by King and Lewellen [5], but deviated substantially from the results reported by Kuo [7].

Let us recall that Kuo's investigation [7] of revolving flows with power-law velocity distributions was motivated by an interest in the three-dimensional flow in the boundary layer beneath a tornado-like vortex with a structure similar to a Rankine vortex, i.e. with a core of large vorticity $(n \approx 1)$ and an outer region of small or zero vorticity $(n \approx 0)$.

It is remarkable that the major disagreement between results obtained by King and Lewellen [5] and Kuo [7] has went unnoticed for a half century. The paper by King and Lewellen [5] was published back in 1964, whereas the comprehensive article by Kuo [7] appeared in 1971. Kuo claimed that his computed results for $n = 1$ agreed well with Bödewadt's [1] original data. Indeed, an excellent agreement was also observed with the present results in Figs. 1–3 for $n = 1$, as well as with the data reported by King and Lewellen [5], as shown in Table 1. For n-values below unity, however, deviations occur and these discrepancies are particularly noteworthy in the axial velocity component H. From the point of view of the present paper, the axial velocity component H is the only velocity component that appears explicitly in the transformed thermal energy Eq. (17).

In a recent paper [10] we argued that physically realistic similarity solutions for the heat transfer problem accompanying the Bödewadtt flow [1] can only be obtained in presence of suction through the planar surface. To this end we also considered surface suction herein. For a given value (-2.0) of the dimensionless suction parameter A, we observed that the actual power $m = 2n - 1$ describing the radial variation of the revolving vortex flow had a decisive effect on the thermal boundary layer. A distinct and monotonically thinning of the thermal boundary layer was observed with increasing values of the power m over the range from $m = -1$ to $m = +1$, i.e. as the revolving flow was altered from a potential vortex $(m = -1)$ to a state of solid-body rotation $(m = +1)$. The gradually decreasing thermal boundary layer thickness was accompanied by an increase of the heat transfer rate through the planar surface above which the flow revolves. These findings were explained as the combined influence of two different effects caused by the different power-law variations of the generalized vortex flow: (i) a variation of the effective Prandtl number $(n + 1)Pr$ affects the thermal diffusion, whereas (ii) a variation of the axial velocity field H affects the thermal convection. These distinctly different effects of $m = 2n - 1$ both alter the thermal boundary layer in the same direction.

Conflict of interest

No conflicts of interests.

References

[1] U.T. Bödewadt, Die Drehströmung über festem Grunde, J. Appl. Math. Mech./Z. Angew. Math. Mech. 20 (1940) 241–253.

[2] G. Nath, B.J. Venkatachala, The effect of suction on boundary layer for rotating flows with or without magnetic field, Proc. Indian Acad. Sci.-Sect. A 85 (1977) 332–337.

[3] B. Sahoo, S. Abbasbandy, S. Poncet, A brief note on the computation of the Bödewadt flow with Navier slip boundary conditions, Comput. Fluids 90 (2014) 133–137.

[4] M. Turkyilmazoglu, Bödewadt flow and heat transfer over a stretching stationary disk, Int. J. Mech. Sci. 90 (2015) 246–250.

[5] W.S. King, W.S. Lewellen, Boundary-layer similarity solutions for rotating flows with and without magnetic interaction, Phys. Fluids 7 (1964) 1674–1680.

[6] B.J. Venkatachala, G. Nath, Mass transfer effects on the generalised vortex flow over a stationary surface with or without magnetic field, Proc. Indian Acad. Sci. Sect. C: Eng. Sci. 3 (1980) 211–223.

[7] H.L. Kuo, Axisymmetric flows in the boundary layer of a maintained vortex, J. Atmos. Sci. 28 (1971) 20–41.

[8] F.K. Moore, Three-dimensional boundary layer theory, Adv. Appl. Mech. 4 (1956) 159–228.

[9] K. Nanbu, Vortex flow over a flat surface with suction, AIAA J. 9 (1971) 1642–1643.

[10] M. Rahman, H.I. Andersson, On heat transfer in Bödewadt flow, Int. J. Heat Mass Transfer 112 (2017) 1057–1061.
[11] L.F. Shampine, J. Kierzenka, M.W. Reichelt, Solving boundary value problems for ordinary differential equations in MATLAB with bvp4c, Tutorial Notes (2000) 437–448.
[12] T. Cebeci, H.B. Keller, Shooting and parallel shooting methods for solving the Falkner-Skan boundary-layer equation, J. Comput. Phys. 7 (1971) 289–300.
[13] N.G. Kafoussias, E.W. Williams, An improved approximation technique to obtain numerical solution of a class of two-point boundary value similarity problems in fluid mechanics, Int. J. Numer. Meth. Fluids 17 (1993) 145–162.
[14] M. Rahimi-Gorji, O. Pourmehran, M. Gorji-Bandpy, D.D. Ganji, Unsteady squeezing nanofluid simulation and investigation of its effect on important heat transfer parameters in presence of magnetic field, J. Taiwan Inst. Chem. Eng. 67 (2016) 467–475.